

AD-A033 712

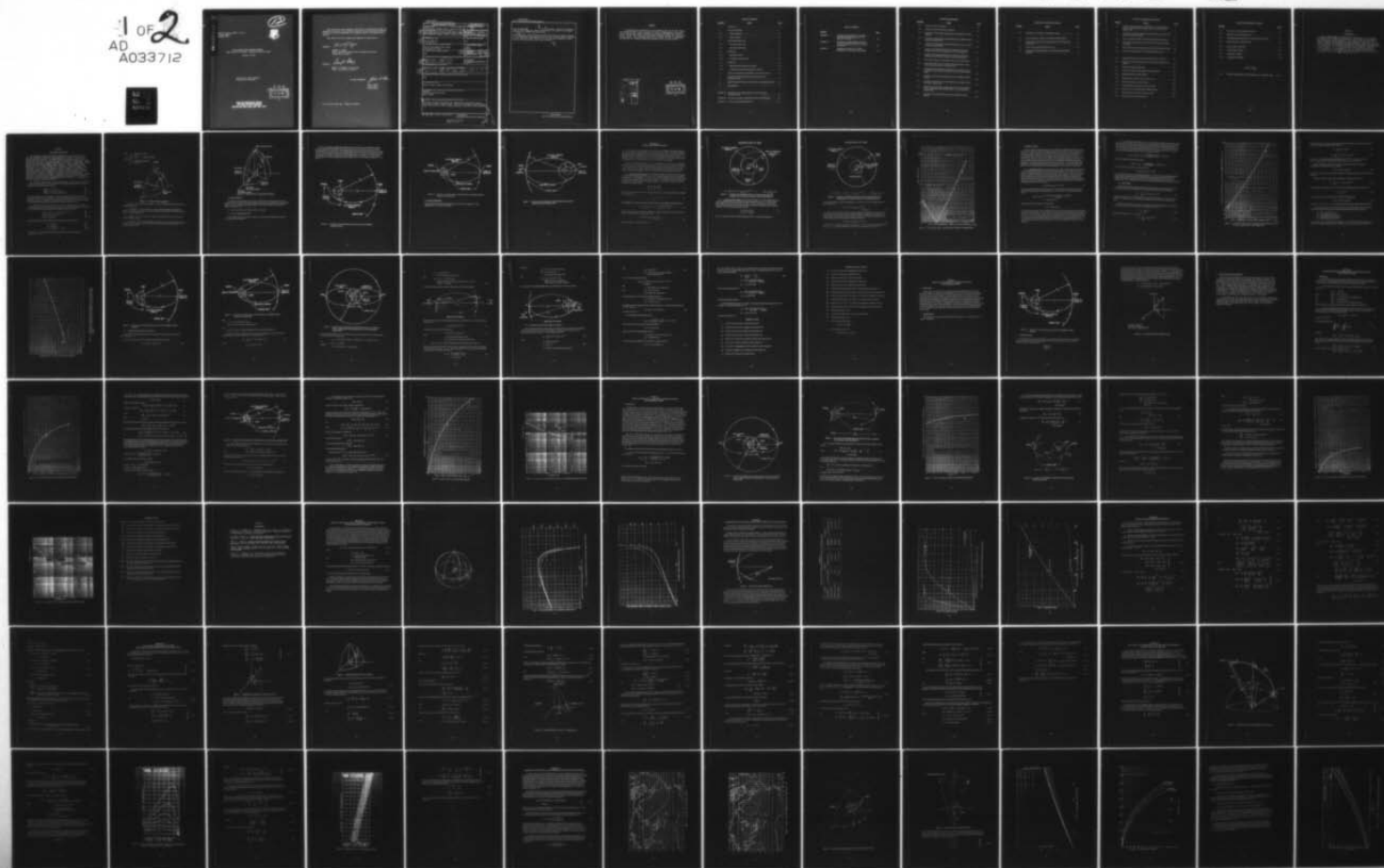
ROME AIR DEVELOPMENT CENTER GRIFFISS AFB N Y
SPACE SURVEILLANCE SOFTWARE SUPPORT. VOLUME I, PART 2. RADC TRA--ETC(U)
OCT 76 @ A ELLIS

F/G 15/3

UNCLASSIFIED

RADC-TR-76-261-VOL-1-PT-2 NL

1 of 2
AD
A033712



1 OF 2
AD
A033712



ADA033712

RADC-TR-76-261, Volume I, Part 2
In-house Report
October 1976

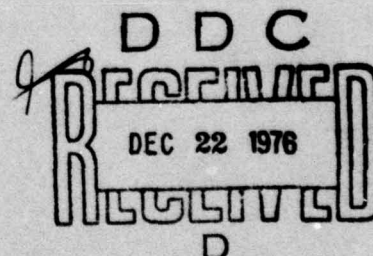
12.



SPACE SURVEILLANCE SOFTWARE SUPPORT
RADC Trajectory Program - Numerical/Analytical Data

George A. Ellis

Approved for Public Release.
Distribution Unlimited.

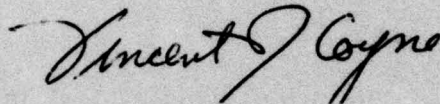


ROME AIR DEVELOPMENT CENTER
AIR FORCE SYSTEMS COMMAND
GRIFFISS AIR FORCE BASE, NEW YORK 13441

This report has been reviewed by the Office of Information, RADC, and approved for release to the National Technical Information Service (NTIS). At NTIS, it will be releasable to the general public, including foreign nations.

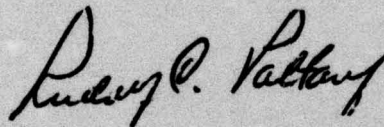
This report has been reviewed and approved for publication.

APPROVED:



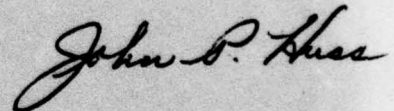
VINCENT J. COYNE
Chief, Space Surveillance and Instrumentation Branch
Surveillance Division

APPROVED:



RUDOLF C. PALTAUF, Lt Col, USAF
Chief, Surveillance Division

FOR THE COMMANDER:



JOHN P. HUSS
Acting Chief
Plans Office

Do not return this copy. Retain or destroy.

UNCLASSIFIED

SECURITY CLASSIFICATION OF THIS PAGE (When Data Entered)

REPORT DOCUMENTATION PAGE		READ INSTRUCTIONS BEFORE COMPLETING FORM
1. REPORT NUMBER RADC-TR-76-261, Volume I, Part 2	2. GOVT ACCESSION NO.	3. RECIPIENT CATALOG NUMBER (9)
4. TITLE (and Subtitle) SPACE SURVEILLANCE SOFTWARE SUPPORT. Volume I, Part 2. Final Rept. RADC Trajectory Program - Numerical/Analytical Data	5. TYPE OF REPORT & PERIOD COVERED Final Rept.	6. PERFORMING ORG. REPORT NUMBER N/A
7. AUTHOR(s) George A. Ellis	8. CONTRACT OR GRANT NUMBER(s) N/A	
9. PERFORMING ORGANIZATION NAME AND ADDRESS Rome Air Development Center (OCSA) Griffiss AFB, NY 13441	10. PROGRAM ELEMENT, PROJECT, TASK AREA & WORK UNIT NUMBERS 62702F 65121205	
11. CONTROLLING OFFICE NAME AND ADDRESS Same	12. REPORT DATE October 1976	13. NUMBER OF PAGES 100
14. MONITORING AGENCY NAME & ADDRESS (if different from Controlling Office) Same	15. SECURITY CLASS. (of this report) UNCLASSIFIED	15a. DECLASSIFICATION/DOWNGRADING SCHEDULE N/A
16. DISTRIBUTION STATEMENT (of this Report) Approved for Public Release. Distribution Unlimited.		
17. DISTRIBUTION STATEMENT (of the abstract entered in Block 20, if different from Report) Same		
18. SUPPLEMENTARY NOTES There are three volumes in this report.		
19. KEY WORDS (Continue on reverse side if necessary and identify by block number) Missiles Satellites-synchronous Orbit Radar coverage		
20. ABSTRACT (Continue on reverse side if necessary and identify by block number) This report contains the numerical and analytical data base useful for the missile/space vehicle mission analyst. Operational constraints considered were: launch site locations, orbital transfer maneuvers, and missile burnout parameters.		

DD FORM 1 JAN 73 1473

EDITION OF 1 NOV 65 IS OBSOLETE

UNCLASSIFIED

SECURITY CLASSIFICATION OF THIS PAGE (When Data Entered)

309050

over
y/B

UNCLASSIFIED

SECURITY CLASSIFICATION OF THIS PAGE(When Data Entered)

Line 20 (continued)

Vol II documents a procedure for punching cards in ASCII format and reading the data onto a HP cassette for subsequent plotting with an HP9820 calculator system.

Vol III documents some Radar Signature and Radar Scattering computer programs. A three dimensional plot program contained in this volume has been incorporated into the Interactive Radar Simulator for plotting three dimensional antenna patterns and cross section aspect angle histories.

UNCLASSIFIED

SECURITY CLASSIFICATION OF THIS PAGE(When Data Entered)

ABSTRACT

To comprehend the formulation of the parametric data for the RADC Trajectory Simulation Model and to increase the field of distribution of this mathematical methodology, certain excerpts of previously published RADC technical reports (by the same author) are being made available, readily and conveniently, by this report. It is intended that this will enable the user to comprehend and exercise the available simulation program with its various options.

* SECTION for	
White Section	<input checked="" type="checkbox"/>
Buff Section	<input type="checkbox"/>
SW/ADDITION	<input type="checkbox"/>
DESCRIPTION	
BY	
SYSTEMS/AVAILABILITY CODE	
DATE, DAY, and/or SPECIAL	
A	

DDC
RECEIVED
 DEC 22 1976
 D

TABLE OF CONTENTS

<u>SECTION</u>	<u>TITLE</u>	<u>PAGE</u>
1	Introduction	1-1
2	Trajectory Simulation	2-1
2.1	Transfer Maneuvers	2-3
2.2	Sensor Locations	2-5
3	Dwell Angle/Transfer Time	3-1
3.1.1	Interceptor Above Target	3-1
3.1.2	Interceptor Below Target	3-2
3.2	Dwell Angle	3-5
3.2.1	High-Altitude-Dwell	3-5
3.2.2	Low/Medium-Altitude-Dwell	3-6
3.3	Flight Time	3-6
3.3.1	High-Altitude-Dwell Flight Time Analysis	3-10
3.3.2	Low/Medium-Altitude-Dwell Flight Time Analysis	3-14
4	Direct Ascent Elliptical Transfer Maneuver to Synchronous Orbit	4-1
5	Low/Medium-Altitude-Dwell Elliptic Transfer Maneuver to Synchronous Orbit	5-1
6	High-Altitude-Dwell Bielliptic Transfer Maneuver to Synchronous Orbit ..	6-1
7	Bibliography.....	7-1
Appendix A	Inertial Geocentric Angular Separation of the Direct Ascent Interceptor/Target	A-1
Appendix B	Interceptor Co-planar Circular/Elliptical Orbit Angular Separation	B-1
Appendix C	Orbital Transfer Energy Requirement	C-1

TABLE OF CONTENTS

<u>SECTION</u>		<u>PAGE</u>
Appendix D	An Analytical Solution to the Three Dimensional Representation of the Ballistic Missile.....	D-1
Appendix E	Evaluation of Approximate Values of the Two Dimensional Ballistic Missile Parameters.....	E-1
Appendix F	Graphical Solution for a Quick Assessment of the Detection Problem	F-1

LIST OF ILLUSTRATIONS

<u>FIGURE</u>	<u>TITLE</u>	<u>PAGE</u>
2-1	Vehicle's Velocity Components	2-2
2-2	Vehicle's Inertial & Tropocentric Coordinates	2-3
2-3	Geometry of the Interceptor's <u>D</u> irect <u>A</u> scent into an Elliptical Transfer Maneuver	2-4
2-4	Geometry of the Interceptor's Transfer Maneuver to the Higher Altitude Synchronous Satellite Orbit	2-5
2-5	Geometry of the Interceptor's Transfer Maneuver to the Lower Altitude Synchronous Satellite Orbit	2-6
3-1	Geometry of the Relative Positions of the Target and an Interceptor (Initially Above the Target) at Initiation of the External Maneuver	3-2
3-2	Geometry of the Relative Positions of the Target and an Interceptor (Initially Below the Target) at Initiation of the Internal Maneuver	3-3
3-3	Dwell Angle vs Ratio of the Interceptor's Radius to the Satellite Orbit	3-4
3-4	Interceptor's Flight Time for an Elliptical Transfer Maneuver vs Ratio of the Interceptor's Radius to the Satellite Orbit	3-7
3-5	Nondimensional Orbital Period of the Interceptor vs the Ratio of the Interceptor's Circular Parking Orbit Radius to the Synchronous Satellite Radius	3-9
3-6	Geometry of the Interceptor's <u>D</u> irect <u>A</u> scent into an Elliptical Transfer Maneuver	3-10
3-7	Geometry of the Interceptor's Transfer Maneuver to the Higher Altitude Synchronous Satellite Orbit	3-11
3-8	Geometry of the Interceptor's Transfer Maneuvers from a <u>L</u> ow- <u>A</u> ltitude- <u>D</u> well to a <u>H</u> igh- <u>A</u> ltitude- <u>D</u> well Parking Orbit to a Final Synchronous Altitude Orbit	3-12
4-1	Geometry of the Interceptor's <u>D</u> irect <u>A</u> scent Into Elliptical Transfer Maneuver	4-2

LIST OF ILLUSTRATIONS (Continued)

<u>FIGURE</u>	<u>TITLE</u>	<u>PAGE</u>
4-2	Interceptor's Intrinsic Coordinate System.....	4-3
5-1	Ratio of Interceptor's Apogee to Parking Orbit Radius (R_a/R_c)	5-2
5-2	Geometry of the Interceptor's Transfer Maneuver to the Synchronous Satellite Orbit	5-4
5-3	Ratio of the Circular Parking Orbits (R_{ss}/R_c)	5-6
5-4	Interceptor's Velocity-Altitude for the Low/Medium-Altitude-Dwell Scenarios	5-7

LIST OF ILLUSTRATIONS (Continued)

<u>FIGURE</u>	<u>TITLE</u>	<u>PAGE</u>
6-1	Geometry of the Interceptor's Transfer Maneuvers from a <u>Low-Altitude-Dwell</u> to a <u>High Altitude-Dwell</u> Parking Orbit to a Final Synchronous Altitude Orbit	6-2
6-2	Interceptor's Intermediate Elliptical Transfer Orbit from an Initial-to-Final (Desired) Circular Parking Orbit	6-3
6-3	Ratio of Interceptor's Apogee to Initial Parking Orbit Radius (R_{ai}/R_{ci})	6-4
6-4	Interceptor's Final Elliptical Transfer Orbit to the Synchronous Satellite Target Orbit	6-5
6-5	Ratio of Interceptor's Final Parking-to-Synchronous Orbits Radii (R_{cf}/R_{ss})	6-8
6-6	Interceptor's Velocity-Altitude for <u>High-Altitude-Dwell</u> Scenario	6-9
A-1	Longitudinal Separation of the Interceptor/Target Prior to Collision	A-3
A-2	Inertial Geocentric Angular Separation of the Interceptor/Target Prior to Collision	A-4
B-1	Interceptor's Angular Displacement	B-1
B-2	Interceptor Co-Planar Circular/Elliptical Angular Separation	B-3
B-3	<u>High-Altitude-Dwell</u> Angular Separation	B-4
D-1	Spherical Polar Coordinates of the Velocity Vector	D-2
D-2	Missile's Initial State Vector Components	D-3
D-3	Unperturbed Planar Trajectory on a Spherical Earth	D-5
E-1	Illustration of the Free Flight Ballistic Missile Geometry	E-2
E-2	Range Angle (Degrees) vs Burnout Reentry Angle	E-5
E-3	Minimum Energy Velocity Requirement	E-7

LIST OF ILLUSTRATIONS (Continued)

<u>FIGURE</u>		<u>PAGE</u>
F-1	Earth Track of a Typical Satellite Trajectory	F-2
F-2	Visibility Contours for Specific Sensors	F-3
F-3	Three-Dimensional Representation of the Subtended Earth Angle	F-4
F-4	Sensor Volumetric Coverage Geometry	F-5
F-5	Viewing Angle vs Slant Range	F-6
F-6	Viewing Angle vs Altitude	F-7
F-7	Slant Range vs Altitude	F-9
F-8	Functional Flow Diagram	F-10

LIST OF TABLES

B-1	Initial State Vector of the Interceptor at Transfer Time.....	B-2
-----	---	-----

SECTION I

INTRODUCTION

This volume documents the mathematical methodology in the conceptual development of the numerical and analytical relationships for the computational trajectory simulation models. These models were exercised for specific targets/sensors complex scenarios tempered by launch site locations, sensor visibility, and performance parameters. These models were represented by a modification of a previously developed RADC Trajectory, Simulation Computer Program. It is to be noted that, for the purpose of clarity, certain mathematical developments of these analytical expressions do not employ the common scalar notation of a vector. However, this scalar form is equivalent to the vector symbol without the arrow.

SECTION 2

TRAJECTORY SIMULATION

The computer program used for the calculation of trajectories is a special perturbation computer program generated at RADC.* It was run on the RADC HIS-635 computer. The double precision program provides sensor metric data and their time rates for specific classes of trajectories. These simulated trajectories encompassed reentry type vehicles: ICBM, SLBM, classes and the interceptor/synchronous target scenarios. These Hohmann and non-Hohmann ballistic flight vehicles were launched from specific geographic locations, i.e., at booster burnout, to impact in specific locations. The interceptor/target scenarios included classes of Hohmann and non-Hohmann trajectories that can be simulated: (i) direct ascent maneuvers, (ii) low-altitude-dwell scenarios (elliptical transfer) to high-altitude-dwell scenarios (bielliptical transfer). The time history of each vehicle's dynamic behavior is influenced by a rotating spherical earth potential, standard atmosphere, earth wind and a variable ballistic coefficient. A discussion of the main subroutine groupings used are:

(1) ICERBM - With an input of a set of initial boundary values unique to each vehicle, the free-flight position and velocity vectors, relative to an inertial geocentric coordinate system, are calculated via the transformation equations:

$$\left. \begin{aligned} dr/dt \Big|_0 &= V_0 \cos \gamma \\ d\theta/dt \Big|_0 &= (V_0 \sin \gamma \cos \beta)/r_0 \\ d\lambda/dt \Big|_0 &= (V_0 \sin \gamma \sin \beta)/r_0 \cos \theta \end{aligned} \right\} \quad (1)$$

where the free flight reentry angle (WRT local vertical), heading angle (WRT North) and the magnitude of the velocity vector (relative to burnout) are given respectively by γ , β , and V_0 (as illustrated in Figure 2-1). In addition, the salient feature of this routine is to provide a corrected set of initial boundary conditions corresponding to a specified impact location.

(2) EQTNX - With respect to the inertial geocentric coordinate system, the vehicle's acceleration components are calculated. These components, in spherical coordinates, are defined by the following set of 2nd order non-linear differential equations of motion.

$$\left. \begin{aligned} d^2 r/d^2 t - r\dot{\theta}^2 - (r \cos^2 \theta) \dot{\Omega}^2 + \mu/r^2 &= Q_1 \\ d(r^2 \dot{\theta})/dt + (r^2 \sin 2\theta) \dot{\Omega}^2/2 &= Q_2 \\ d(r^2 \dot{\Omega} \cos^2 \theta)/dt &= Q_3 \end{aligned} \right\} \quad (2)$$

where Q_i represents the nongravitational force arising from atmospheric drag i.e.,

$$\left. \begin{aligned} Q_1 &= -\rho Z_d V \dot{r} \\ Q_2 &= -\rho Z_d V r^2 \dot{\theta} \\ Q_3 &= -\rho Z_d V r^2 (\dot{\lambda} - \dot{\Omega}) \cos^2 \theta \end{aligned} \right\} \quad (3)$$

*Ellis, G.A., et al., "Simulation Program for Three Degrees of Freedom Trajectories," EMA-TM-66-5, Sep 66.

where; ρ = atmospheric density
 $\Omega = \omega + \lambda$
 $Z_d = C_d A / 2$ = ballistic coefficient
 (unit mass)
 ω_e = earth's angular velocity
 ω = earth wind

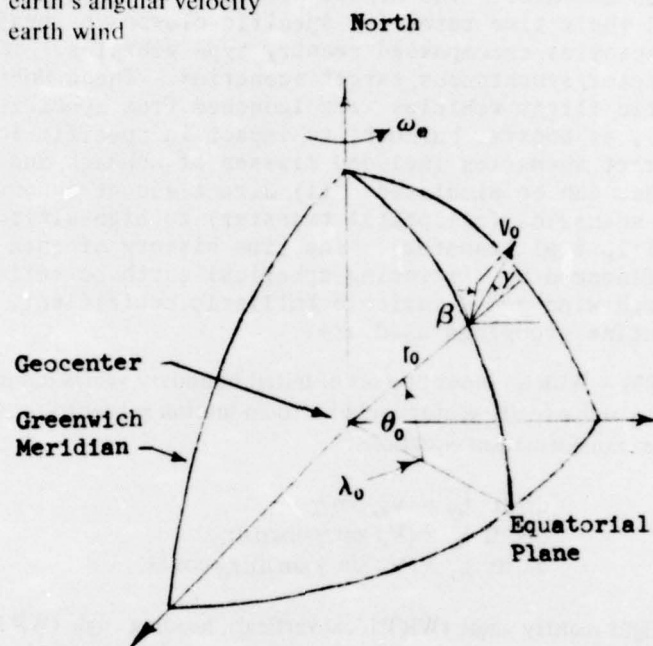


Figure 2-1 – Vehicle's Velocity Components

- (3) RKG – Using a 4th order Runge Kutta – Gill, the differential equations of motion are numerically integrated.
- (4) CONVERT – For a specified sensor location (latitude, longitude and height) the vehicle's metric data and their time rates were calculated for that portion of its flight within the sensor's 2.0° right circular cone.
- (5) PRINT – The time histories of the trajectories are presented in geocentric and topocentric coordinate systems.
- (6) BALCOF – Provides a variable ballistic coefficient generated from metric data for each specific vehicle. The altitude dependent coefficients were extensively employed for the 3° of freedom simulation study.

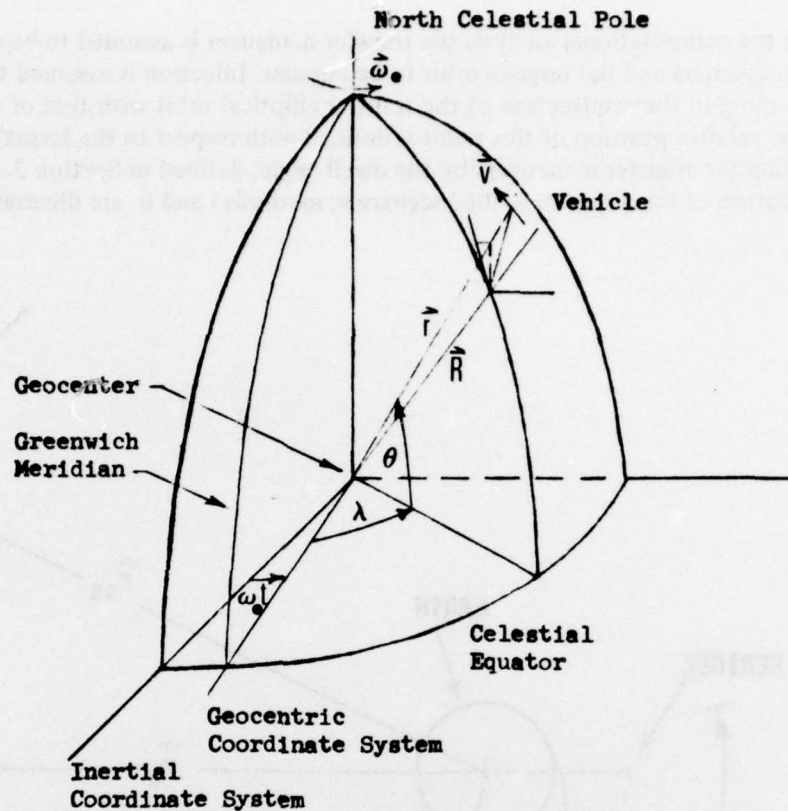


Figure 2-2 – Vehicle's Inertial & Tropocentric Coordinates

2.1 Transfer Maneuvers

The analysis of an interception with a vehicle requires that the velocity and radius vectors of the target vehicle be matched. The analytical analysis was reduced to the problem of coplanar orbital transfer. The transfer maneuver required a definition of the launch timing for the two general coplanar methods. These are:

- i) Direct ascent to the synchronous altitude of the target.
- ii) Launch utilizing parking orbits.

These methods neglect perturbative accelerations and assume the burning time of the interceptor stages to be infinitesimal.

For the computational analysis the transfer maneuver is assumed to be elliptical (coplanar and non-coplanar) and the target's orbit to be circular. Injection is assumed to occur at a point corresponding to the intersection of the transfer elliptical orbit with that of the synchronous target orbit. The relative position of this point is defined with respect to the target's position (at the time of initiating the transfer maneuver) by the dwell angle, defined in Section 3. A two-dimensional representation of the above described scenarios; methods i and ii are illustrated in Figures 2-3, 2-4 and 2-5.

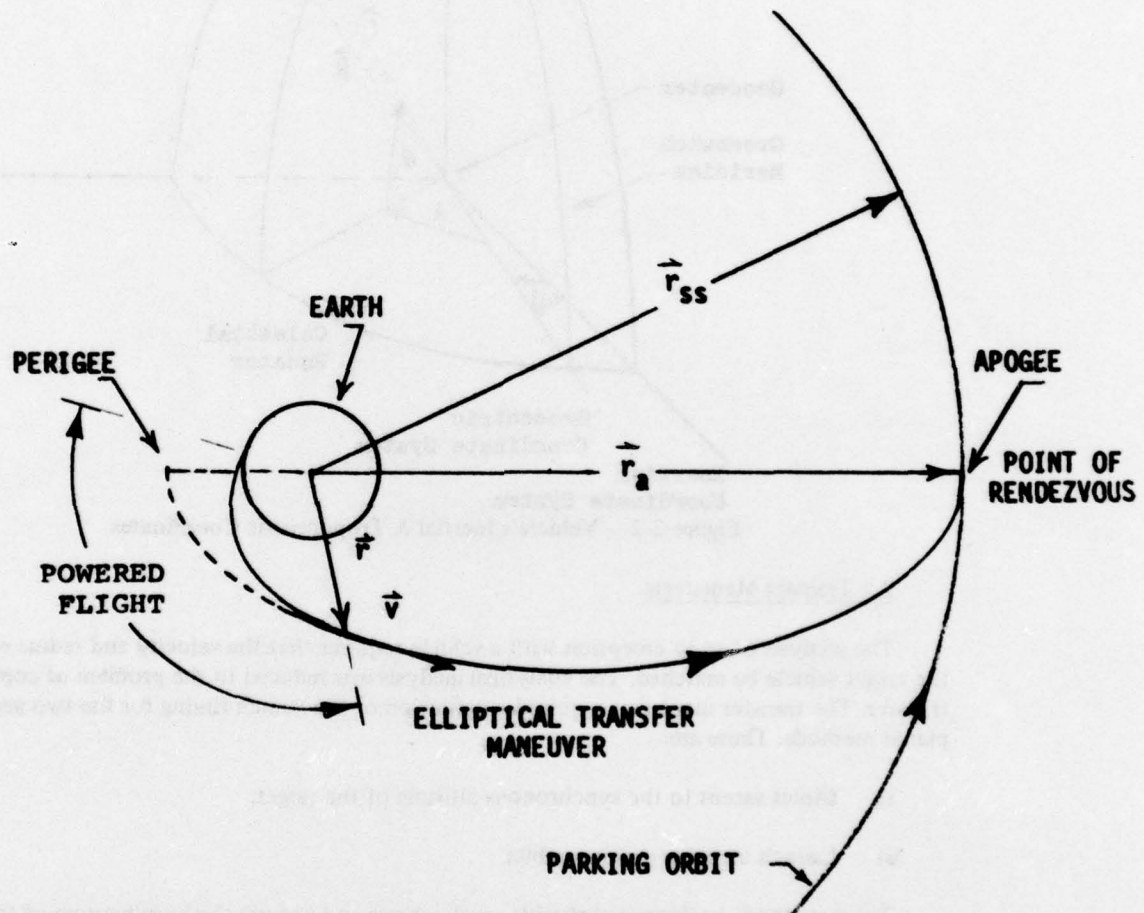


Figure 2-3 – Geometry of the Interceptor's Direct Ascent into an Elliptical Transfer Maneuver

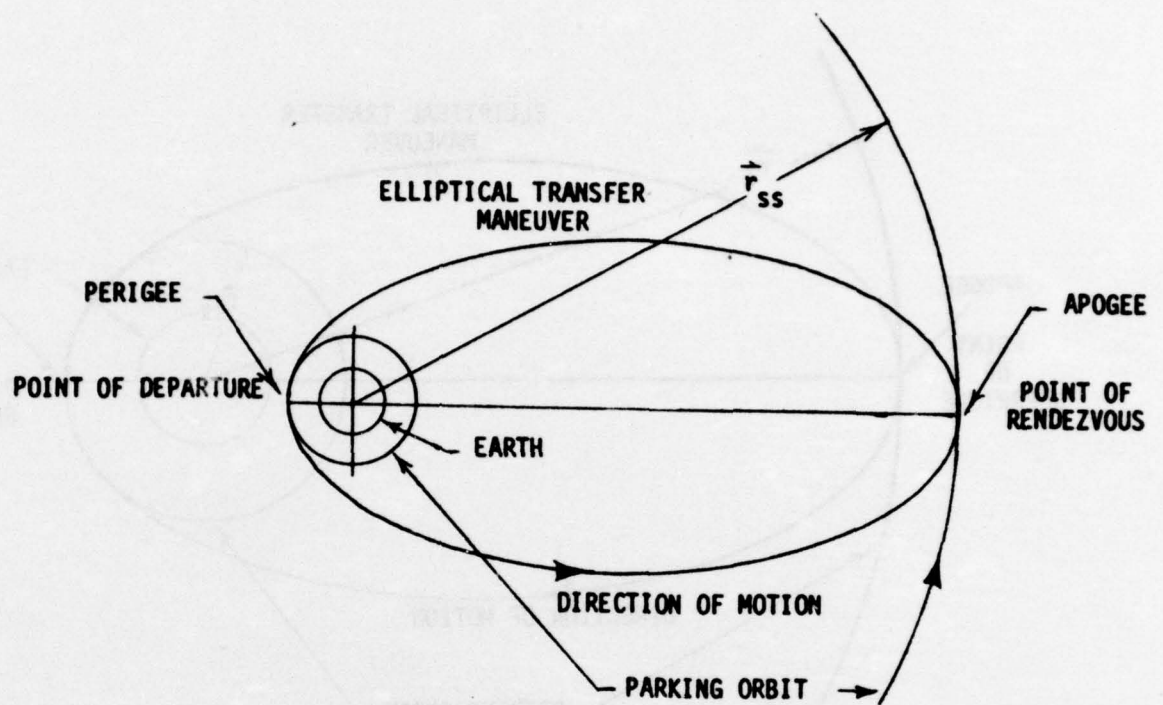


Figure 2-4 — Geometry of the Interceptor's Transfer Maneuver to the Higher Altitude Synchronous Satellite Orbit

2.2 Sensor Locations

The previously described scenarios can be exercised against a pre-selected set of sensor locations.

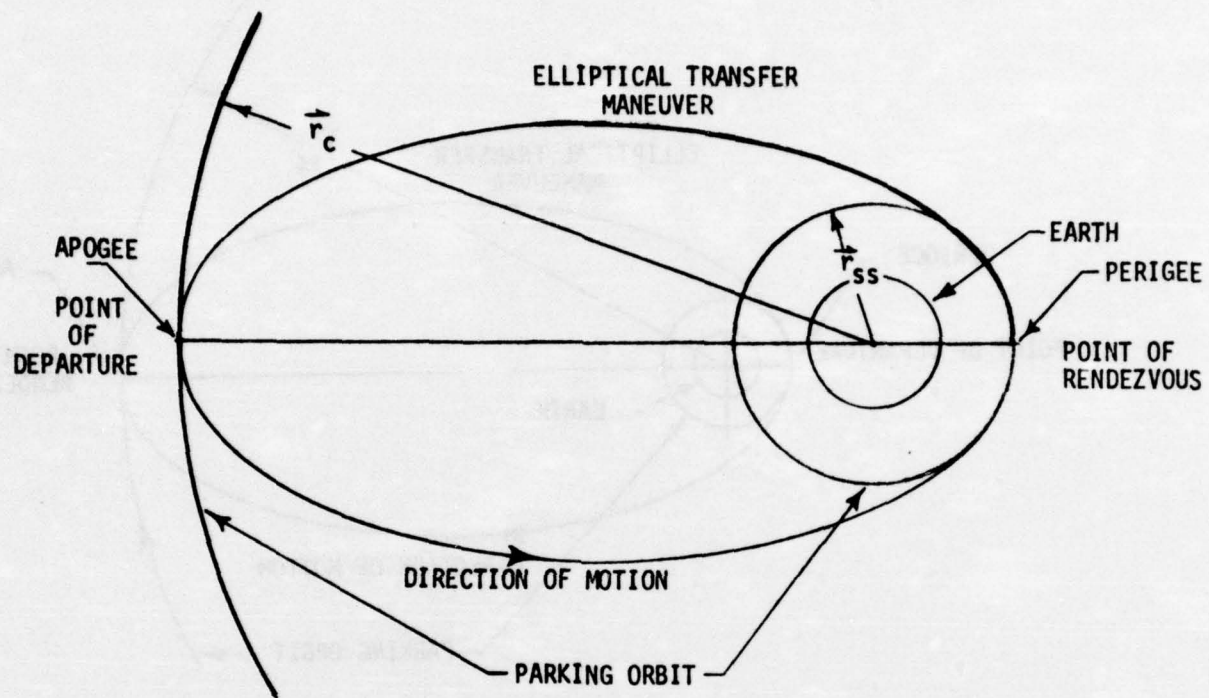


Figure 2-5 – Geometry of the Interceptor's Transfer Maneuver to the Lower Altitude Synchronous Satellite Orbit

SECTION 3 DWELL ANGLE/TRANSFER TIME

An interceptor is launched from a specific launch site on a ballistic trajectory for injecting into a low-altitude-dwell parking orbit at a specific inclination. A "time" is calculated to initiate a maneuver to enable the interceptor to execute a Hohmann elliptical transfer maneuver. For the Hohmann transfer, the maneuver is initiated at the mode opposite that at which rendezvous is to take place. Thus the timing must be precise, that is, at the initiation of the transfer maneuver, the synchronous equatorial satellite target must be at a prescribed orbital position.

The "time" at which this transfer is to be initiated is defined in terms of an angular displacement, Θ . This angle, defined at the point of departure of the interceptor, is a function of the ratio of the orbital radii between the interceptor and the target. Defining the radial distance from the earth's center to the interceptor's circular orbit and the distance from the earth's center to the target's circular orbit as r_i and r_{ss} , respectively, the following type of maneuver is presented.

3.1.1 Interceptor Above Target. The interceptor is initially on a circular orbit with a radius r_i greater than that of the target's radius r_{ss} , i.e., the interceptor leads the target by the angle Θ (see Figure 3-1). Let the flight time of the interceptor's elliptical transfer maneuver (apogee-perigee, π) initiated by an impulsive velocity increment at apogee, be equivalent to the target's flight time during an angular displacement ($\pi + \Theta$). Since the target exercises uniform angular velocity, the following relationship is formed:

$$\left\{ \frac{\pi + \Theta}{T_c} \right\} = \left\{ \frac{2\pi}{T} \right\} \quad (1)$$

where T_{ss} is the period of the (target's) circular orbit and $2T_c$ equal to the period of the elliptical orbit. Therefore,

$$T_{ss} = \frac{2\pi}{\mu^{1/2}} r_{ss}^{3/2} \quad (2)$$

and the flight time of the interceptor is reduced (in terms of the variables (r_a, r_{ss})) to the form:

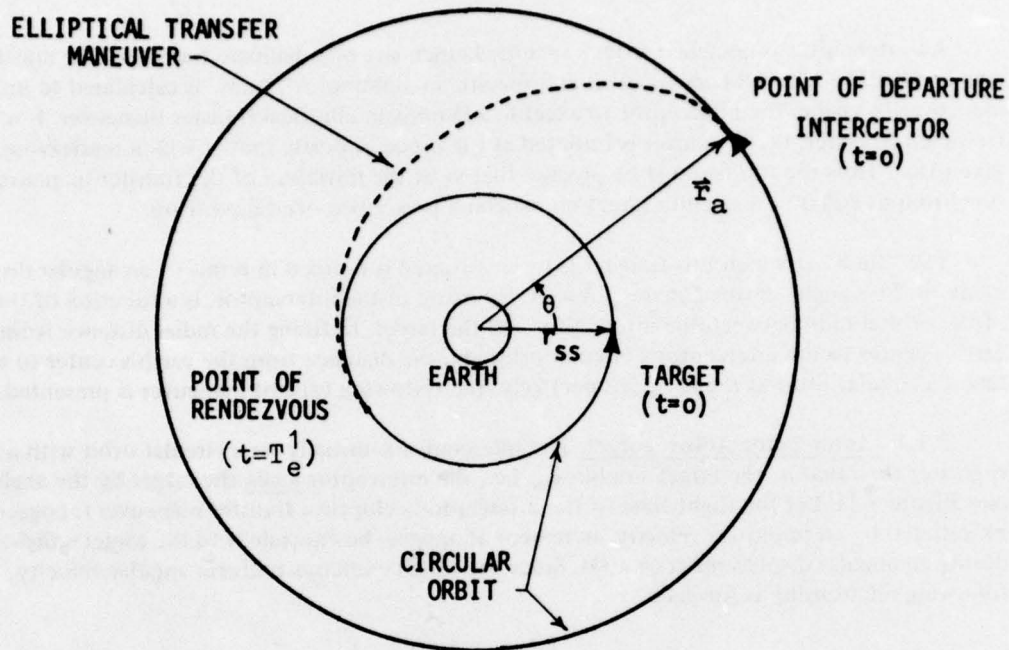
$$2T_c = \frac{2\pi}{\mu^{1/2}} a^{3/2} \Rightarrow T_c = \frac{\pi}{\mu^{1/2}} \left\{ \frac{r_a + r_{ss}}{2} \right\}^{3/2} \quad (3)$$

Substituting equations (2) and (3) into equation (1) yields the following expression for the lead angle, i.e., the interceptor is 'ahead' of the target:

$$\Theta = \pi \left\{ \left[\frac{1}{2} \left(\frac{r_a}{r_{ss}} + 1 \right) \right]^{3/2} - 1 \right\} \quad \text{For } r_a/r_{ss} \geq 1 \quad (4)$$

The above function is illustrated in Figure 3-1.

INTERCEPTOR LEADS THE TARGET



$$\theta = \pi \left\{ \left[\frac{1}{2} \left(1 + \frac{r_a}{r_{ss}} \right) \right]^{3/2} - 1 \right\} \quad \text{FOR } \frac{r_a}{r_{ss}} \geq 1$$

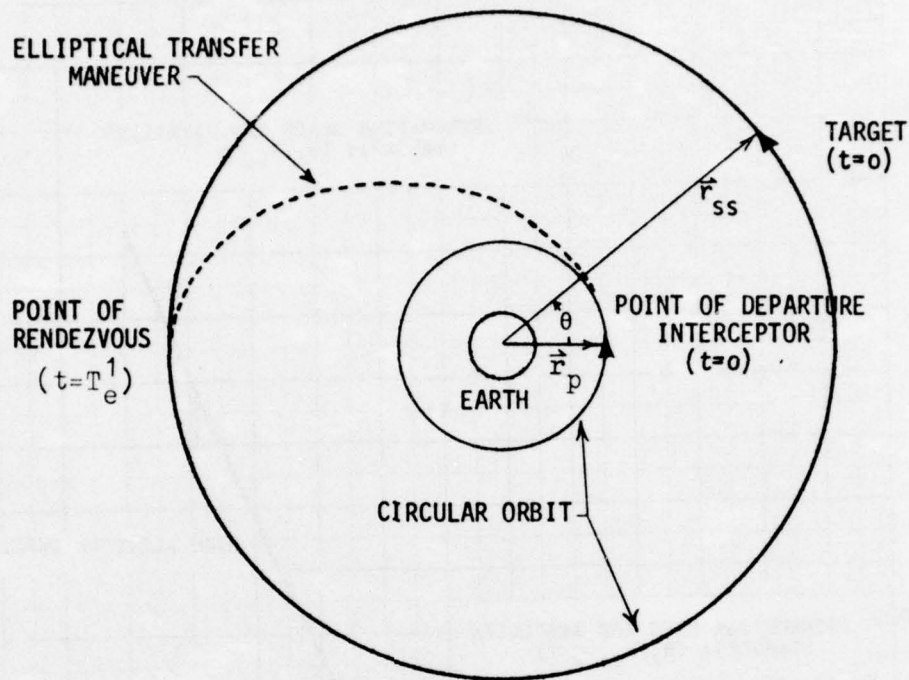
Figure 3-1 – Geometry of the Relative Positions of the Target and an Interceptor (Initially Above the Target) at Initiation of the External Maneuver

3.1.2. Interceptor Below Target. The interceptor is initially on a circular parking orbit with a radius r_p less than that of the synchronous equatorial satellite radius r_{ss} , i.e., the interceptor lags the target by the angle Θ . As before, the "time" to execute the maneuver is given by this angle. Employing the same notations, the lag angle is defined in the following manner. Referring to Figure 3-2, the following relationship is formed:

$$\left\{ \frac{\pi - \Theta}{T_e^1} \right\} = \left\{ \frac{2\pi}{T_{ss}} \right\} \quad (5)$$

where T_e^1 represents the time the target uniformly orbits a $(\pi - \Theta)$ angular displacement.

INTERCEPTOR LAGS THE TARGET



$$\theta = \pi \left\{ 1 - \left[\frac{1}{2} \left(1 + \frac{r_p}{r_{ss}} \right) \right]^{3/2} \right\} \quad \text{FOR } r_p/r_{ss} \leq 1$$

Figure 3-2 — Geometry of the Relative Positions of the Target and an Interceptor (Initially Below the Target) at Initiation of the Internal Maneuver

From the definitions of T_{ss} and T_e^1 (equations 2, 3), equation (5) may be written in terms of the variables r_p , r_{ss} :

$$\Theta = \pi \left\{ 1 - \left[\frac{1}{2} \left(\frac{r_p}{r_{ss}} + 1 \right) \right]^{3/2} \right\} \quad \text{for } r_p/r_{ss} \leq 1 \quad (6)$$

where the position of the interceptor at its point of departure is equivalent to the perigee of the elliptical transfer maneuver ($r_i = r_p$) and its point of rendezvous equivalent to the radius of the satellite/target's non-coplanar synchronous parking orbit ($r_a = r_{ss}$). The general expression for the angular displacement of an interceptor at a radius r_i is given by;

$$\Theta = \pi \left\{ 1 - \left[\frac{1}{2} \left(\frac{r_i}{r_{ss}} + 1 \right) \right]^{3/2} \right\} \quad (7)$$

where the interceptor may lead ($r_i/r_{ss} \geq 1$) or lag ($r_i/r_{ss} \leq 1$) the synchronous satellite/target. The above function is graphically illustrated in Figure 3-3 for the values of $0 < r_i/r_{ss} \leq 3.0$.

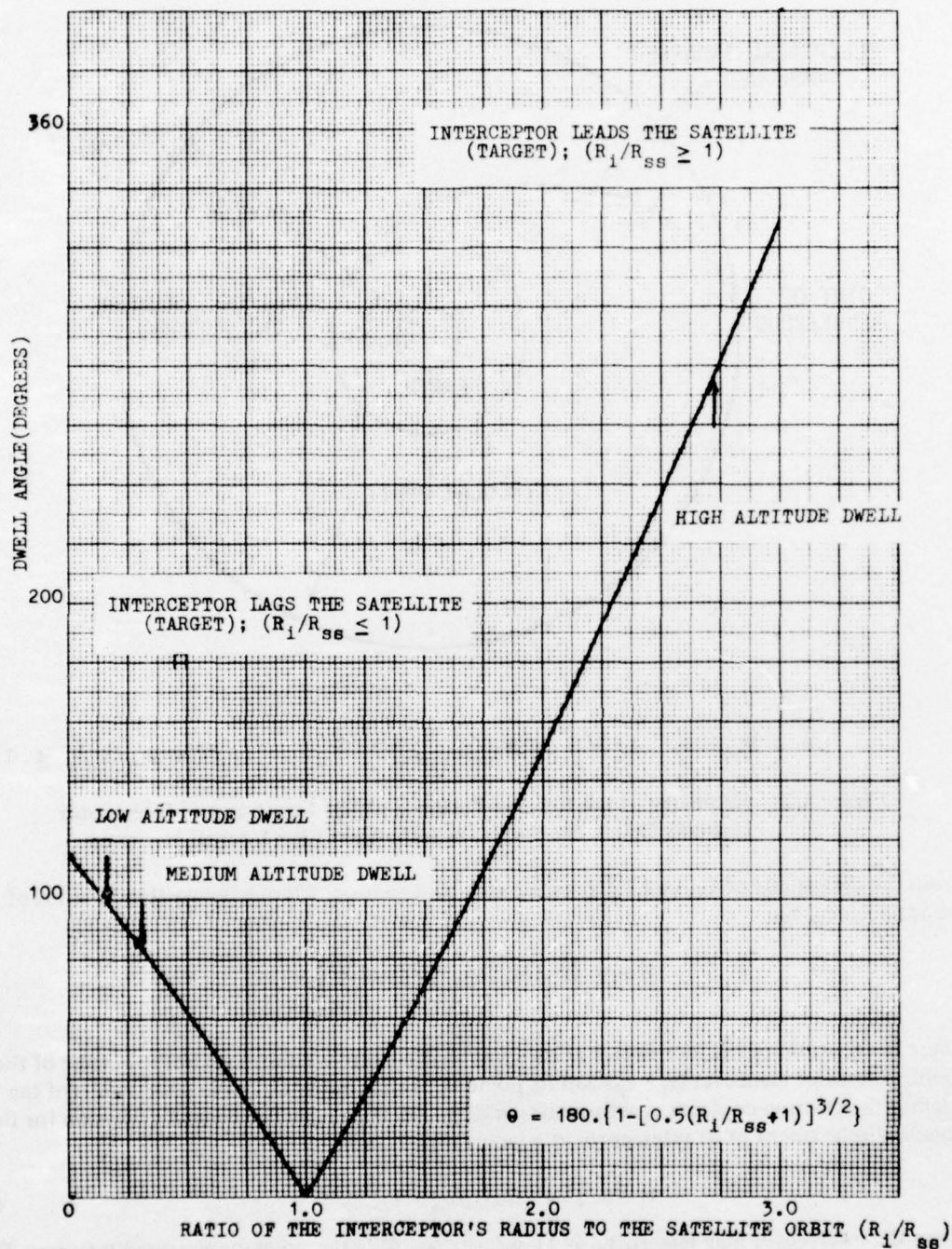


Figure 3-3 - Dwell Angle vs. Ratio of the Interceptor's Radius to the Satellite Orbit

3.2. DWELL ANGLE

The time at which a transfer maneuver is to be initiated to accomplish a desired operational mission can be defined in terms of the angular separation of the relative geocentric positions of the synchronous satellite (target) and the interceptor. This so-called "dwell" angle is defined for the final elliptical transfer maneuver, i.e., the designed point of departure from the interceptor's parking orbit to the point of rendezvous with the target's equatorial parking (synchronous) orbit. These parking orbits may or may not be coplanar. The dwell angles are given by equations (4) and (6) for the High-Altitude-Dwell Scenario and the Low-and Medium-Altitude-Dwell Scenarios, respectively. A numerical evaluation of these equations is presented. For these specified scenarios, the subsatellite position is located at 0° latitude and 80° longitude at the initialization of the interceptor's final point of departure.

3.2.1. High-Altitude-Dwell. This particular maneuver defines the final elliptical transfer stage of the bielliptic transfer scenario. These transfer Hohmann ellipses (intermediate and final) are unique to the High-Altitude-Dwell Scenario and are illustrated in Figure 3-8. Thus, the dwell angle, given by equation (4), will define the relative geocentric angular separation of the interceptor's point of departure (from its final circular parking orbit) and the synchronous satellite orbital position. At the point of rendezvous ($t = T_c^1$), the satellite and interceptor's total angular displacements are $(\pi + \Theta)$ and π , respectively. Rewriting equation (4), the dwell angle for the interceptor's final elliptical transfer maneuver becomes;

$$\Theta = \pi \left\{ \left[1/2(r_{af}/r_{ss} + 1) \right]^{3/2} - 1 \right\} \quad (7)$$

where r_{af} is the interceptor's radius at the apogee of the final elliptical orbit and is equivalent to the radius of the interceptor's final parking orbit, r_{cf} . From Table 5-1, the nondimensionalized ratio:

$$\begin{aligned} r_{af}/r_{ss} = r_{cf}/r_{pf} &= \frac{(3*19310.54113/6080.28 + 20925640.)}{13833730.1} \\ &= 2.697461494 > 1 \end{aligned}$$

resulting in the following value for the dwell angle,

$$\Theta = 272.469278 \text{ deg.}$$

The functional dependency of the dwell angle on the non-dimensionalized ratio of the interceptor's radius at the point of departure to the radius of the satellite's synchronous parking orbit is illustrated in Figure 3-3. In the interest of mathematical expediency, the interceptor's final point of departure for all scenarios occurred at the intersection of the orbital planes (i.e., at the ascending node). Thus, the angular separation (dwell angle) was easily translated into a longitudinal displacement. The above numerical value for Θ , may be expressed as $7.^\circ 5370722$ W longitude (interceptor's point of departure).

3.2.2. Low/Medium-Altitude-Dwell. In the Low and Medium-Altitude-Dwell, the interceptor's elliptical transfer maneuver is executed from a circular parking orbit of altitude 100 NM and 3000 NM, respectively. In both scenarios, the interceptor (which is below the target) lags the target, i.e., the interceptor's and target's total angular displacements are π and $(\pi - \theta)$, respectively (see Figure 3-2). Since equation (6) is applicable for these specific scenarios, the numerical value of θ follows. For the Low-Altitude-Dwell scenario, Table 5-1 provides the values of

$$r_i/r_{ss} \equiv r_c/r_{ss} = r_p/r_a = \frac{2.1533640 \cdot 10^7 \text{ ft}}{13.83337301 \cdot 10^7 \text{ ft}} = 0.1556644$$

and, for the Medium-Altitude-Dwell scenario,

$$r_i/r_{ss} \equiv r_c/r_{ss} = \frac{3.9165640 \text{ ft}}{13.83337301 \text{ ft}} = 0.2881243 < 1$$

In the evaluation of equation (6) for these two cases;

$$\theta = \pi \left\{ 1 - \left[\frac{1}{2} (r_i/r_{ss} + 1) \right]^{3/2} \right\} \quad (8)$$

$\theta = 100.936656$ deg. for the Low-Altitude-Dwell and $\theta = 87.502370$ deg. for the Medium-Altitude-Dwell. With the satellite located at its previously defined longitudinal position (80.0° E), the angular displacement of the interceptor at its point of departure is given by 20.936656 W longitude and 7.502370 W longitude for the Low- and Medium-Altitude dwell scenarios, respectively.

3.3. FLIGHT TIME

With the definition of the target's period in a circular orbit about a spherical earth, the interceptor's flight time during the elliptical transfer (Hohmann) maneuver may be rewritten as:

$$T_e^1 = \frac{\pi}{\mu^{1/2}} r_{ss}^{3/2} \left[\frac{1}{2} (r_i/r_{ss} + 1) \right]^{3/2} \quad (9)$$

regardless of whether or not the interceptor leads or lags the target. Figure 3-4 is a plot of T_e^1 as a function of the parameter r_i/r_{ss} , with equation (9) applicable in this case for the entire range of r_i/r_{ss} .

Another factor of interest is the period of the elliptical orbits being considered. The Keplerian equation for the period of an interceptor in an elliptical orbit is given by:

$$T_e = \frac{2\pi}{\mu^{1/2}} a^{3/2} \quad (10)$$

where the semi-major axis: $a \equiv (r_a + r_p)/2$

$$\therefore T_e = \frac{2\pi}{\mu^{1/2}} [(r_p + r_a)/2]^{3/2} \quad (11)$$

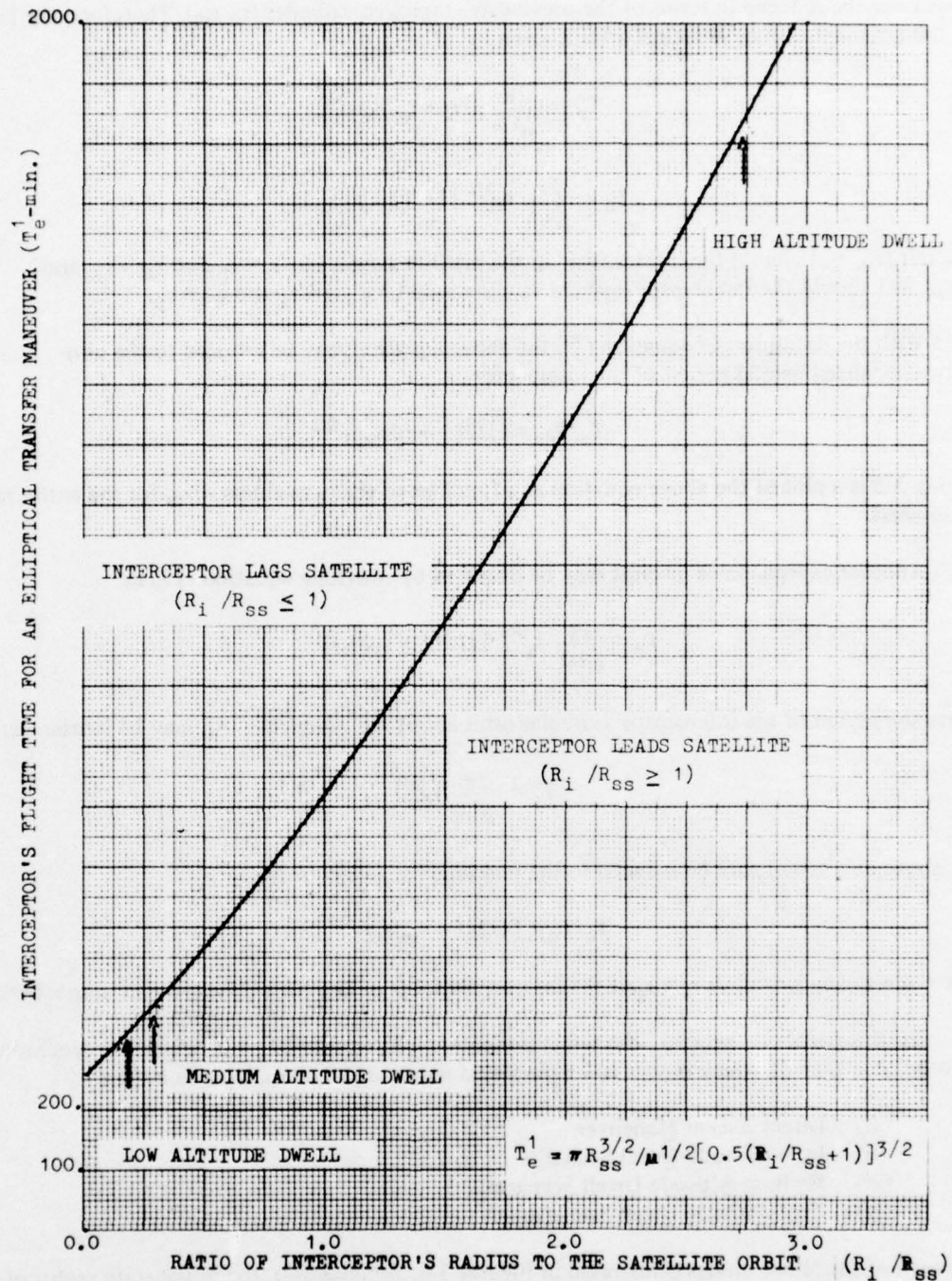


Figure 3-4 – Interceptor's Flight Time for an Elliptical Transfer Maneuver vs. Ratio of the Interceptor's Radius to the Satellite Orbit

which may be reduced in terms of the previously employed variables (r_i , r_{ss}). Therefore, the period of the interceptor in an elliptical orbit is given by:

$$T_e = \frac{2\pi}{\mu^{1/2}} [(r_i + r_{ss})/2]^{3/2} \quad (12)$$

$$T_e = \frac{2\pi}{\mu^{1/2}} r_{ss}^{3/2} [1/2(1 + r_i/r_{ss})]^{3/2} \quad (13)$$

where $r_i/r_{ss} \leq 1$ should the interceptor lag the satellite target, i.e., $r_i = r_p$ and $r_{ss} = r_a$, and $r_i/r_{ss} \geq 1$ should the interceptor lead the satellite target, i.e., $r_i = r_a$ and $r_{ss} = r_p$.

With the definition of equation (2), the above equation may be reduced to the non-dimensionalized orbital period of the interceptor:

$$T_e/T_{ss} = [1/2(1 + r_i/r_{ss})]^{3/2} \quad (14)$$

Figure 3-5 is a plot of the above equation as a function of the parameters r_i/r_{ss} for the entire range of interest.

Another expression of interest may be obtained by rewriting equation (12) as:

$$T_e = \frac{2\pi}{\mu^{1/2}} r_i^{3/2} [1/2(1 + r_{ss}/r_i)]^{3/2} \quad (15)$$

Since the period of the interceptor's circular orbit about the spherical earth may be written as:

$$T_c = \frac{2\pi}{\mu^{1/2}} r_c^{3/2} \quad (16)$$

the above expression may be reduced to the nondimensionalized form:

$$T_e/T_c = [1/2(1 + r_{ss}/r_i)]^{3/2} \quad (17)$$

where $r_i = r_c$ and $r_c = r_a$ or $r_c = r_p$ if the interceptor leads or lags the satellite/target, respectively.

For this particular exercise, the target is located in an equatorial parking orbit at synchronous altitude. The type of attack modes to be simulated required the interceptor to initiate a:

- (i) Direct Ascent Maneuver
- (ii) Low-Altitude-Dwell Scenario
- (iii) Medium-Altitude-Dwell Scenario
- (iv) High-Altitude-Dwell Scenario

For each of the above modes (illustrated in Figures 3-6, 3-7, and 3-8), the initial state vector of the interceptor and target required the values of the dwell angle Θ and the interceptor's flight time.

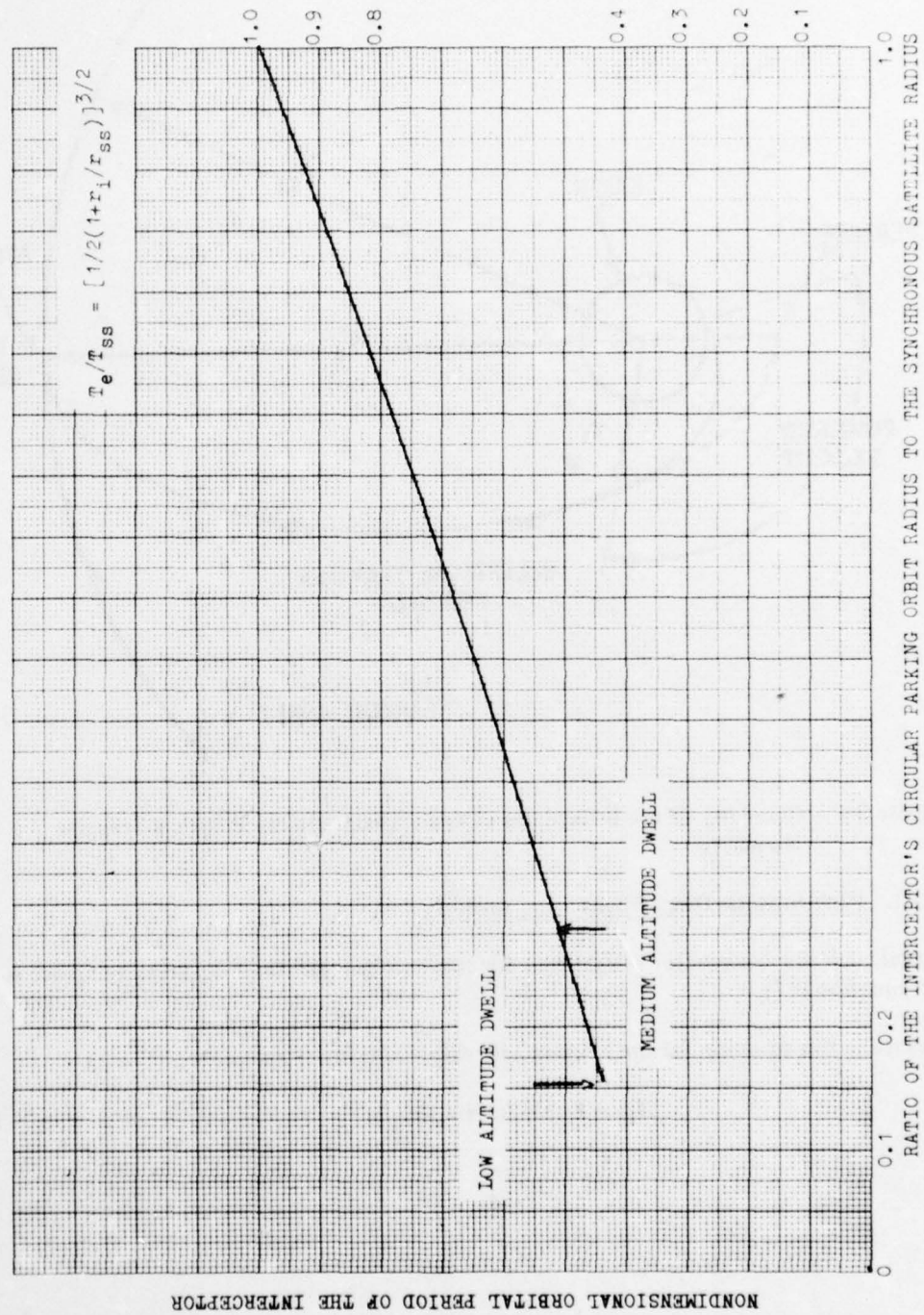


Figure 3-5 — Nondimensional Orbital Period of the Interceptor vs. the Ratio of the Interceptor's Circular Parking Orbit Radius to the Synchronous Satellite Radius

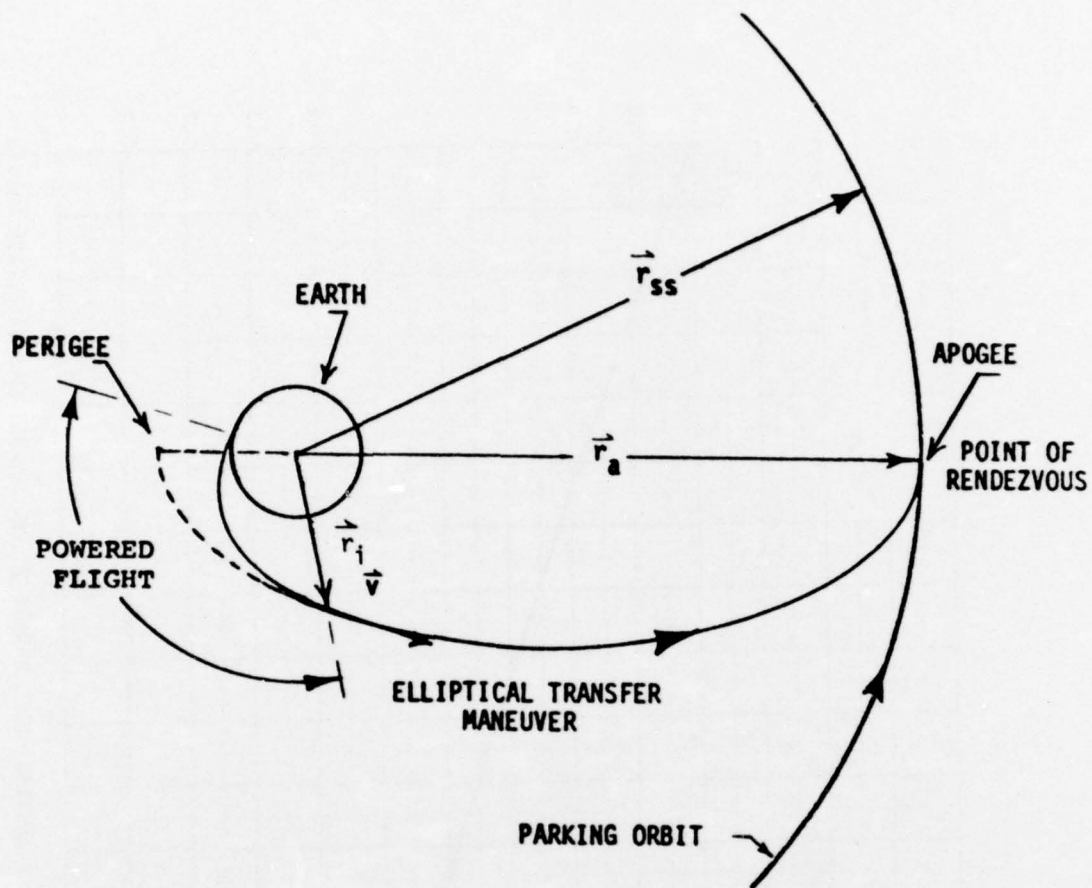


Figure 3-6 – Geometry of the Interceptor's Direct Ascent into an Elliptical Transfer Maneuver

3.3.1. High-Altitude-Dwell Flight Time Analysis

To calculate the interceptor's flight time for the elliptical transfer maneuvers, reference is made to equation (17).

Rewriting this equation for the intermediate elliptical transfer maneuver;

$$T_{ei} = T_{ci} [1/2(1 + r_{ai}/r_{ci})]^{3/2} \quad (18)$$

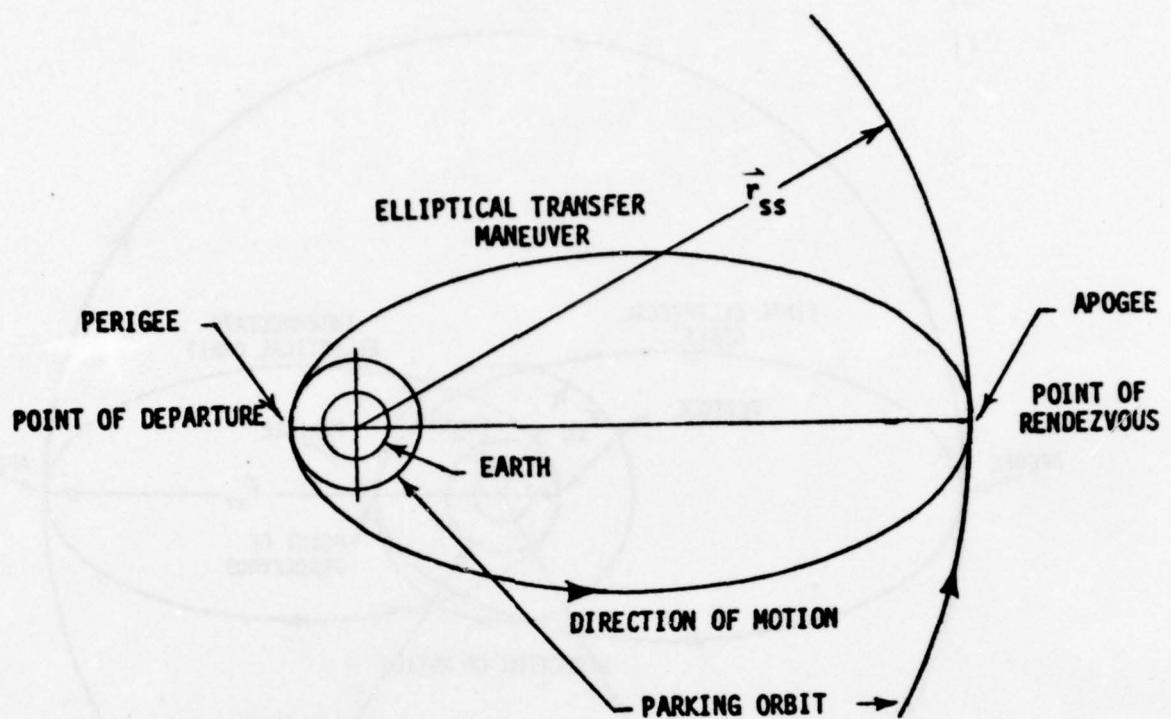


Figure 3-7 – Geometry of the Interceptor's Transfer Maneuver to the Higher Altitude Synchronous Satellite Orbit

where;

T_{ei} = period of the Hohmann ellipse

T_{ci} = period of the initial circular parking orbit

and

$(r_{ai}/r_{ci}) \equiv (r_{ai}/r_{pi})$ = nondimensionalized ratio of apogee/perigee parameter

To calculate the value of the period for the initial circular parking orbit, with an altitude of 100 NM, reference is made to equation (10). Its numerical value is:

$$T_{ci} = \frac{2\pi}{\mu^{1/2}} r_{ci}^{3/2} = 88.19808282 \text{ min.} \quad (19)$$

where;

$$r_{ci} = 2.1533640 \times 10^7 \text{ Ft}$$

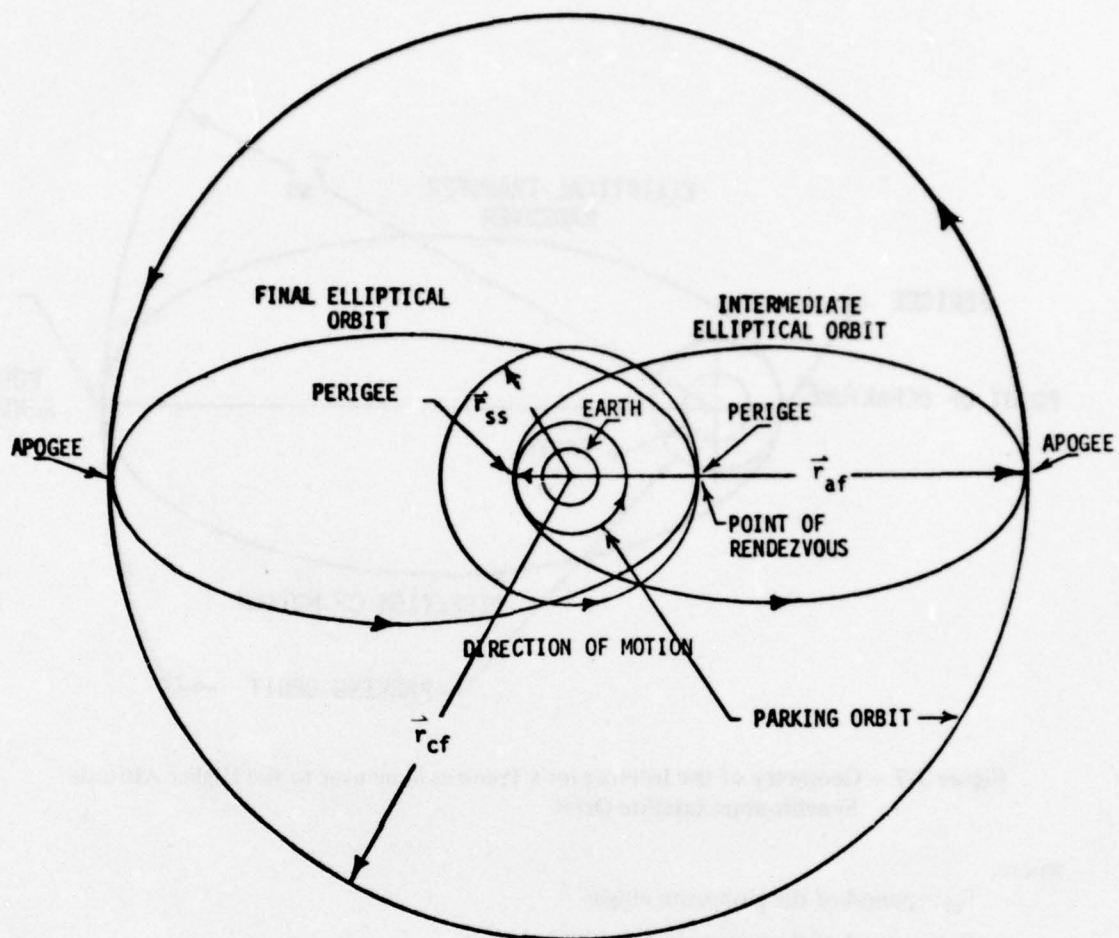


Figure 3-8 – Geometry of the Interceptor's Transfer Maneuvers from a Low-Altitude-Dwell to a High-Altitude-Dwell Parking Orbit to a Final Synchronous Altitude Orbit

Since the apogee radius r_{ai} is to be equivalent to three times the altitude of the synchronous orbit, its numerical value is determined by

$$r_{ai} = 3 * 19310.54113 / 6080.28 + 20925640.) = 37.31499103 * 10^7 \text{ Ft.}$$

and

$$r_{ai}/r_{ci} = 17.32869624$$

resulting in

$$T_{ei} = 88.19808282 (27.74293305) \text{ min.}$$

or

$$T_{ei} = 2446.873507 \text{ min.}$$

= period of the intermediate ellipse

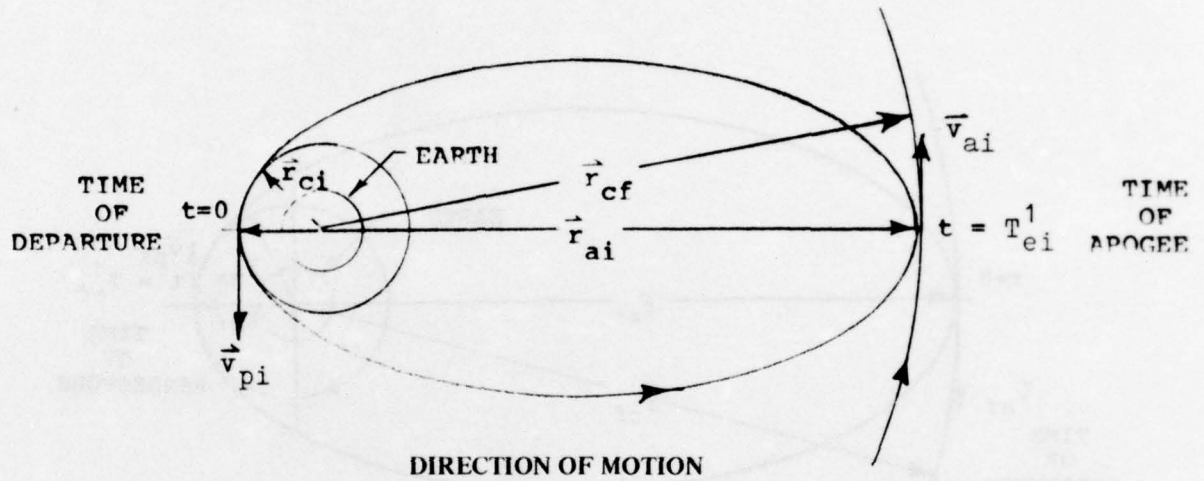
and

$$T_{ei}^1 = T_{ei}/2 = 1223.436754 \text{ min.}$$

= flight time of the intermediate elliptical transfer maneuver
(perigee - to - apogee).

(20)

The elliptical transfer maneuver pattern is illustrated in the following diagram.



The interceptor's second (or final) elliptical transfer maneuver flight time can be determined from equation (11), i.e.

$$T_e = 2\pi/\mu^{1/2} [(r_p + r_a)/2]^{3/2} \quad (11)$$

which reduces to (for the specific maneuver)

$$T_f = T_{ss} [1/2(1 + r_{af}/r_{ss})]^{3/2} \quad (21)$$

where

T_f = period of the Hohmann ellipse

T_{ss} = period of the synchronous satellite orbit

and

$(r_{af}/r_{ss}) = (r_{af}/r_{pf})$ = nondimensionalized ratio of apogee/perigee parameters

The numerical value of the perigee, equivalent to the synchronous orbit radius, was an additional constraint imposed. Since $r_{ai} = r_{cf} = r_{af}$ and solving equation (2) for r_{ss} , the previously defined nondimensionalized ratio takes on a value of

$$\begin{aligned} r_{af}/r_{ss} &= \frac{37.31499103 * 10^7 \text{ Ft}}{13.83337301 * 10^7 \text{ Ft}} \\ &= 2.697461494 \end{aligned} \quad (22)$$

resulting in

$$T_{ef} = (24 \cdot 60) (2.513682932) \text{ min.}$$

$$T_{ef} = 3619.703422 \text{ min.}$$

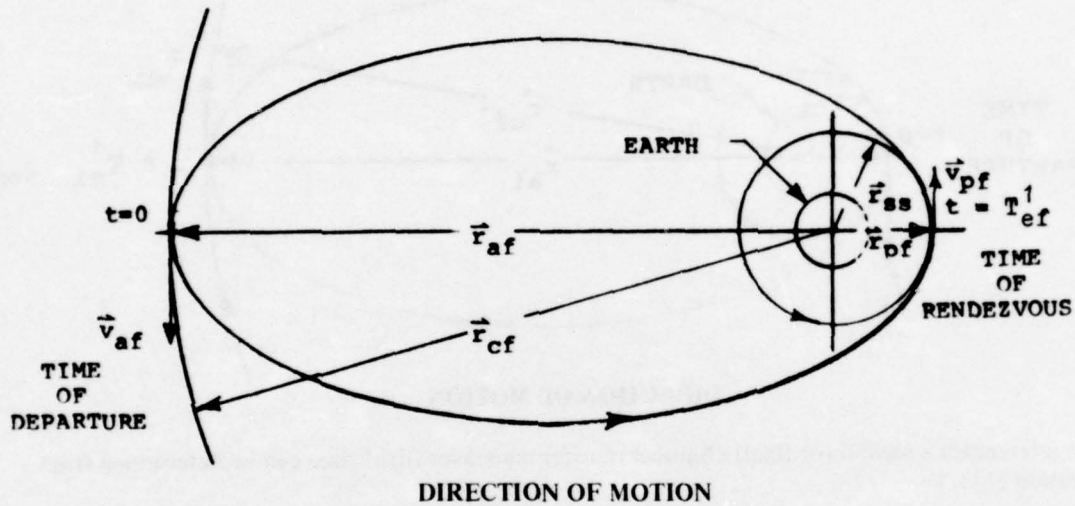
= period of the final elliptical orbit

and

$$T_{ef}^1 = T_{ef}/2 = 1809.851711 \text{ min.} \quad (23)$$

= flight time of the final elliptical transfer maneuver (apogee-to-perigee)

The interceptor's final elliptical flight maneuver is illustrated in the following diagram.



3.3.2. Low/Medium-Altitude-Dwell Flight Time Analysis

Having previously defined the flight sequence associated with the Low-Altitude and Medium Altitude scenarios, the interceptor's time of flight in its elliptical transfer maneuver can be numerically evaluated by equation (13). This equation is given by:

$$T_e = \frac{2\pi}{\mu^{1/2}} r_{ss}^{3/2} [1/2(r_i/r_{ss} + 1)]^{3/2} \quad (13)$$

where

T_e = period of the ellipse

$$T_c = \frac{2\pi}{\mu^{1/2}} r_c^{3/2} \quad (24)$$

T_c = period of the interceptor's parking orbit

and

$$T_{ss} = 2\pi r_{ss}^{3/2} / \mu^{1/2} \quad (25)$$

T_{ss} = period of the synchronous satellite's
equatorial parking orbit

For the Low-Altitude-Dwell scenario

$$\begin{aligned} r_i/r_{ss} &= 2.1533640 * 10^7 \text{ Ft} / 13.83337301 * 10^7 \text{ Ft} \\ &= 0.155664421 \end{aligned}$$

and

$$T_c = 88.19808282 \text{ min. parking orbit}$$

and

$$T_{ss} = (24. * 60.) \text{ min.}$$

$$T_{ss} = 1440.0 \text{ min. parking orbit}$$

The numerical value for the period of the ellipse is given by

$$T_e = 1440.0 [1/2 (1.155664421)]^{3/2} \text{ min.}$$

$$T_e = 632.5066752 \text{ min.}$$

The flight time of the interceptor from its point of departure ($t = 0$) to its point of rendezvous ($t = T_e^1$) is given by

$$T_e^1 = T_e/2 = 316.2533376 \text{ min.} \quad (26)$$

as verified by Figure 3-4.

For the Medium-Altitude-Dwell scenario

$$r_i/r_{ss} = \frac{3.9165640 * 10^7 \text{ Ft}}{13.83337301 * 10^7 \text{ Ft}} = 0.283124296$$

with the period of the interceptor's parking orbit given by

$$T_c = 216.341987 \text{ min.}$$

and the period for the elliptical transfer orbit by

$$T_e = 1440.0 [1/2 (1.283124296)]^{3/2} \text{ min.}$$

$$T_e = 739.9810384 \text{ min.}$$

Thus the interceptor's flight time (from perigee to apogee) is given by

$$T_e^1 = T_e/2 = 369.99052 \text{ min.} \quad (27)$$

Since the satellite exhibits a uniform angular motion ($d\Theta/dt$) equivalent to the earth's rotational velocity (ω_e), for an angular displacement of $(\pi - \Theta)$, the corresponding flight time T_e^1 , can be simply calculated by letting

$$T_e^1 = \frac{(\pi - \Theta)}{d\Theta/dt} = \frac{(\pi - \Theta)}{\omega_e} \quad (28)$$

$$T_e^1 = \frac{(180 - 100.936656) \text{ Deg.}}{360./1440. \text{ Deg/Min}}$$

$$T_e^1 = 316.253376 \text{ Min.}$$

for the Low-Altitude-Dwell and

$$T_e^1 = \frac{(180. - 87.502370) \text{ Deg.}}{360./1440 \text{ Deg/Min}}$$

$$T_e^1 = 369.99052 \text{ Min.}$$

for the Medium-Altitude-Dwell.

For the High-Altitude-Dwell, the satellite's total angular displacement is given by $(\pi + \Theta)$ resulting in a corresponding flight time of;

$$T_e^1 = \frac{(180. + 272.4629278) \text{ Deg.}}{360./1440 \text{ Deg/Min}}$$

$$T_e^1 = 1809.851711 \text{ Min}$$

as verified by equation (23).

NOMENCLATURE

T_c = period of the interceptor's circular parking orbit

T_{ci} = period of the interceptor's initial circular parking orbit

T_{cf} = period of the interceptor's final circular parking orbit

T_{si} = period of the interceptor's synchronous parking orbit

T_{ss} = period of the equatorial synchronous satellite/target parking orbit

T_e^1 = interceptor's maneuver (elliptical transfer) flight time

T_{ei}^1 = interceptor's intermediate maneuver (elliptical transfer) flight time

T_{ef}^1 = interceptor's final maneuver (elliptical transfer) flight time

T_e = period of the interceptor's elliptical orbit

NOMENCLATURE (Continued)

T_{ei} = period of the interceptor's intermediate elliptical orbit

T_{ef} = period of the interceptor final elliptical orbit

\vec{r}_c = radius of the interceptor's circular parking orbit

\vec{r}_{ci} = radius of the interceptor's initial circular parking orbit

\vec{r}_{cf} = radius of the interceptor's final circular parking orbit

\vec{r}_p = radius of the interceptor at the perigee of the elliptical transfer maneuver

\vec{r}_{pi} = radius of the interceptor at the perigee of the intermediate elliptical transfer orbit

\vec{r}_{ai} = radius of the interceptor at the apogee of the intermediate elliptical transfer orbit

\vec{r}_a = radius of the interceptor at the apogee of the elliptical transfer maneuver

\vec{r}_{pf} = radius of the interceptor at the perigee of the final elliptical transfer maneuver

\vec{r}_{af} = radius of the interceptor at the apogee of the final elliptical transfer maneuver

\vec{r}_i = interceptor's position vector

\vec{r}_{ss} = radius of the satellite/target's synchronous parking orbit

\vec{V} = interceptor's velocity vector

μ = earth's gravitational constant =

$$1.407639 * 10^{16} \frac{\text{ft}^3}{\text{sec}^2}$$

ω_e = earth's rotational velocity =

$$0.4375269048 * 10^{-2} \text{ rad/sec}$$

Amold

8/ 3-17

SECTION 4

DIRECT ASCENT ELLIPTICAL TRANSFER MANEUVER TO SYNCHRONOUS ORBIT

1. Methodology

An interceptor is launched from a specified launch site on a ballistic trajectory which intercepts a satellite in a synchronous equatorial orbit. The direct ascent trajectories are defined at the termination of the final-impulse of a multi-stage booster by an initial state vector of the interceptor. By the definition of the interceptor's initial state vector (a six-element column matrix) numerical integration of the differential equations of motion (previously defined) provides the time history of the interceptor's elliptical transfer orbit thus, encompassing the free flight maneuver to the point of rendezvous, as illustrated by Figure 4-1. In addition, the Trajectory Simulation Program outputs (when appropriate) a time-correlated observation data set (topocentric system) for a specified sensor. This data provides an observed set of metric data and their rates. This data is pertinent to the assignment of a figure-of-merit to each of the specified trajectory/sensor scenario.

2. Launch Sites

The previously described can be exercised against a preselected set of sensor locations.

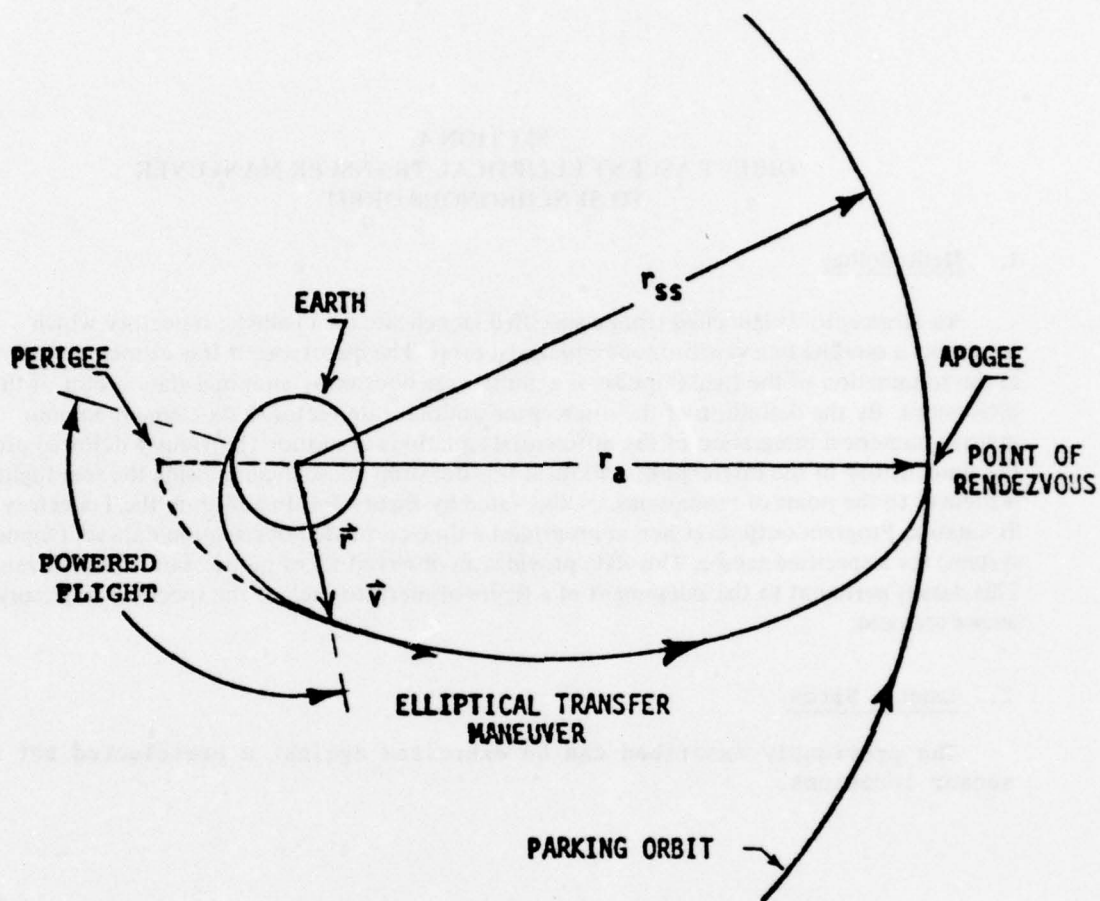


Figure 4-1 – Geometry of the Interceptor's Direct Ascent Into Elliptical Transfer Maneuver

3. Initial State Vectors

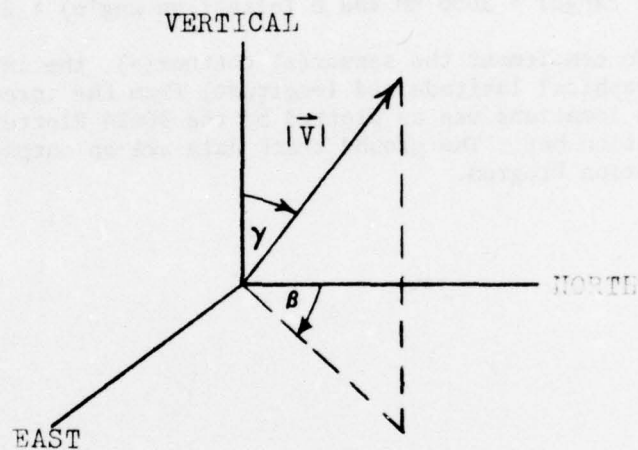
The initial state vector of the interceptor and the satellite target are defined at the termination of the final-impulse (burnout). Mathematically, the state of the interceptor, at time t_i , may be represented by the partitioned matrix.

$$\begin{bmatrix} \vec{r}(t_i) \\ \vec{v}(t_i) \end{bmatrix}$$

The six-element column matrix (previously mentioned) defines the interceptor's position coordinates (latitude; ϕ , longitude; λ , altitude; H) and velocity coordinates with their numerical values (for each of the three launch sites) specified in Tables 4-1 and 4-2. For each launch site, the components of the interceptor's velocity vector (\vec{V} , γ , β) are defined within the frame of reference, illustrated in Figure 4-3. Since the timing must be precise, the initial state vector of the interceptor must initiate a collision-type course when the satellite target (designated -S1) is at a prescribed position. The initial state vector of S1 is implicit in the definition of a synchronous equatorial satellite at a specific longitude, i.e.,

$$\gamma = \beta = \pi/2; |\vec{V}| = (R_E + H) \omega_E = 10087.4548 \text{ FT/S}$$

$$H = 19,310.54 \text{ NM}; \theta = 0.0^\circ; \lambda = 80.0^\circ \text{E}$$



REENTRY ANGLE γ
 HEADING ANGLE β
 VELOCITY MAGNITUDE $|\vec{V}|$

Figure 4-2 - Interceptor's Intrinsic Coordinate System

4. Sensor Location/Ground Track

The direct ascent scenario can be exercised against a set of sensor locations preselected within some geographical latitude perimeter. The geographical locations of these sensors and their physical locations can be illustrated by visibility contours plotted upon a Mercator Projection Map. These contours were generated by programming the mathematical equations on the RADC/HP 9820A Calculator and plotting their solutions (by an appropriate coordinate transformation) with the RADC/HP9862A Plotter. A description of these equations and the procedure employed are described in Reference 5. It must be emphasized that these contours are restricted, but by no means limited, to a specific set of parameters, such as R_s (slant range) = 2000 NM and E (elevation angle) = 2.0 degrees.

To complement the sensor(s) contour(s), the interceptor's earth trace (geographical latitude and longitude) from the three (previously discussed) launch locations can be plotted by the 9862A Plotter on the Mercator Projection Map. The ground track data are an output of the Trajectory Simulation Program.

SECTION 5 LOW/MEDIUM-ALTITUDE-DWELL ELLIPTIC TRANSFER MANEUVER TO SYNCHRONOUS ORBIT

1. Methodology

The basic dynamical equations describing the flight sequence of the interceptor launched from a near earth circular parking orbit dwell into a Hohmann transfer ellipse for rendezvous with the synchronous orbit satellite target can be defined by the following equations.

i. On the interceptor's inertial velocity in a circular parking orbit of radius \vec{r}_c , its speed can be given by

$$|\vec{V}_c| = \sqrt{\mu / |\vec{r}_c|} \quad (1)$$

where

$$|\vec{V}_c| = 25,567.4209 \text{ Ft/s}$$

for

$$|\vec{r}_c| = 2.1533640 * 10^7 \text{ Ft (100 NM altitude)}$$

and

$$|\vec{V}_c| = 18,958.02238 \text{ Ft/s}$$

for

$$|\vec{r}_c| = 3.9165640 * 10^7 \text{ Ft (3000 NM Altitude)}$$

with $|\vec{r}_c| < |\vec{r}_{ss}|$; i.e., \vec{r}_{ss} is equal to the radius of the synchronous satellite orbit.

ii. The point of departure of the interceptor from this dwell orbit is accomplished by an impulse velocity $\Delta \vec{V}_1$ initiating a Hohmann elliptical transfer maneuver (refer to Figure 5-2). From the inverse-square law equation (unit mass)

$$\vec{F} = -\mu \hat{r} / |\vec{r}|^3 = -\mu \vec{r} / |\vec{r}|^2 \quad (2)$$

where $\vec{a} \equiv \vec{V} d \vec{V} / d \vec{r}$

The energy integral becomes:

$$\int_{V_a}^{V_p} \vec{V} d \vec{V} = -\mu \int_{r_a}^{r_p} d\vec{r} / |\vec{r}|^2 \quad (3)$$

resulting in

$$|\vec{V}_p|^2 = |\vec{V}_a|^2 + 2\mu \{1/|\vec{r}_p| - 1/|\vec{r}_a|\}$$

where \vec{V}_p, \vec{V}_a = interceptor's velocity at perigee (\vec{r}_p) and apogee (\vec{r}_a) respectively. Since the impulse initiates a point of departure at $\vec{r}_p = \vec{r}_c$ and a point of rendezvous at $\vec{r}_a = \vec{r}_{ss}$, where $\vec{r}_c < \vec{r}_{ss}$

$$|\vec{V}_p|^2 = |\vec{V}_a|^2 + 2\mu \{1/|\vec{r}_c| - 1/|\vec{r}_{ss}|\} \quad (4)$$

or with equation (1), the above reduces to the form

$$|\vec{V}_p|^2 = |\vec{V}_a|^2 + 2 |\vec{V}_c|^2 \{1 - |\vec{r}_c| / |\vec{r}_{ss}|\} \quad (5)$$

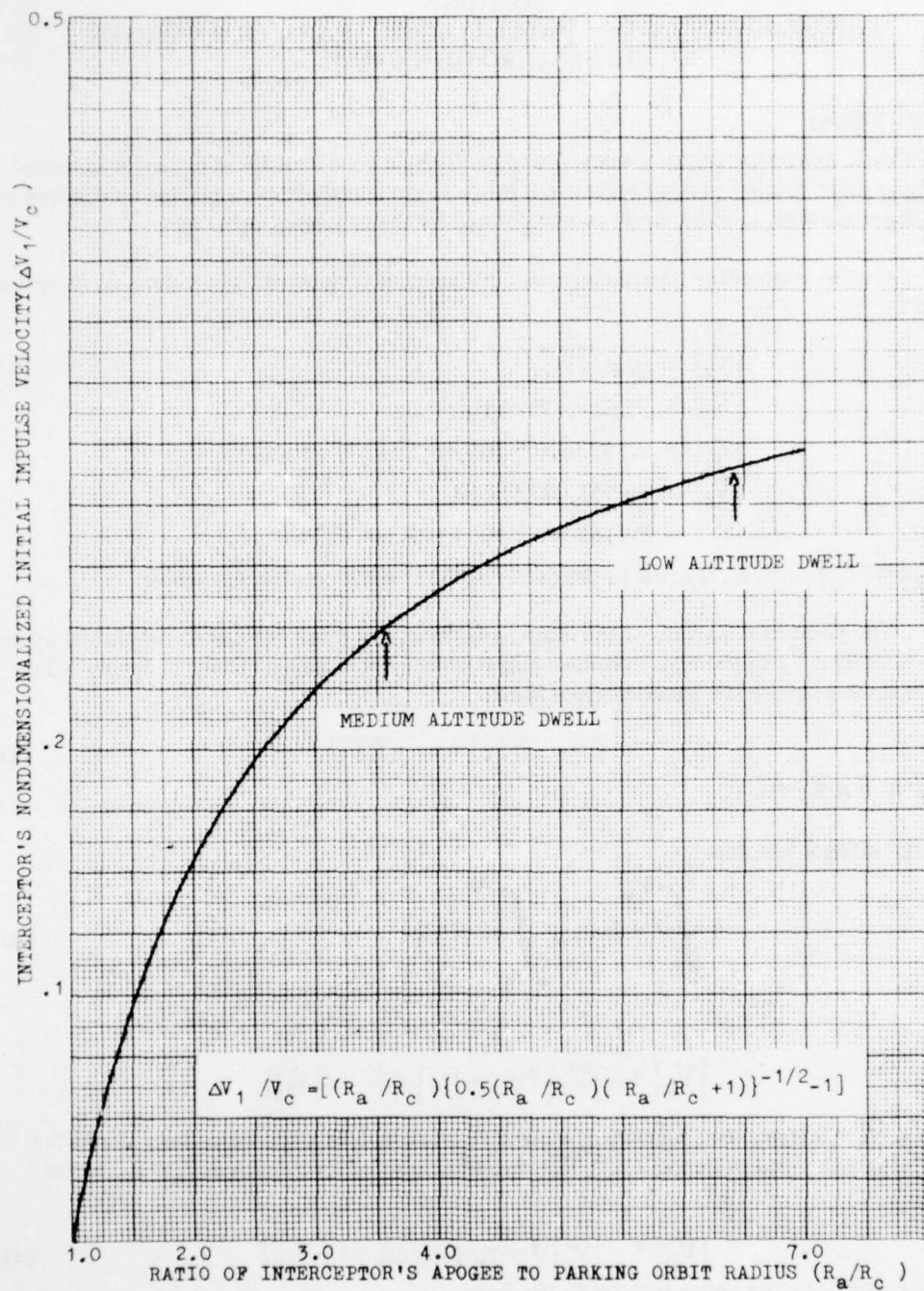


Figure 5-1 – Ratio of Interceptor's Apogee to Parking Orbit Radius (R_a/R_c)

Since $\vec{V}_p > \vec{V}_c$ an impulsive velocity is to be added at \vec{r}_p to initiate the transfer. This quantity can be determined by the following method. From the law of the conservation of angular momentum

$$\vec{r} \times \vec{V} = \text{constant} \quad (6)$$

applied at \vec{r}_p and \vec{r}_a (scalar form)

$$|\vec{r}_a| |\vec{V}_a| = |\vec{r}_p| |\vec{V}_p| \Rightarrow |\vec{V}_a| = \left\{ |\vec{r}_p| / |\vec{r}_a| \right\} |\vec{V}_p| \quad (7)$$

Equation (5) reduces to:

$$|\vec{V}_p|^2 = \left\{ |\vec{r}_p| / |\vec{r}_a| \right\}^2 |\vec{V}_p|^2 + 2 |\vec{V}_c|^2 \left\{ 1 - |\vec{r}_c| / |\vec{r}_{ss}| \right\} \quad (8)$$

where

$$\left\{ |\vec{V}_p| / |\vec{V}_c| \right\} = \left\{ 1/2(1 + |\vec{r}_c| / |\vec{r}_a|) \right\}^{-1/2} \quad (9)$$

and

$$\vec{r}_a \equiv \vec{r}_{ss}$$

Since the impulse velocity increment required to initiate this specific transfer maneuver is given by;

$$|\Delta \vec{V}_1| = |\vec{V}_p| - |\vec{V}_c| = \left\{ (|\vec{V}_p| / |\vec{V}_c|) - 1 \right\} |\vec{V}_c|$$

and substituting equation (9) for the value of $(|\vec{V}_p| / |\vec{V}_c|)$ results in

$$|\Delta \vec{V}_1| = |\vec{V}_c| \left[\left(|\vec{r}_a| / |\vec{r}_c| \right)^{1/2} \left\{ 1/2 (|\vec{r}_a| / |\vec{r}_c| + 1) \right\}^{-1/2} - 1 \right] \quad (10)$$

or

$$|\Delta \vec{V}_1| = |\vec{V}_c| \left[\left(|\vec{r}_a| / |\vec{r}_c| \right) \left\{ 1/2 (|\vec{r}_a| / |\vec{r}_c|) (|\vec{r}_a| / |\vec{r}_c| + 1) \right\}^{-1/2} - 1 \right]$$

Rewriting equation (10), the nondimensionalized ratio of the interceptor's initial velocity impulse to its initial parking orbit velocity is graphically illustrated (by Figure 5-1) as a function of its apogee (of the elliptical transfer maneuver) to the parking orbit radius. The numerical evaluation of the above equation, required a value of the apogee radius \vec{r}_a to be equivalent to the radius of the synchronous satellite orbit. Hence,

$$|\vec{r}_a| = |\vec{r}_{ss}| = 13.8333730 * 10^7 \text{ Ft}$$

$$\text{and } \left\{ |\vec{r}_a| / |\vec{r}_c| \right\} = \frac{13.8333730 * 10^7 \text{ Ft}}{2.1533640 * 10^7 \text{ Ft}} = 6.4240755$$

for 100 NM parking orbit altitude resulting in

$$|\Delta \vec{V}_1| = 8067.16206 \text{ Ft/s}$$

$$\text{and } |\vec{V}_c| < |\vec{V}_p| = 33634.58296 \text{ Ft/s}$$

for the Low-Altitude-Dwell scenario.

The Medium-Altitude-Dwell scenario, results in

$$\left\{ |\vec{r}_a| / |\vec{r}_c| \right\} = \frac{13.8333730 * 10^7 \text{ Ft}}{3.9165640 * 10^7 \text{ Ft}} = 3.5320176$$

and the incremental velocity numerical value (equation 10) becomes; $|\Delta \vec{V}_1| = 4710.63729 \text{ Ft/s}$ and $|\vec{V}_c| < |\vec{V}_p| = 23,668.65967 \text{ Ft/s}$. The direction of the applied impulse is illustrated in the following Figure 5-2.

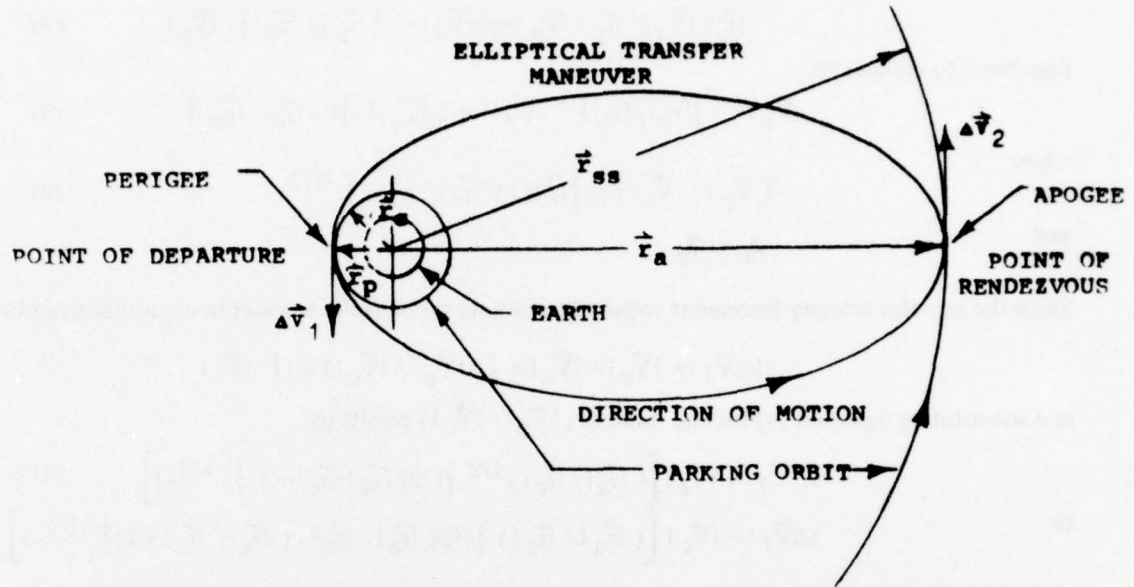


Figure 5-2 – Geometry of the Interceptor's Transfer Maneuver to the Synchronous Satellite Orbit

iii. On the elliptical transfer orbit, the magnitude of the interceptor's free-flight velocity can be obtained from the energy integral, i.e.,

$$|\vec{V}|^2 = |\vec{V}_p|^2 + 2\mu \left\{ 1/|\vec{r}| - 1/|\vec{r}_p| \right\} \quad (11)$$

where

\vec{r} is the interceptor's elliptical position vector.

With the results of equation (9) and letting $\vec{r}_p = \vec{r}_c$; the magnitude of the interceptor's velocity at the apogee position is given by:

$$|\vec{V}_a| = |\vec{V}_c| \left\{ 1/2 \left(|\vec{r}_a|/|\vec{r}_c| \right) \left(|\vec{r}_a|/|\vec{r}_c| + 1 \right) \right\}^{-1/2} \quad (12)$$

Using the previously defined numerical values, the above equation reduces to:

$$|\vec{V}_a| = 5235.70788 \text{ Ft/s}$$

for the Low-Altitude-Dwell scenario (i.e., 100 NM orbit) and for the Medium-Altitude-Dwell;

$$|\vec{V}_a| = 6701.172606 \text{ Ft/s}$$

iv. The impulsive velocity increment to circularize the interceptor at apogee (point of rendezvous, as illustrated in Figure 5-2) is

$$\Delta \vec{V}_2 = \vec{V}_{ss} - \vec{V}_a \quad (13)$$

where the direction of the impulse velocity, determined by

$$|\vec{V}_{ss}| = \sqrt{\mu / |\vec{r}_{ss}|} = 10,087.4548 \text{ Ft/s} \quad (14)$$

required an addition to the interceptor's "deficient" circular speed (i.e., $|\vec{V}_a| < |\vec{V}_{ss}|$.) The magnitude of the impulse velocity can be shown to be functionally dependent upon the ratio of the parking orbits radii. With the scalar form of equation (13) and equation (12),

$$|\Delta \vec{V}_2| = |\vec{V}_{ss}| - |\vec{V}_a| \quad (13.1)$$

and

$$|\Delta \vec{V}_2| = |\vec{V}_{ss}| - |\vec{V}_c| \left\{ \frac{1}{2} \left(\frac{|\vec{r}_a|}{|\vec{r}_c|} \right) \left(\frac{|\vec{r}_a|}{|\vec{r}_c|} + 1 \right) \right\}^{-1/2} \quad (15)$$

Since

$$|\vec{V}_c| = \sqrt{\mu / |\vec{r}_c|} \left(\frac{|\vec{r}_{ss}|}{|\vec{r}_{ss}|} \right)^{1/2} = |\vec{V}_{ss}| \left(\frac{|\vec{r}_{ss}|}{|\vec{r}_c|} \right)^{1/2} \quad (16)$$

and $\vec{r}_{ss} \equiv \vec{r}_a$, equation (15) reduces to

$$|\Delta \vec{V}_2| = |\vec{V}_{ss}| \left\{ 1 - \left[\frac{1}{2} \left(\frac{|\vec{r}_{ss}|}{|\vec{r}_c|} + 1 \right) \right]^{-1/2} \right\} \quad (17)$$

with a numerical value of

$$|\Delta \vec{V}_2| = 4851.74692 \text{ Ft/s}$$

for the Low-Altitude-Dwell scenario, and

$$|\Delta \vec{V}_2| = 3386.28219 \text{ Ft/s}$$

for the Medium-Altitude-Dwell.

Rewriting equation (17) in a nondimensionalized form, i.e.,

$$\left(\frac{|\Delta \vec{V}_2|}{|\vec{V}_{ss}|} \right) = \left\{ 1 - \left[\frac{1}{2} \left(\frac{|\vec{r}_{ss}|}{|\vec{r}_c|} + 1 \right) \right]^{-1/2} \right\} \quad (18)$$

a plot of $\left(\frac{|\Delta \vec{V}_2|}{|\vec{V}_{ss}|} \right)$ vs the ratio of the circular parking orbits radii $\left(\frac{|\vec{r}_{ss}|}{|\vec{r}_c|} > 1 \right)$ is illustrated in Figure 5-3.

In the performance of these specific elliptical transfer maneuvers, the "time" associated with the interceptor/satellite (target) relative positions is calculated in Section 3. A graphical display of the interceptor's velocity and altitude at these specified events for the two scenarios is illustrated in Figure 5-4.

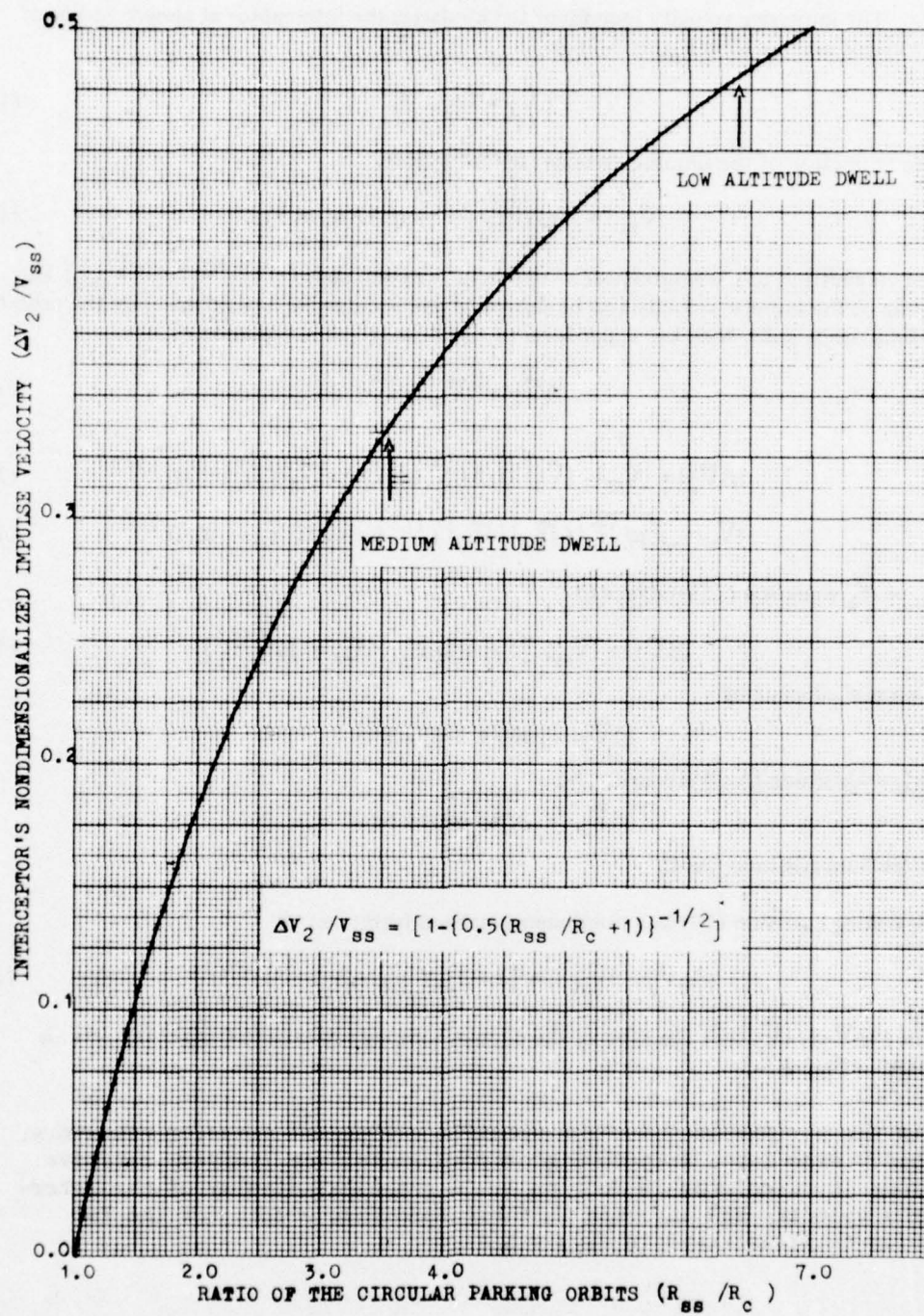


Figure 5-3 – Ratio of the Circular Parking Orbits (R_{ss}/R_c)

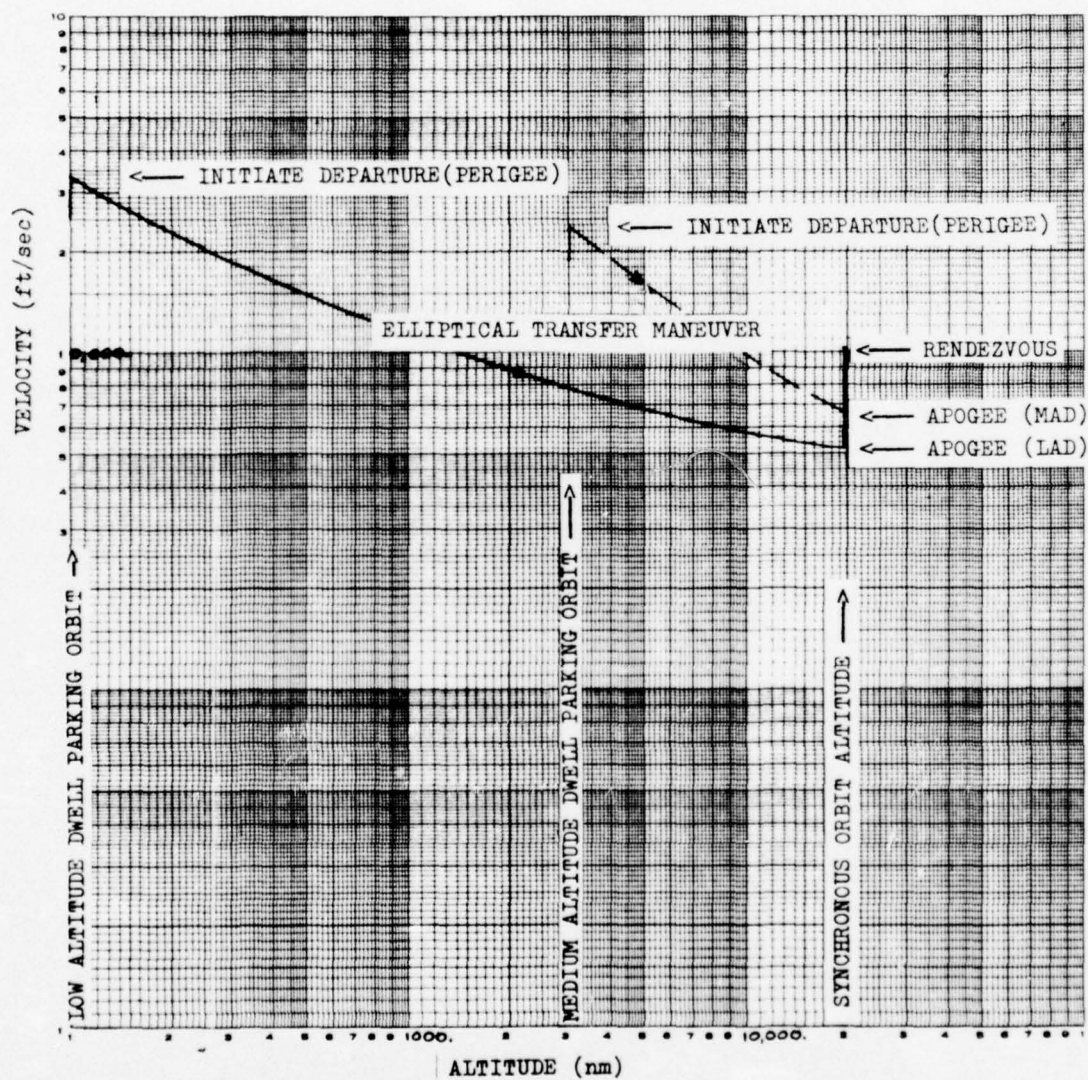


Figure 5-4 — Interceptor's Velocity-Altitude for the Low- and Medium-Altitude-Dwell Scenarios

SECTION 6

HIGH ALTITUDE DWELL - BIELLIPTIC TRANSFER MANEUVER TO SYNCHRONOUS ORBIT*

1. Methodology

The flight sequence of the interceptor illustrated in Figure 6-1, consists of a power flight from a specific launch site to injection into a low-altitude-dwell circular parking orbit of radius $-r_{ci}$ and orbital velocity \vec{V}_{ci} . At a specific launch "time", defined in terms of an angular displacement, an applied impulsive velocity increment, defined below by equation (2), injects the interceptor in an Hohmann transfer ellipse of an apogee radius $-r_{ai}$, illustrated in Figure 6-2. The point of departure of the interceptor from its parking orbit constitutes the perigee radius \vec{r}_{pi} ($= \vec{r}_{ci}$) of the elliptical transfer maneuver of the intermediate (first) orbit. Note that the establishment of an elliptic orbit of a given parameter was by means of an impulsive velocity $-\Delta\vec{V}_1$. As the radius of the interceptor approaches the value of the apogee radius, a successive stage of the interceptor's booster is ignited to provide an impulsive incremental velocity $-\Delta\vec{V}_2$. This impulse circularizes the interceptor orbit at apogee (infinitesimal burning time), with a radius $-r_{cf}$. Since the velocity vector of the interceptor approaching apogee has a "deficient" circular speed, the applied velocity increment provided the corrective maneuver i.e., an acceleration. With this maneuver the interceptor is now in a High-Altitude-Dwell circular parking orbit of radius $-r_{cf}$.

Since "time", at which these transfers are to be initiated, is very crucial, the final elliptical transfer maneuver must be executed at the node opposite the point of rendezvous (perigee), to provide the necessary correlation with the target's flight time and hence its angular displacement with respect to the point of departure. The Hohmann transfer is initiated at the apogee (point of departure) illustrated in Figure 6-4, by the execution of an impulsive velocity increment $-\Delta\vec{V}_3$, in the direction opposite the velocity vector since the interceptor has an "excessive" apogee velocity $-\vec{V}_{af}$.

The equations used for each of the transfer maneuvers illustrated in Figures 6-2, 6-4 are:

- i.) On the near-earth (initial) circular parking orbit of radius $-r_{ci}$, the speed of the velocity vector is given by

$$|\vec{V}_{ci}| = \sqrt{\frac{\mu}{r_{ci}}} = \sqrt{\frac{5.0675004 * 10^{19} \text{ FT}^3/\text{MIN}^2}{2.153364 * 10^7 \text{ FT}}} \quad (1)$$

$$|\vec{V}_{ci}| = 25567.4209 \text{ FT/S}$$

for a parking orbit altitude of 100 NM.

*Bielliptic Transfer: The apogee altitude of the intermediate (first) transfer ellipse is set at an altitude three times the altitude of the 24-hour altitude. The final ellipse is then required to have its perigee at the 24-hour orbit altitude.

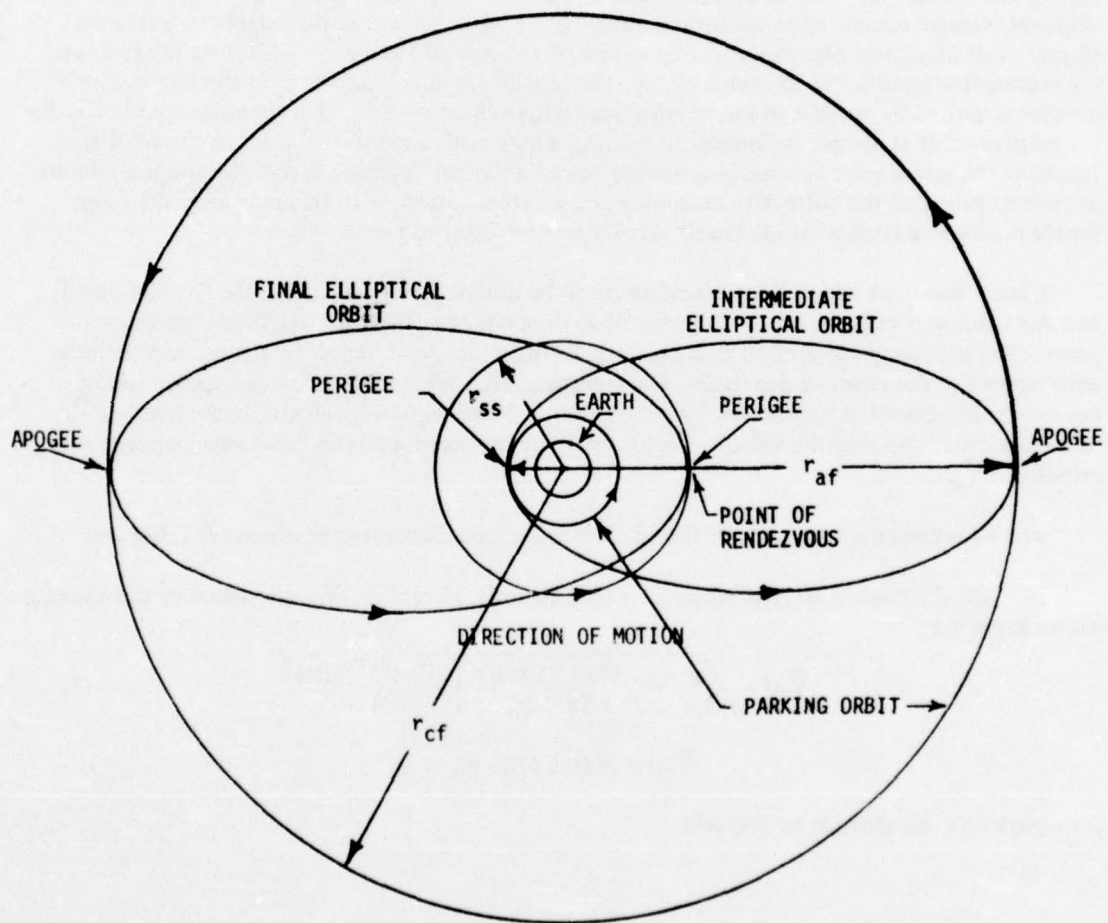


Figure 6-1 – Geometry of the Interceptor's Transfer Maneuvers from a Low-Altitude-Dwell to a High-Altitude-Dwell Parking Orbit to a Final Synchronous Altitude Orbit

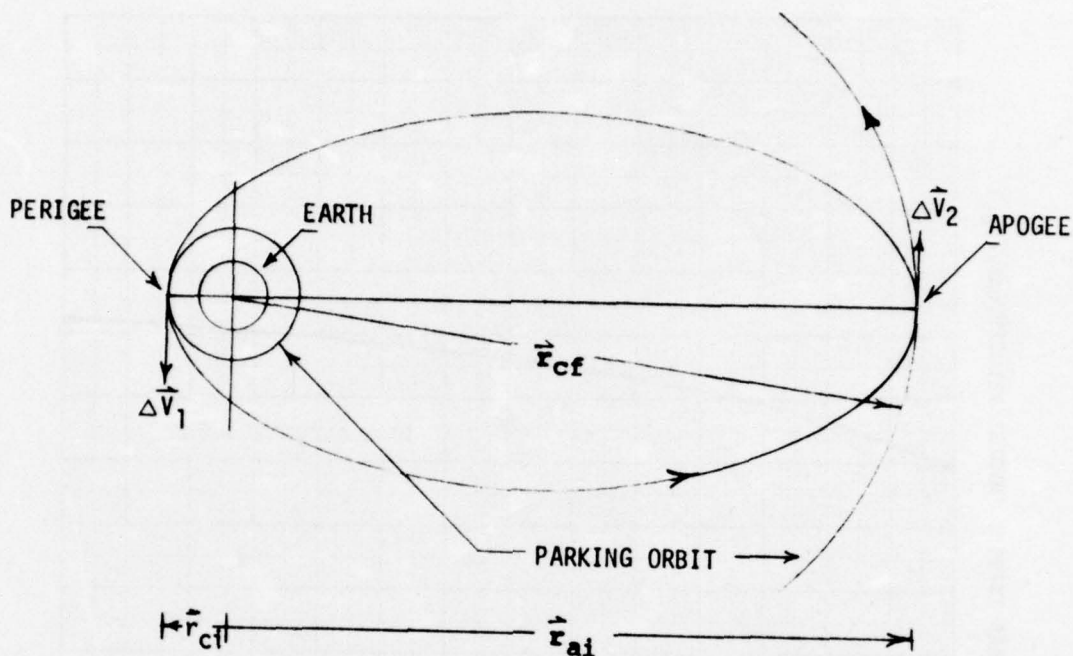


Figure 6-2 – Interceptor's Intermediate Elliptical Transfer Orbit from an Initial-to-Final (Desired) Circular Parking Orbit

ii.) The impulse velocity increment required to initiate the intermediate elliptical orbit is given by;

$$\Delta \vec{V}_1 = \vec{V}_{pi} - \vec{V}_{ci}$$

where

$$|\Delta \vec{V}_1| = |\vec{V}_{ci}| \left[(r_{ai}/r_{ci})^{1/2} \left\{ \frac{1}{2} \left(\frac{r_{ai}}{r_{ci}} + 1 \right) \right\}^{-1/2} - 1 \right] \quad (2)$$

(at the perigee)

For the numerical evaluation of the above equation, an additional constraint required the value of the apogee radius - r_{ai} , to the equivalent to three times the altitude of the equatorial synchronous satellite orbit. Therefore;

$$|r_{ai}| = (3 * 19310.54113/6080.28 + 20925640.) = 373,149,910.3 \text{ FT}$$

and

$$(|r_{ai}|/|r_{ci}|) = 17.32869642 = (r_{cf}/r_{pi}) = (r_{af}/r_{pi})$$

resulting in $|\Delta \vec{V}_1| = 9590.1674 \text{ FT/S}$

The direction of the applied impulse is illustrated in Figure 6-2. Rewriting equation (2) in the form of the nondimensionalized ratio of the interceptor's velocity impulse to its initial parking orbit velocity, the following equation is graphically illustrated in Figure 6-3.

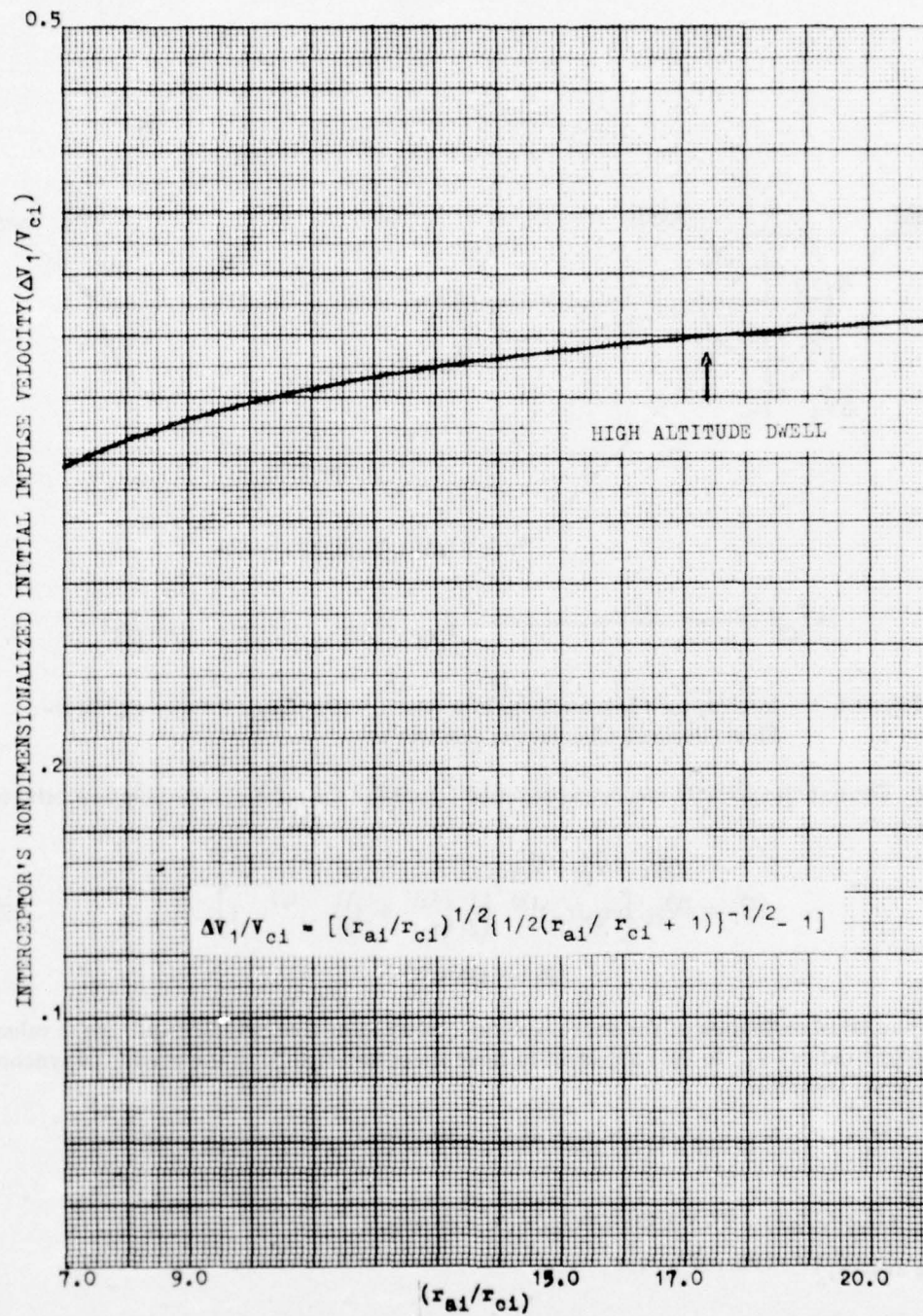


Figure 6-3 – Ratio of Interceptor's Apogee to Initial Parking Orbit Radius

iii.) On the intermediate elliptical transfer orbit, the magnitude of the interceptor's velocity, functionally dependent on the ratio of the apogee to initial circular parking orbit radii, is given by;

$$|\vec{V}_{pi}| = |\vec{V}_{ci}| (r_{ai}/r_{ci})^{1/2} \left\{ \frac{1}{2} \left(\frac{r_{ai}}{r_{ci}} + 1 \right) \right\}^{-1/2} \quad (3)$$

(at the perigee)

And from the conservation of angular momentum, the magnitude of the apogee velocity may be expressed by;

$$|\vec{V}_{ai}| = |\vec{V}_{pi}| (|\vec{r}_{pi}| / |\vec{r}_{ai}|). \quad (4)$$

Substitution of equation (3) for $|\vec{V}_{pi}|$ reduces the above expression to

$$|\vec{V}_{ai}| = |\vec{V}_{ci}| \left\{ \frac{1}{2} \left(\frac{r_{ai}}{r_{ci}} \right) \left(\frac{r_{ai}}{r_{ci}} + 1 \right) \right\}^{-1/2} \quad (5)$$

(at the apogee)

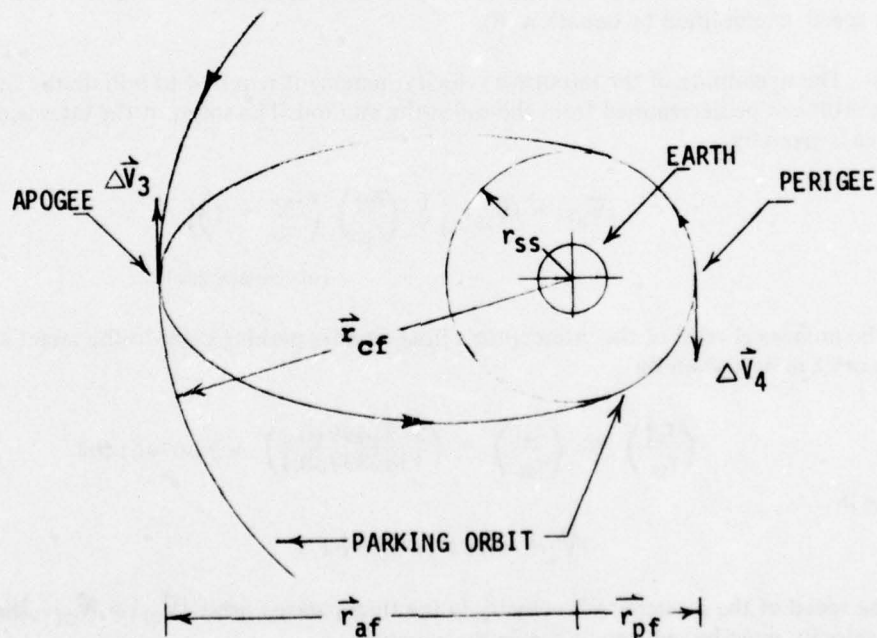


Figure 6-4 – Interceptor's Final Elliptical Transfer Orbit to the Synchronous Satellite Target Orbit

With the numerical values, previously defined, equations (3), (5) become

$$|\vec{V}_{pi}| = 35157.58831 \text{ FT/S}$$

$$|\vec{V}_{ai}| = 2028.86515 \text{ FT/S}$$

(in a CCW direction, as illustrated on page 3-13).

iv.) The impulsive velocity increment required to circularize the interceptor's final parking orbit is

$$\Delta \vec{V}_2 = \vec{V}_{cf} - \vec{V}_{ai} \quad \text{for } |\vec{V}_{cf}| > |\vec{V}_{ai}| \quad (6)$$

with

$$|\vec{V}_{cf}| = \sqrt{\frac{\mu}{r_{cf}}} = 6141.91744 \text{ FT/S} \quad (7)$$

and the previously calculated value for $|\vec{V}_{ai}|$, results in

$$|\Delta \vec{V}_2| = 4113.05229 \text{ FT/S}$$

applied in the direction of motion (clockwise — illustrated in Figure 6-2) due to a "deficient" circular speed, exemplified by equation (6).

v.) The magnitude of the impulsive velocity increment required to initiate the final elliptical transfer orbit can be determined from the following method. The speed of the interceptor's velocity at apogee is given by

$$|\vec{V}_{af}| = |\vec{V}_{ss}| \left\{ \frac{1}{2} \left(\frac{r_{af}}{r_{ss}} \right) \left(\frac{r_{af}}{r_{ss}} + 1 \right) \right\}^{-1/2} \quad (8)$$

(at the apogee)

where the numerical ratio of the interceptor's final circular parking orbit-to-the target's synchronous parking orbit radii is given by

$$\left(\frac{r_{cf}}{r_{ss}} \right) \equiv \left(\frac{r_{af}}{r_{ss}} \right) = \left(\frac{373149910.3}{138333730.1} \right) = 2.697461494$$

resulting in

$$|\vec{V}_{af}| = 4517.17736 \text{ FT/S}$$

Since the speed of the interceptor's velocity in the final parking orbit $|\vec{V}_{cf}| > |\vec{V}_{af}|$, the "excessive" apogee velocity must be reduced at \vec{r}_{af} via the equation

$$\Delta \vec{V}_3 = \vec{V}_{cf} - \vec{V}_{af}$$

where

$$\begin{aligned} |\Delta \vec{V}_3| &= |\vec{V}_{cf}| - |\vec{V}_{af}| \\ &= 6141.91744 - 4517.17736 \\ |\Delta \vec{V}_3| &= 1624.74008 \text{ FT/S} \end{aligned} \quad (9)$$

(counter to the interceptor's direction).

vi.) The magnitude of the impulsive velocity increment required to circularize the interceptor into the target's equatorial synchronous parking orbit is

$$|\Delta \vec{V}_4| = |\vec{V}_{pf}| - |\vec{V}_{ss}| \quad (10)$$

or

$$|\Delta \vec{V}_4| = |\vec{V}_{ss}| \left[\left(\frac{r_{cf}}{r_{ss}} \right) \left\{ \frac{1}{2} \left(\frac{r_{cf}}{r_{ss}} \right) \left(\frac{r_{cf}}{r_{ss}} + 1 \right) \right\}^{-1/2} - 1 \right] \quad (11)$$

(at the perigee)

for $r_{cf} > r_{ss}$

From the previously defined numerical values of $|\vec{V}_{ss}|$ and the radii ratio; (r_{cf}/r_{ss}) , the interceptor's "excessive" circular velocity requirement is reduced by

$$\begin{aligned} |\Delta \vec{V}_4| &= 12184.91199 - 10087.4548 \text{ FT/S} \\ |\Delta \vec{V}_4| &= 2097.45719 \text{ FT/S} \end{aligned}$$

Since the flight of the interceptor on a Hohmann elliptical transfer maneuver is on a collision-type course, it need not circularize at the synchronous satellite target orbit. This concept reduces the total required incremental velocities (i.e. $\Delta \vec{V}_4 \rightarrow 0$) for the sequence of maneuvers.

Rewriting equation (11), a plot of the interceptor's nondimensionalized final impulse required to circularize its perigee velocity, \vec{V}_{pf} at synchronous altitude is given by Figure 6-5.

In summary, the interceptor's altitude and inertial velocity for each of its specified events during the transfer maneuvers are **presented in Figure 6-6.**

With the above-defined numerical values, the simulation of the interceptor's final elliptical transfer maneuver to the point of rendezvous (with the target - S1) was accomplished by the previously defined Trajectory Simulation Program. This simulation (of the interceptor's flight time of ≈ 1800 min) was restricted to the single, zero-inclination elliptical transfer orbit, and employed the data (flight time, dwell angle) derived in Section 3.

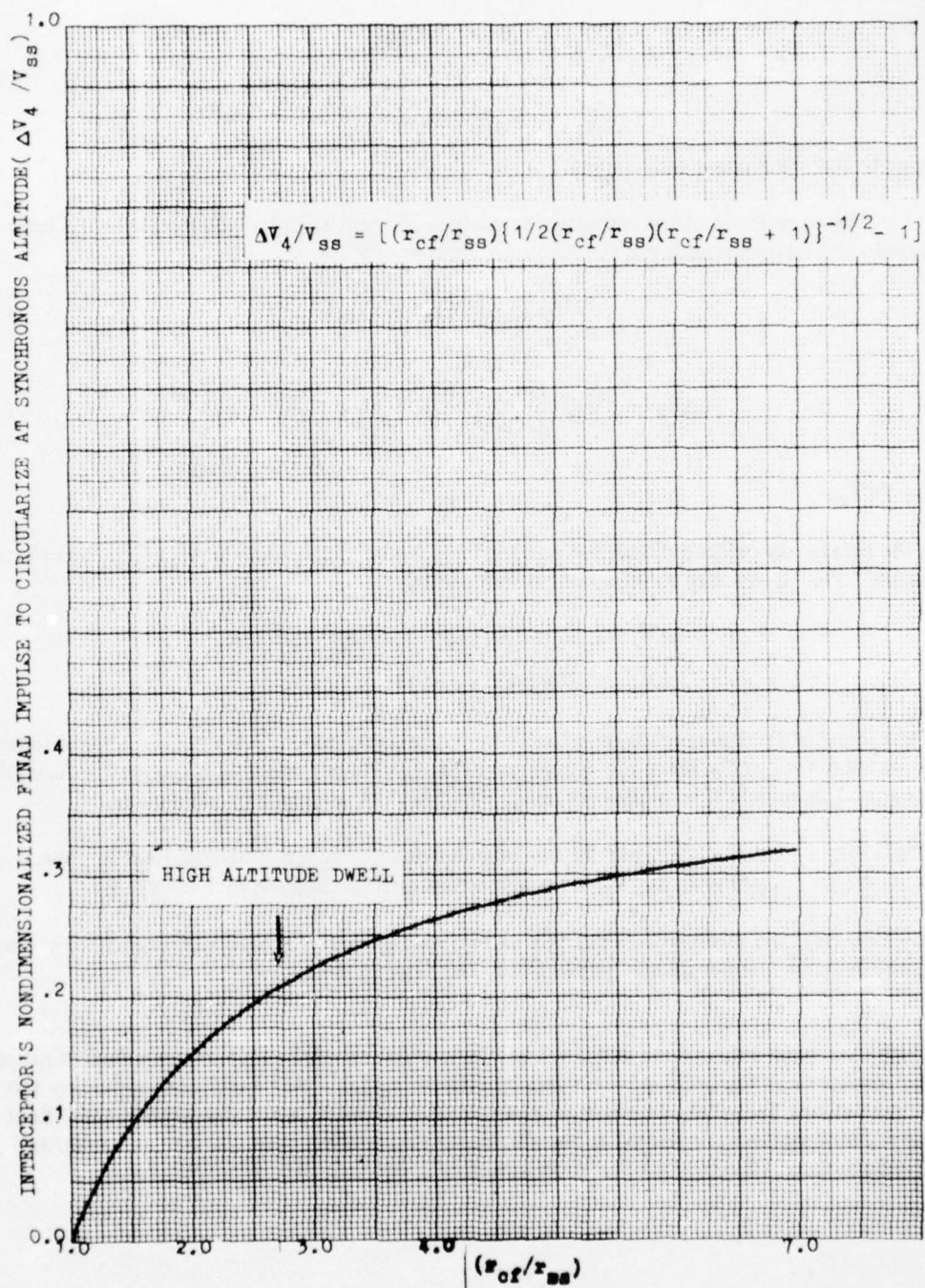


Figure 6-5 — Ratio of Interceptor's Final Parking-to-Synchronous Orbits Radii

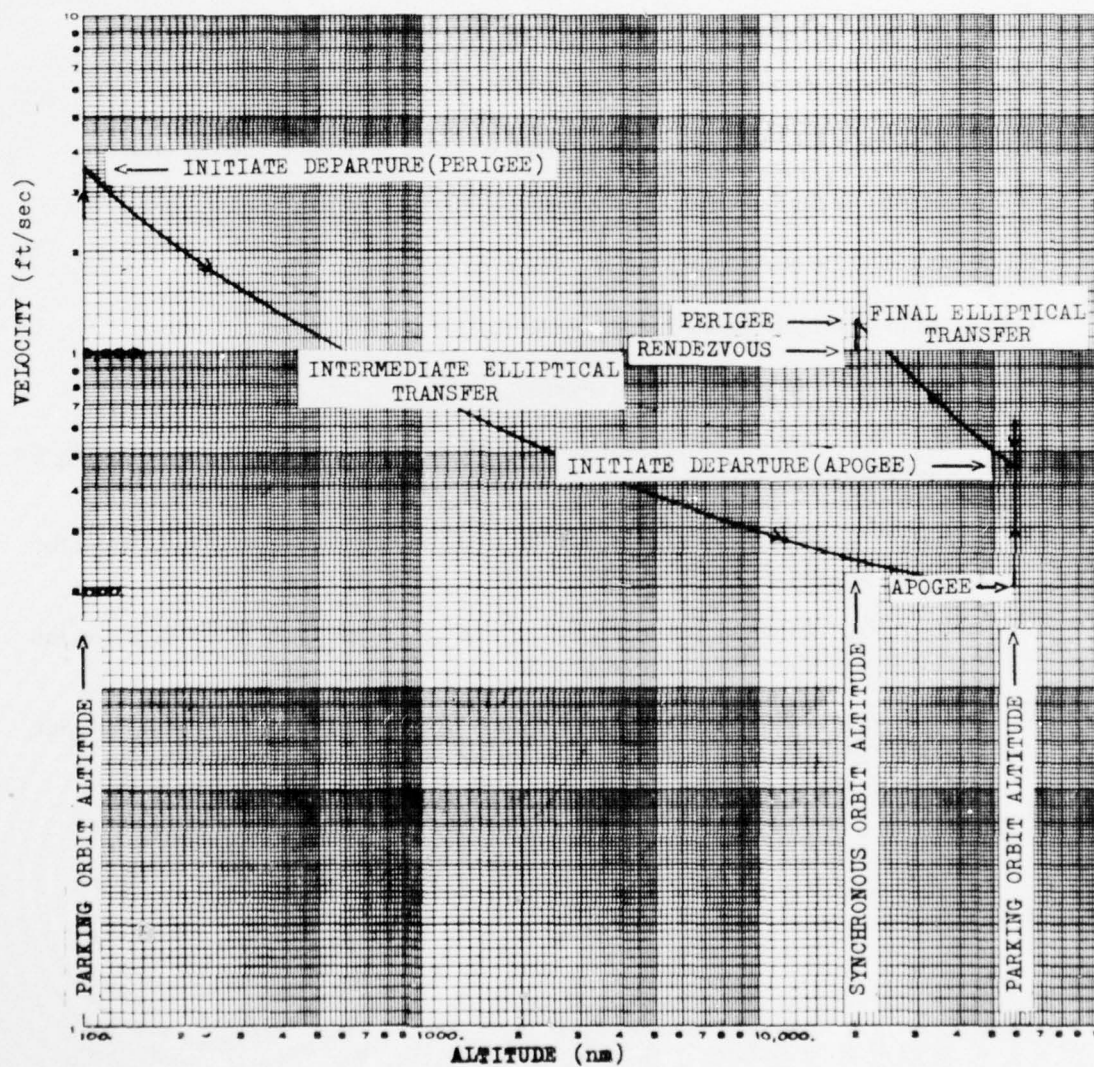


Figure 6-6 — Interceptor's Velocity-Altitude for High-Altitude-Dwell Scenario

NOMENCLATURE

(Applicable to the High-Altitude-Dwell – Bielliptic Transfer Maneuver)

\vec{V}_{pi} = velocity of the interceptor at the perigee of the intermediate elliptical transfer orbit.

\vec{V}_{ai} = velocity of the interceptor at the apogee of the intermediate elliptical transfer orbit.

\vec{V}_{ci} = velocity of the interceptor in the initial circular parking orbit.

\vec{V}_{cf} = velocity of the interceptor in the final circular parking orbit.

\vec{V}_{ss} = velocity of the target in the equatorial synchronous parking orbit.

\vec{V}_{pf} = velocity of the interceptor at the perigee of the final elliptical transfer orbit.

\vec{V}_{af} = velocity of the interceptor at the apogee of the final elliptical transfer orbit.

\vec{r}_{ci} = radius of the interceptor's initial circular parking orbit.

\vec{r}_{cf} = radius of the interceptor's final circular parking orbit.

\vec{r}_{ss} = radius of the target's synchronous parking orbit.

$\Delta \vec{V}_1 \equiv \vec{V}_{pi} - \vec{V}_{ci}$ = difference in the interceptor's perigee velocity and its circular velocity for the intermediate (initial) transfer orbit.

$\Delta \vec{V}_2 \equiv \vec{V}_{cf} - \vec{V}_{ai}$ = difference in the interceptor's velocity in the final circular orbit and the apogee velocity in the initial transfer orbit.

$\Delta \vec{V}_3 \equiv \vec{V}_{cf} - \vec{V}_{af}$ = difference in the interceptor's velocity in the final circular orbit and the apogee velocity in the final transfer orbit.

$\Delta \vec{V}_4 \equiv \vec{V}_{pf} - \vec{V}_{ss}$ = difference in the interceptor's perigee velocity in the final transfer orbit and the circular velocity in the desired (synchronous) orbit.

SECTION 7

BIBLIOGRAPHY

1. Ellis, G. A.; Femia, J. F.; Kalynycz, John Jr.; Proctor, A.H. "Simulation Program for Three Degrees of Freedom Trajectories", Technical Memorandum No. EMA-TM-66-5, Sept 1966, Unclassified.
2. Wolverton, Raymond W., Flight Performance Handbook for Orbital Operations, John Wiley & Sons, Inc., New York, 1961, Unclassified.
3. White, J. Frederick, Flight Performance Handbook for Powered Flight Operations, John Wiley & Sons, Inc., New York, 1962, Unclassified.
4. Jensen, Jorgen; Townsend, George; Kork, Jyri and Kraft, Donald, Design Guide to Orbital Flight, McGraw-Hill Book Company, Inc., New York, 1962, Unclassified.
5. Ellis, G. A.; Hoffman, P. R. "An Analysis of the Satellite/Missile Trajectory and Ground Sensor Visibility Coverage Using the Mercator Projection", RADC-TR-75-238, Sept 1975, Unclassified.

APPENDIX A **INERTIAL GEOCENTRIC ANGULAR SEPARATION OF THE DIRECT ASCENT** **INTERCEPTOR/TARGET SCENARIO**

For the purpose of early warning, a time related angular separation of specific interceptor launch/target location scenarios were calculated by the Trajectory Simulation Program and plotted with the HP 9862A plotter. These plots, the longitudinal, and inertial geocentric angular separation include the Direct Ascent interceptor maneuver to the equatorial synchronous satellite/target and are illustrated in Figures A-1 and A-2 for the three launch locations. These angular separations are calculated during the interceptor's total flight time ($\cong 149.4$ minutes) referenced to the zero time at collision. Specifying the interceptor burnout state vector and the target's time corresponding state vector, the time-dependent angular separation was calculated by the Trajectory Simulation Program and the results plotted by the HP 9862A plotter. The mathematical derivation of the angular displacement is given by

$$a(t) = \cos^{-1} [\cos (\Delta\lambda) \cos \theta_i \cos \theta_t + \sin \theta_i \sin \theta_t] \quad (A-1)$$

where

$$\Delta\lambda \equiv [\lambda_i(t) - \lambda_t(t)] \quad (A-2)$$

$\Delta\lambda$ = longitudinal separation of the
interceptor/target

and

$\theta_i(t)$ = interceptor's geocentric latitude

$\theta_t(t)$ = target's geocentric latitude

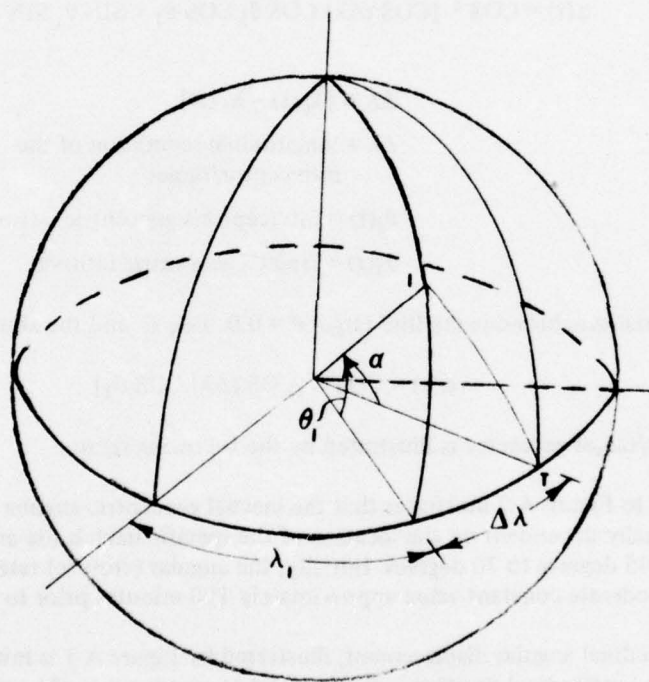
For the equatorial synchronous satellite target $\theta = 0.0$. Deg E and the above expression reduces to;

$$a(t) = \cos^{-1} [\cos (\Delta\lambda) \cos \theta_t] \quad (A-3)$$

The interceptor/target geometry is illustrated by the following figure.

Reference to Figure A-2 illustrates that the inertial geocentric angular separation at burnout time is functionally dependent on the location of the specific launch site and may vary from approximately 45 degrees to 70 degrees. Initially, the angular (closure) rate is relatively high and approaches a moderate constant value approximately 100 minutes prior to the intercept.

The longitudinal angular displacement, illustrated by Figure A-1 is initially negative, illustrating that the target's longitudinal position is further East as compared to the interceptor position. The angular rate is quite high and does not approach a constant value until about 100 minutes prior to collision.



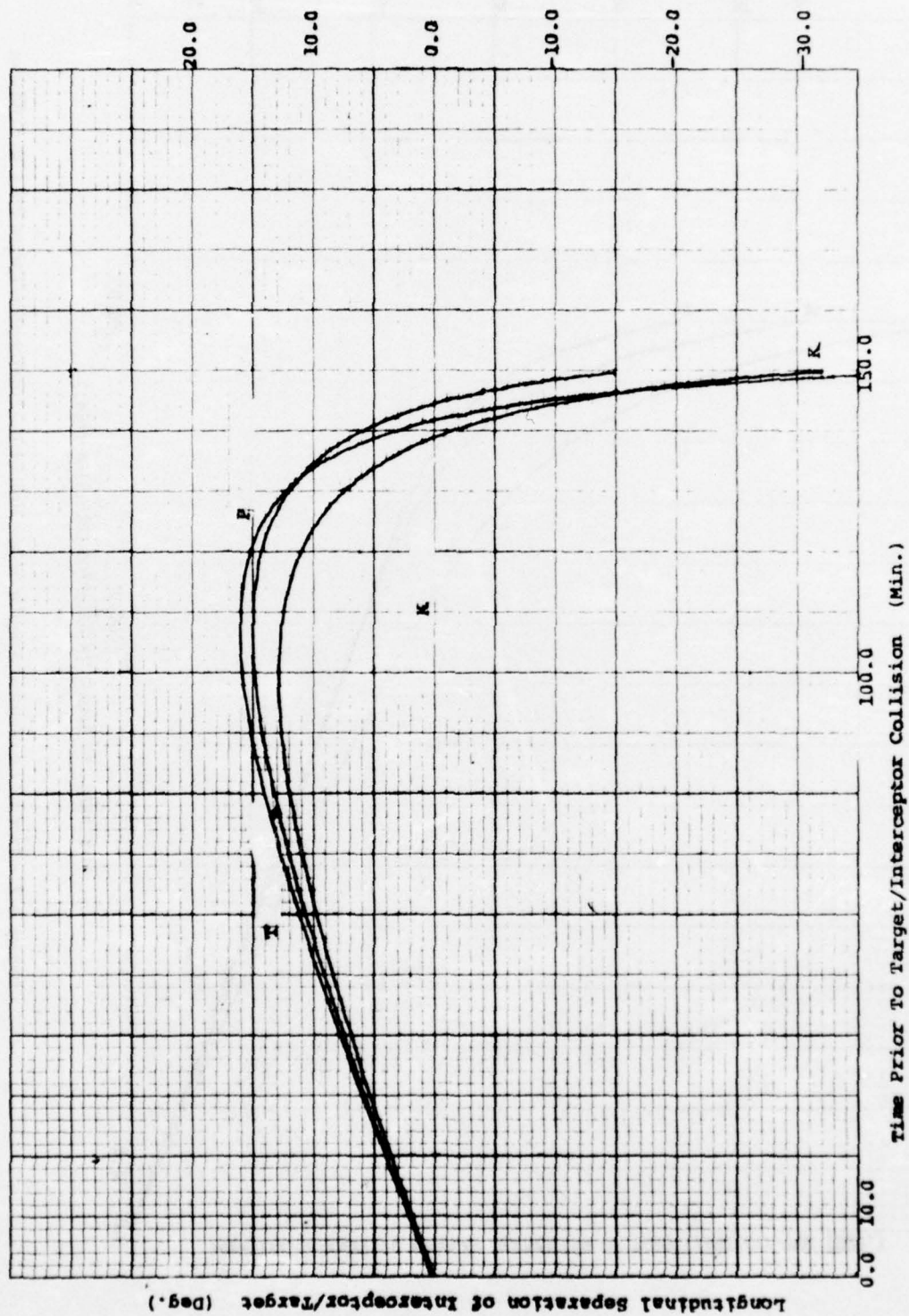


Figure A-1. Longitudinal Separation of the Interceptor/Target Prior to Collision

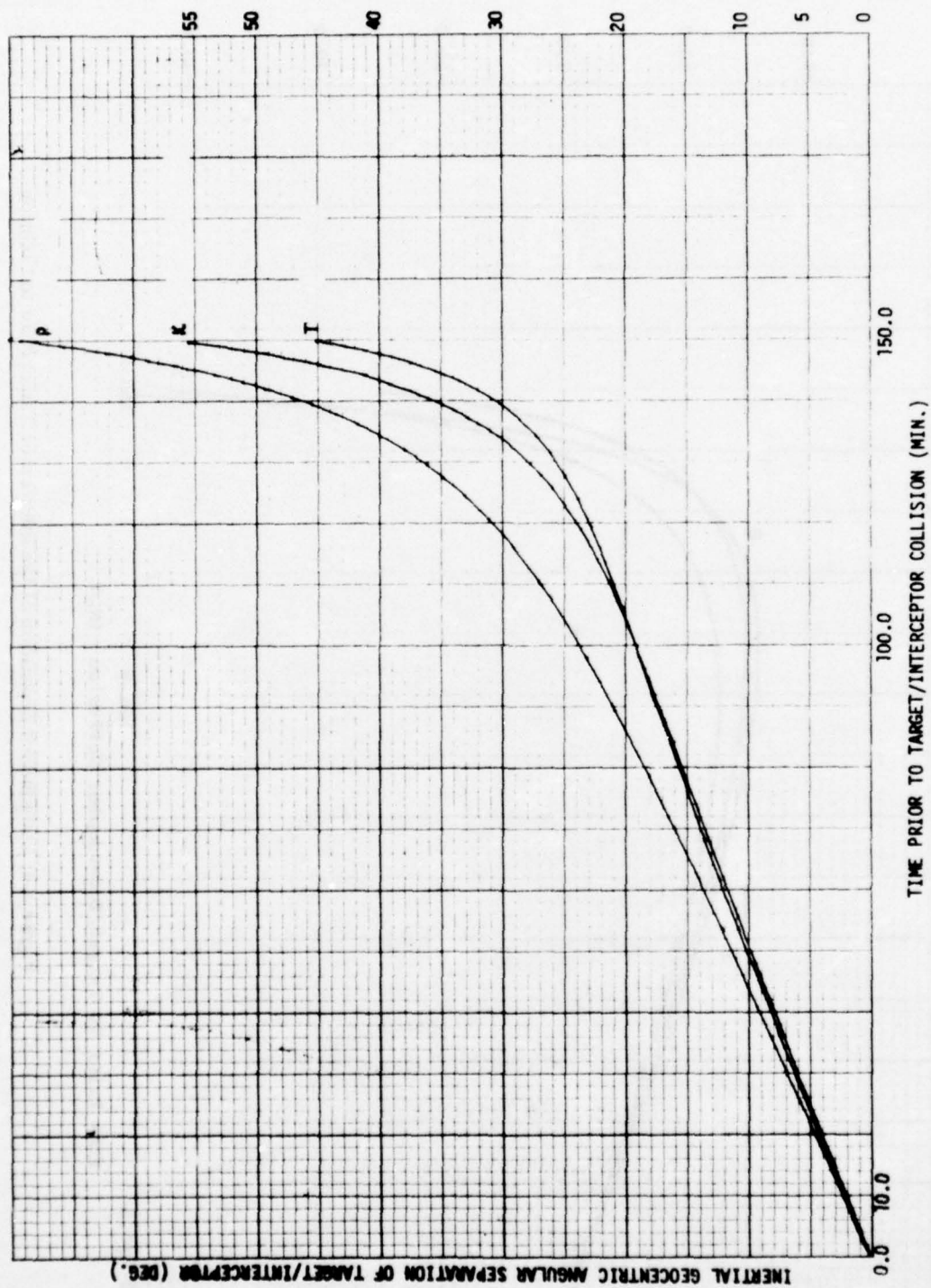


Figure A-2 - Inertial Geocentric Angular Separation of the Interceptor/Target Prior to Collision

APPENDIX B

INTERCEPTOR CO-PLANAR CIRCULAR/ELLIPTICAL ORBIT ANGULAR SEPARATION

In order to be able to detect the time of departure of an interceptor from its circular parking orbit onto a Hohmann elliptical transfer maneuver to the point of rendezvous, a study was made to determine the time-correlated angular separation.

With the Trajectory Simulation Computer Program, a circular equatorial parking orbit and a coplanar elliptical transfer orbit were simulated for the three altitude-dwell scenarios. The initial position and velocity of the interceptor in a circular and elliptical motion are given in Table B-1.

For each simulated scenario, the interceptor's time-dependent longitudinal position (incremented in 0.1 minute intervals) in the circular parking orbit was correlated with its elliptical transfer maneuver (time-sequenced with-respect-to the point of final departure, illustrated in Figure B-1). The elliptical transfer maneuver for the Low/Medium-Altitude-Dwell Scenarios occurred at the perigee and the interceptor's longitudinal angular displacement is equivalent to the true anomaly whereas the High-Altitude-Dwell Scenario required the interceptor's elliptical transfer maneuver to be initiated at apogee, (equivalent to a true anomaly value of 180. degrees).

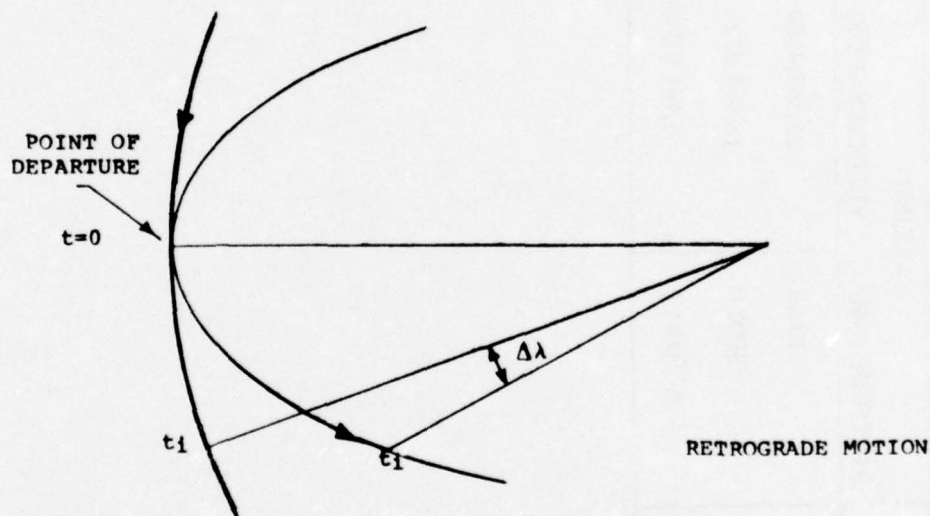


Figure B-1 – Interceptor's Angular Displacement

In each of the Altitude-Dwell Scenarios, these longitudinal angular separations ($\Delta\lambda$) were plotted as a function of the transfer initiation time (T). In Figure B-2, the Low-Altitude-Dwell Scenario exhibits a greater time rate-of-change of angular separation ($\Delta\lambda/\Delta t$) with a value of $6.^\circ$ in approximately 5. minutes whereas the Medium-Altitude-Dwell Scenario required approximately 21. minutes. In Figure B-3, the High-Altitude-Dwell Scenario with the least rate-of-change required approximately 450. minutes of elliptical flight time prior to achieving this value. These values represent: 1.6%, 5.7% and 24.9% of the total elliptical transfer maneuver flight time for the Low, Medium and High-Altitude Dwell Scenarios respectively.

TABLE B-1
INITIAL STATE VECTOR OF THE INTERCEPTOR AT TRANSFER TIME

ORBIT SCENARIO	PARKING		ELLIPTICAL	
	ALTITUDE (NM)	VELOCITY (FT/S)	POSITION	VELOCITY (FT/S)
LOW ALTITUDE	100.0	25,567,4209	PERIGEE	33,634,58296
MEDIUM ALTITUDE	3000.0	18,958,022	PERIGEE	23,668,65967
HIGH ALTITUDE	57,931.62	6,141,91744	APOGEE	4,517,17736

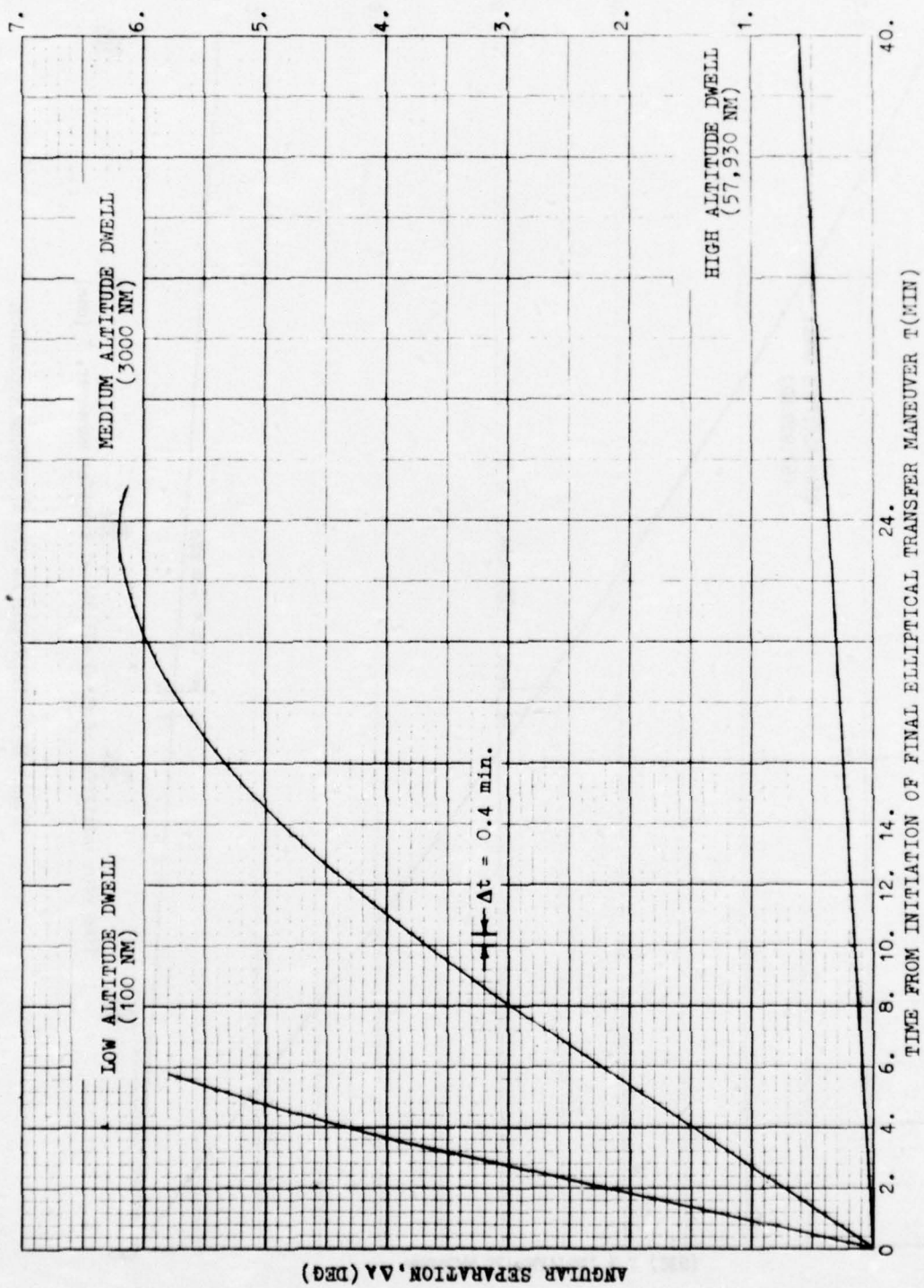


Figure B-2 - Interceptor Co-Planar Circular/Elliptical Angular Separation

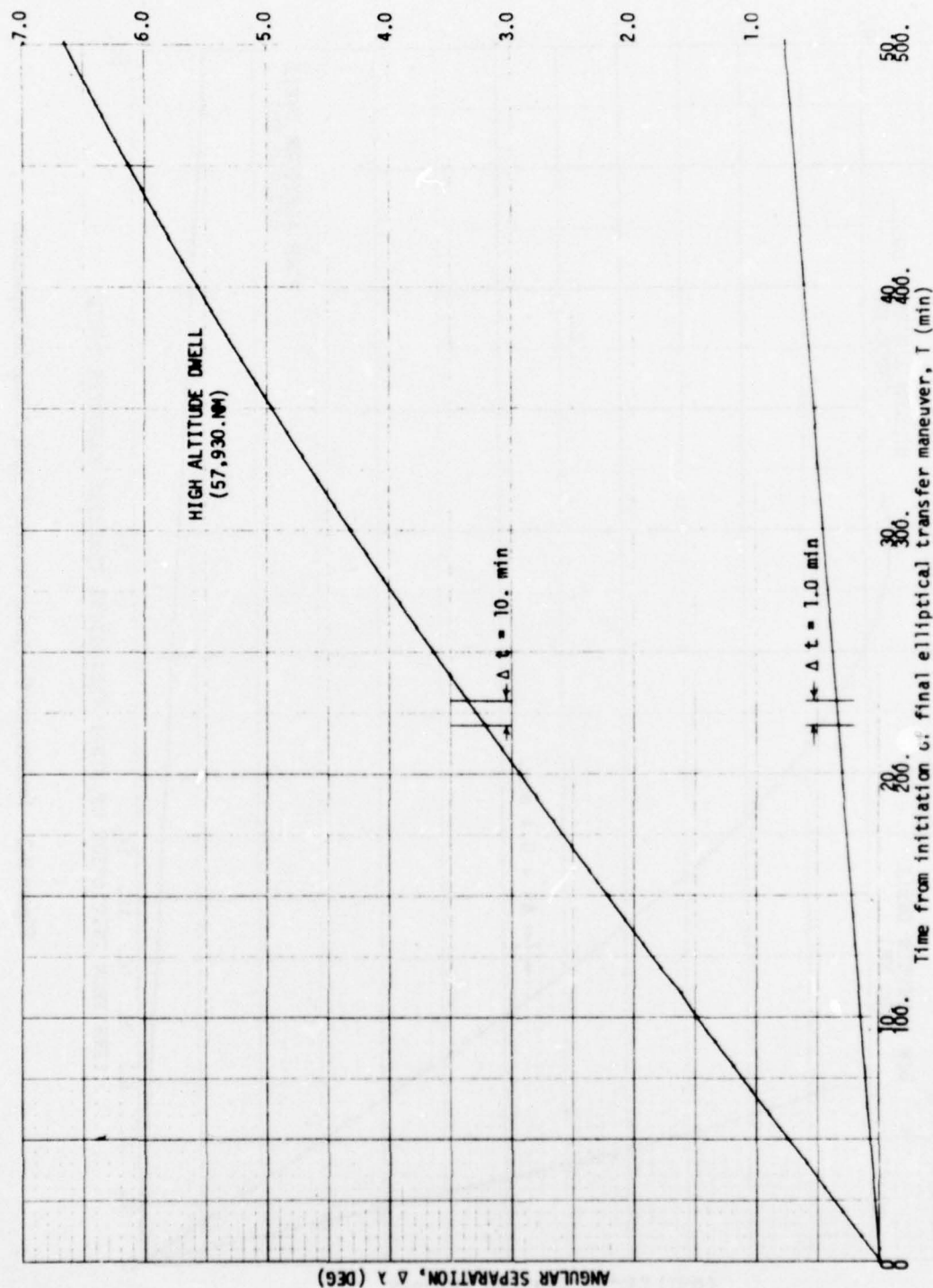


Figure B-3 - High Altitude-Dwell Angular Separation

APPENDIX C ORBITAL TRANSFER ENERGY REQUIREMENT

The total velocity increment $-\Delta \vec{v}_T$, required by an interceptor to execute the bielliptic transfer to a coplanar synchronous satellite target orbit, as demonstrated by the High-Altitude-Dwell Scenario is defined by:

- i. difference in the initial circular parking orbit velocity and the initial perigee velocity for the intermediate (initial) elliptical transfer maneuver $-\Delta \vec{v}_1$, plus
- ii. difference in the initial apogee velocity for the initial elliptical orbit and the interceptor's circular velocity in its parking orbit (final) $-\Delta \vec{v}_2$, plus
- iii. difference in the circular velocity and the apogee velocity for the final elliptical transfer maneuver $-\Delta \vec{v}_3$ plus
- iv. difference in the perigee velocity in the final elliptical orbit and the circular velocity of the desired orbit $-\Delta \vec{v}_4$; i.e.,

$$\Delta \vec{v}_T = \Delta \vec{v}_1 + \Delta \vec{v}_2 + \Delta \vec{v}_3 + \Delta \vec{v}_4 \quad (C-1)$$

A four-velocity increment transfer between the circular (initial) and desired circular orbits.

$$\begin{aligned} |\Delta \vec{v}_T| &= |\Delta \vec{v}_1| + |\Delta \vec{v}_2| + |\Delta \vec{v}_3| + |\Delta \vec{v}_4| \\ &= (|\vec{v}_{pi}| - |\vec{v}_{ci}|) + (|\vec{v}_{cf}| - |\vec{v}_{ai}|) + \\ &\quad (|\vec{v}_{cf}| - |\vec{v}_{af}|) + (|\vec{v}_{pf}| - |\vec{v}_{ss}|), \end{aligned} \quad (C-2)$$

for $\vec{r}_{cf} > \vec{r}_{ss} > \vec{r}_{ci}$.

To evaluate $|\Delta \vec{v}_1| = (|\vec{v}_{pi}| - |\vec{v}_{ci}|)$ (C-3)

$$|\vec{v}_{pi}| = |\vec{v}_{ci}| \sqrt{2} \left\{ 1 + \frac{r_{ci}}{r_{cf}} \right\}^{-1/2} = v_{ci} \sqrt{2} \left\{ \frac{r_{cf}}{r_{cf} + r_{ci}} \right\}^{1/2} \quad (C-4)$$

$$|\vec{v}_{pi}| = |\vec{v}_{ci}| \sqrt{2} \left\{ \frac{r_{cf}/r_{ci}}{(r_{cf}/r_{ci}) + 1} \right\}^{1/2} = |\vec{v}_{ci}| \left\{ \frac{2X}{1 + X} \right\}^{1/2}$$

$$\boxed{\left(\frac{v_{pi}}{v_{ci}} \right) = \left\{ \frac{2X}{1 + X} \right\}^{1/2}} \quad (C-5)$$

and

$$\frac{\Delta v_1}{v_{ci}} = \left(\frac{v_{pi}}{v_{ci}} - 1 \right) = \left[\left\{ \frac{2X}{1+X} \right\}^{1/2} - 1 \right] \quad (C-6)$$

or

$$\boxed{\frac{|\Delta \vec{v}_1|}{|\vec{v}_{ci}|} = \left[\left\{ \frac{2X}{1+X} \right\}^{1/2} - 1 \right]} \quad (C-7)$$

where $X \equiv (r_{cf}/r_{ci})$

$$\text{To evaluate: } |\Delta \vec{v}_2| = (|\vec{v}_{cf}| - |\vec{v}_{ai}|) \quad (C-8)$$

$$|\vec{v}_{ai}| = |\vec{v}_{pi}| \left(\frac{r_{pi}}{r_{ai}} \right) = |\vec{v}_{pi}| \left(\frac{r_{ci}}{r_{cf}} \right) = |\vec{v}_{pi}| \left(\frac{1}{X} \right) \quad (C-9)$$

$$|\vec{v}_{ai}| = |\vec{v}_{ci}| \left(\frac{1}{X} \right) \left\{ \frac{2X}{1+X} \right\}^{1/2}$$

$$|\vec{v}_{cf}| = \left(\frac{\mu}{r_{cf}} \right)^{1/2} = \left(\frac{\mu}{r_{ci}} \right)^{1/2} \left(\frac{r_{ci}}{r_{cf}} \right)^{1/2} \quad (C-10)$$

$$|\vec{v}_{cf}| = |\vec{v}_{ci}| \left(\frac{1}{X} \right)^{1/2} \quad (C-11)$$

$$(|\vec{v}_{cf}| - |\vec{v}_{ai}|) = |\vec{v}_{ci}| \left(\frac{1}{X} \right)^{1/2} \left(1 - \left\{ \frac{2}{1+X} \right\}^{1/2} \right) \quad (C-12)$$

and

$$\boxed{\left(\frac{|\Delta \vec{v}_2|}{|\vec{v}_{ci}|} \right) = \left(\frac{|\vec{v}_{cf}|}{|\vec{v}_{ci}|} \right) \left(1 - \left\{ \frac{2}{1+X} \right\}^{1/2} \right)} \quad (C-13)$$

$$\text{To evaluate: } |\Delta \vec{v}_3| = (|\vec{v}_{cf}| - |\vec{v}_{af}|) \quad (C-14)$$

$$\left. \begin{aligned} |\vec{v}_{af}| &= |\vec{v}_{ss}| \left\{ \frac{1}{2} \left(\frac{r_{af}}{r_{ss}} \right) \left(\frac{r_{af}}{r_{ss}} + 1 \right) \right\}^{-1/2} \\ |\vec{v}_{af}| &= |\vec{v}_{ss}| \left\{ \left(\frac{r_{ss}}{r_{cf}} \right)^{1/2} \left(\frac{2r_{ss}}{r_{cf} + r_{ss}} \right)^{1/2} \right\} \\ |\vec{v}_{af}| &= |\vec{v}_{ss}| \left(\frac{r_{ss}}{r_{cf}} \right)^{1/2} \left\{ \left(\frac{2(r_{ss}/r_{cf})}{1 + (r_{ss}/r_{cf})} \right)^{1/2} \right\} \end{aligned} \right\} \quad (C-15)$$

since
$$|\vec{v}_{cf}| = \left(\frac{\mu}{r_{cf}} \right)^{1/2} = \left(\frac{\mu}{r_{ss}} \right)^{1/2} \left(\frac{r_{ss}}{r_{cf}} \right)^{1/2} = |\vec{v}_{ss}| \left(\frac{r_{ss}}{r_{cf}} \right)^{1/2} \quad (C-16)$$

$$|\Delta \vec{v}_3| = |\vec{v}_{ss}| \left(\frac{r_{ss}}{r_{cf}} \right)^{1/2} - |\vec{v}_{ss}| \left(\frac{r_{ss}}{r_{cf}} \right)^{1/2} \left\{ \frac{2(r_{ss}/r_{cf})}{1 + r_{ss}/r_{cf}} \right\}^{1/2} \quad (C-17)$$

$$\boxed{\frac{|\Delta \vec{v}_3|}{|\vec{v}_{ci}|} = \left(\frac{|\vec{v}_{ss}|}{|\vec{v}_{ci}|} \right) (Y)^{1/2} \left[1 - \left\{ \frac{2Y}{1+Y} \right\}^{1/2} \right]} \quad (C-18)$$

where $Y \equiv (r_{ss}/r_{cf})$

To evaluate: $|\Delta \vec{v}_4| = (|\vec{v}_{pf}| - |\vec{v}_{ss}|)$ (C-19)

where
$$|\vec{v}_{pf}| = |\vec{v}_{af}| \left(\frac{r_{af}}{r_{pf}} \right) = |\vec{v}_{af}| \left(\frac{r_{cf}}{r_{ss}} \right) \quad (C-20)$$

$$|\vec{v}_{pf}| = |\vec{v}_{ss}| \left(\frac{r_{cf}}{r_{ss}} \right) \left(\frac{r_{ss}}{r_{cf}} \right)^{1/2} \left\{ \frac{2(r_{ss}/r_{cf})}{1 + (r_{ss}/r_{cf})} \right\}^{1/2} \quad (C-21)$$

$$|\vec{v}_{pf}| = |\vec{v}_{ss}| \left(\frac{r_{cf}}{r_{ss}} \right)^{1/2} \left\{ \frac{2Y}{1+Y} \right\}^{1/2} = |\vec{v}_{ss}| \left(\frac{1}{Y} \right)^{1/2} \left\{ \frac{2Y}{1+Y} \right\}^{1/2} \quad (C-22)$$

$$\boxed{\frac{|\Delta \vec{v}_4|}{|\vec{v}_{ci}|} = \frac{|\vec{v}_{ss}|}{|\vec{v}_{ci}|} \left[\left\{ \frac{2}{1+Y} \right\}^{1/2} - 1 \right]} \quad (C-23)$$

$$\frac{|\Delta \vec{v}_4|}{|\vec{v}_{ci}|} \left[\sqrt{\frac{2X}{1+X}} - 1 \right] + \left(\frac{|\vec{v}_{cf}|}{|\vec{v}_{ci}|} \right) \left(1 - \sqrt{\frac{2}{1+X}} \right) \quad (C-24)$$

since
$$+ \left(\frac{|\vec{v}_{ss}|}{|\vec{v}_{ci}|} \right) \left(\sqrt{Y} \right) \left(1 - \sqrt{\frac{2Y}{1+Y}} \right) + \left(\frac{|\vec{v}_{ss}|}{|\vec{v}_{ci}|} \right) \left(\sqrt{\frac{2}{1+Y}} - 1 \right)$$

for $X > 1, Y < 1$

Since the Hohmann transfer ellipse has long been recognized as the minimum energy for a two-impulse velocity increment between coplanar circular orbits, an analysis to determine whether this is the most efficient means of transfer, as compared to the four-velocity increment is required. For the two-velocity increment, the transfer between the initial and desired circular orbits, equation reduces to;

$$\left. \frac{|\Delta \vec{v}_T|}{|\vec{v}_{ci}|} \right|_H = \left[\sqrt{\frac{2X}{1+X}} - 1 \right] + \frac{|\vec{v}_{ss}|}{|\vec{v}_{ci}|} \left[1 - \sqrt{\frac{1}{X}} \sqrt{\frac{2X}{1+X}} \right] \quad (C-25)$$

where $X = r_{cf}/r_{ci} = r_{ss}/r_{ci} > 1$

and $|\Delta \vec{p}_3| = |\Delta \vec{p}_4| = 0$ since $Y = 1$

Given the following numerical values for the four-impulse transfer, equation is evaluated.

$$X = (r_{cf}/r_{ci}) = 373149910.3/21533640.0 \quad (C-26)$$

$$X = 17.32866942$$

$$Y = (r_{ss}/r_{cf}) = 138333730.1/373149910.3 \quad (C-27)$$

$$Y = 0.3707189156$$

$$(v_{cf}/v_{ci}) = 6141.917441/25567.4209 \quad (C-28)$$

$$= 0.2402243646$$

$$(v_{ss}/v_{ci}) = 10087.4548/25567.4209 \quad (C-29)$$

$$= 0.3945433073$$

resulting in;

$$\begin{aligned} \left(\frac{|\Delta \vec{p}_T|}{|\vec{p}_{ci}|} \right) &= 0.375074432 + 0.6696690938 + \\ &0.635472812 + 0.0820369968 \\ \left(\frac{|\Delta \vec{p}_T|}{|\vec{p}_{ci}|} \right) &= 0.6815288426 \text{ total energy requirement for the } \underline{\text{four-impulse}} \text{ coplanar transfer} \\ &\text{between circular orbits } \vec{r}_{ci} \text{ and } \vec{r}_{ss}. \end{aligned} \quad (C-30)$$

For the two-impulse energy requirement between the coplanar initial and desired circular parking orbits, equation is evaluated with the following numerical data.

$$\text{Let } X = (r_{ss}/r_{ci}) = 138333730.1/21533640. \quad (C-31)$$

$$X = 6.424075544$$

$$Y = (r_{ss}/r_{ss}) = 1.0 \quad (C-32)$$

$$(v_{ss}/v_{ci}) = 10087.4548/25567.4209 \quad (C-33)$$

$$= 0.3945433073$$

resulting in;

$$\left(\frac{|\Delta \vec{p}_T|}{|\vec{p}_{ci}|} \right) = 0.5052879217 \text{ total energy required for the } \underline{\text{two-impulse}} \text{ coplanar transfer maneuver.} \quad (C-34)$$

Thus, the Hohmann two-impulse transfer is the most economical approach for this specific data set.

APPENDIX D
AN ANALYTICAL SOLUTION TO THE THREE
DIMENSIONAL REPRESENTATION OF THE BALLISTIC MISSILE

The motion of a ballistic missile, after thrust termination, is described by means of a non-rotating spherical polar coordinate system (r, θ, λ) with origin at the earth's center and the polar axis coincident with that of the earth.

The Lagrangian in this system is

$$L = T - V \quad (D-1)$$

where T = kinetic energy

$$T = m(\vec{v} \cdot \vec{v}) / 2$$

and $V = V(r) = \mu m/r$ (potential energy)

(D-2)

From this, the equations of motion are derived from the Euler-Lagrange equation in general coordinates

$$\frac{d}{dt} \left(\frac{\partial L}{\partial \dot{q}_j} \right) - \left(\frac{\partial L}{\partial q_j} \right) = Q_j \quad j = 1, 2, 3 \quad (D-3)$$

where Q_j represents the nongravitational forces.

Since the velocity, in the nonrotating system, may be expressed in terms of the spherical coordinates as

$$\vec{v} = \dot{r} \hat{r} + r \dot{\theta} \hat{\theta} + (r \cos \theta) \dot{\lambda} \hat{\lambda}$$

and

$$v^2 \equiv \vec{v} \cdot \vec{v} = \dot{r}^2 + (r \dot{\theta})^2 + (r \cos \theta)^2 \dot{\lambda}^2 \quad (D-4)$$

$$\therefore L = \frac{m}{2} [\dot{r}^2 + r^2 \dot{\theta}^2 + (r \cos \theta)^2 \dot{\lambda}^2] + \frac{\mu m}{r} \quad (D-5)$$

Letting q_j and \dot{q}_j be equivalent to the spherical polar coordinates and their rates respectively equation D-3 reduces to the following equations of motion i.e.,

$$\left. \begin{aligned} \frac{d^2 r}{dt^2} - r \dot{\theta}^2 - (r \cos^2 \theta) \dot{\lambda}^2 + \frac{\mu}{r^2} &= Q_1 \\ \frac{d}{dt} (r^2 \dot{\theta}) + \left(\frac{r^2}{2} \sin \theta \right) \dot{\lambda}^2 &= Q_2 \\ \frac{d}{dt} [(r^2 \cos^2 \theta) \dot{\lambda}] &= Q_3 \end{aligned} \right\} \quad (D-6)$$

The initial state vector of the missile may be written as

$$\left. \begin{aligned} \frac{dr}{dt} \Big|_0 &= v_o \cos \gamma \\ \frac{d\theta}{dt} \Big|_0 &= \frac{v_o}{r_o} \sin \gamma \cos \beta \\ \frac{d\lambda}{dt} \Big|_0 &= \frac{v_o}{r_o} \frac{\sin \gamma \sin \beta}{\cos \theta_o} \end{aligned} \right\} \quad (D-7)$$

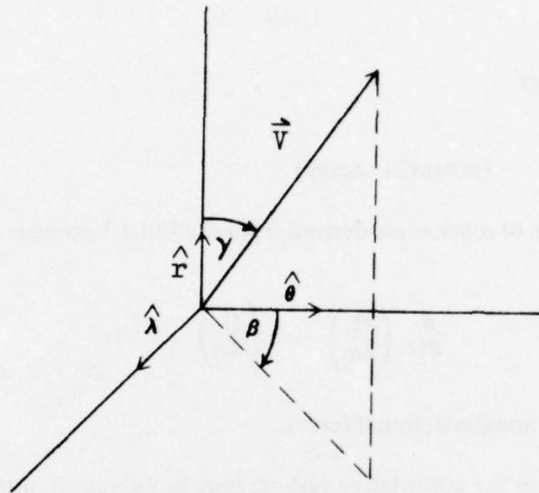


Figure D-1 — Spherical Polar Coordinates of the Velocity Vector

The above 2nd order non-linear differential equations of motion were numerically integrated by the 4th order Runge Kutta-Gill Method (1,5). Since the Q's will give rise to a torque and an analytical solution is required to establish the initial state vector on the missile, the right hand side is set equal to zero. This results in the angular momentum (time rate of change of torque) being conserved and the Lagrangian equation can be rewritten as

$$(r^2 \cos^2 \theta) \dot{\lambda} = \text{constant} \quad (D-8)$$

and the remaining equations reduce to

$$\frac{d^2 r}{dt^2} - r \dot{\theta}^2 - (r \cos^2 \theta) \dot{\lambda}^2 + \frac{\mu}{r^2} = 0 \quad (D-9)$$

$$\frac{d}{dt} (r^2 \dot{\theta}) + \frac{r^2}{2} \sin 2\theta \dot{\lambda}^2 = 0 \quad (D-10)$$

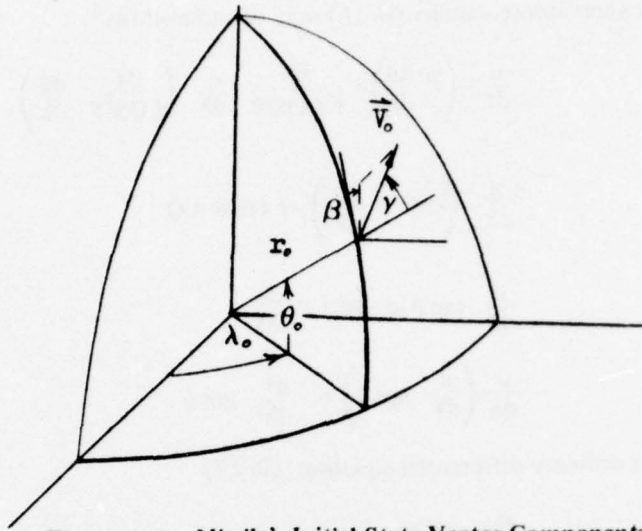


Figure D-2 -- Missile's Initial State Vector Components

Since the angular momentum is conserved, the expression, as given by equation (D-8) may be rewritten as

$$H \equiv (r^2 \cos^2 \theta) \frac{d\lambda}{dt} \quad (D-11)$$

$$H = r_0 v_0 \cos \theta_0 \sin \gamma \sin \beta$$

To eliminate the time dependency of the Lagrangian equations (i.e., $r(t)$, $\theta(t)$, $\lambda(t)$), the expression for angular momentum provides the functional dependency of the differential change in time, dt to the corresponding change in $d\lambda$.

$$\frac{d}{dt} \equiv \frac{d\lambda}{dt} \frac{d}{d\lambda} = \frac{H}{r^2 \cos^2 \theta} \frac{d}{d\lambda} \quad (D-12)$$

Rewriting equation (D-10)

$$\frac{d}{dt} (r^2 \dot{\theta}) + (r^2 \sin \theta \cos \theta) \dot{\lambda}^2 = 0 \quad (D-13)$$

Since

$$\frac{d\lambda}{dt} = \frac{H}{r^2 \cos^2 \theta} \quad (D-14)$$

$$\frac{d}{dt} (r^2 \dot{\theta}) + \frac{H^2 \tan \theta}{r^2 \cos^2 \theta} = 0 \quad (D-15)$$

First term of the above expression (equation (D-15)) may be reduced to:

$$\frac{d}{dt} \left(r^2 \frac{d\theta}{dt} \right) = \frac{H}{r^2 \cos^2 \theta} \frac{d}{d\lambda} \left(\frac{H}{\cos^2 \theta} \frac{d\theta}{d\lambda} \right) \quad (D-16)$$

resulting in:

$$\frac{d}{d\lambda} \left(\sec^2 \theta \frac{d\theta}{d\lambda} \right) + \tan \theta = 0 \quad (D-17)$$

since

$$\frac{d}{d\lambda} \tan \theta \equiv \sec^2 \theta \frac{d\theta}{d\lambda} \quad (D-18)$$

$$\frac{d}{d\lambda} \left(\frac{d}{d\lambda} \tan \theta \right) = \frac{d^2}{d\lambda^2} \tan \theta \quad (D-19)$$

Solution to the 2nd order ordinary differential equation (D-17)

$$\frac{d^2}{d\lambda^2} \tan \theta + \tan \theta = 0 \quad (D-20)$$

Let $S = \tan \theta$ and $ds/d\lambda \equiv T$

(D-21)

Rewrite the above equation as a first order equation,

$$\frac{d^2 S}{d\lambda^2} = \frac{dT}{d\lambda} (S) = \left(\frac{dT}{dS} \right) \left(\frac{dS}{d\lambda} \right) = T \frac{dT}{dS} \quad (D-22)$$

$$T \frac{dT}{dS} + S = 0$$

Solution of the above first order equation, yields a constant of integration given by:

$$C_2 = T^2 + S^2 = \left(\frac{d}{d\lambda} \tan \theta \right)^2 + \tan^2 \theta \quad (D-23)$$

where

$$\frac{d}{d\lambda} \tan \theta = \sec^2 \theta (d\theta/d\lambda) \quad (D-24)$$

and

$$\left(\frac{d\theta}{d\lambda} \right) \equiv (d\theta/dt) / (d\lambda/dt) \quad (D-25)$$

From the initial boundary conditions given by equation (D-7)

$$\frac{d}{d\lambda} \tan \theta \Big|_0 = \left(\frac{\text{ctn} \beta}{\cos \theta_0} \right) \quad (D-26)$$

and

$$\sqrt{C_2} = (\text{ctn}^2 \beta + \sin^2 \theta_0)^{1/2} / \cos \theta_0 \quad (D-27)$$

Rewriting equation (D-21)

$$T \equiv \frac{dS}{d\lambda} = \sqrt{C_2 - S^2} \quad (D-28)$$

and integrating again, results in

$$\tan \theta = \sqrt{C_2} \sin(\lambda + C_1) \quad (D-29)$$

and

$$\sec \theta = [1 + C_2 \sin^2(\lambda + C_1)]^{1/2} \quad (D-30)$$

with C_1, C_2 as arbitrary constants of integrations. Differentiating of equation (D-29) and imposing the initial set of boundary values on the two equations, results in

$$\tan \theta_0 = \sqrt{C_2} \sin(\lambda_0 + C_1) \quad (D-31)$$

and

$$\left. \frac{d}{d\lambda} \tan \theta \right|_0 = \sqrt{C_2} \cos(\lambda_0 + C_1) \quad (D-32)$$

Substituting equation (D-26) into the above differential equation and dividing into equation (D-31), results in an expression representing the intersection of a trajectory plane with a sphere (see Figure D-3).

$$\tan(\lambda_0 + C_1) = \sin \theta_0 \tan \beta \quad (D-33)$$

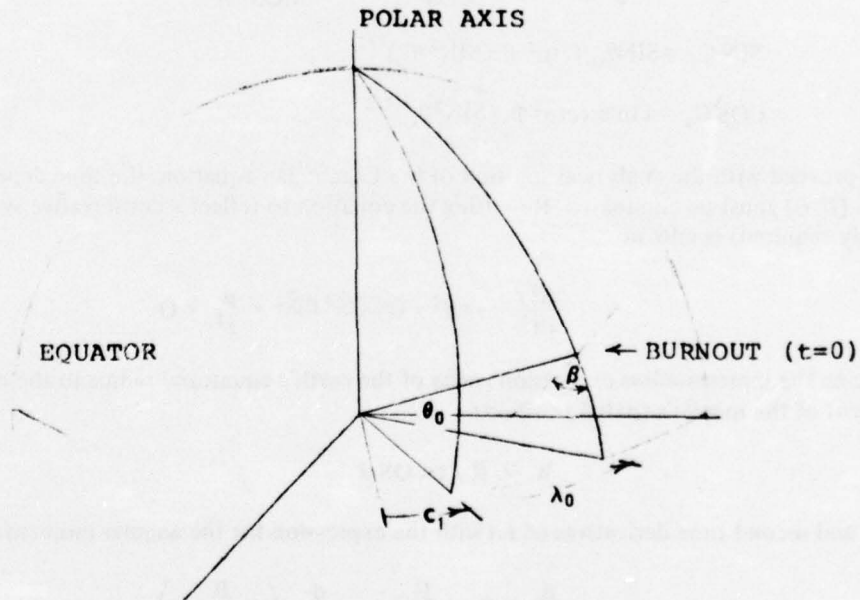


Figure D-3— Unperturbed Planar Trajectory on a Spherical Earth

To impose an additional constraint upon the initial state vector, let $\lambda_0 = 0$ and with the substitution of equation (D-26) in equation (D-32), the resulting equation and equation (D-31) reduces to:

$$\frac{\text{ctn } \beta}{\text{COS } \theta_0} = \sqrt{C_2} \text{COS } C_1 \quad (\text{D-34})$$

$$\tan \theta_0 = \sqrt{C_2} \text{SIN } C_1 \quad (\text{D-35})$$

$$\tan \theta \text{COS } \theta_0 = \text{SIN } \lambda \text{ctn } \beta + \text{COS } \lambda \text{SIN } \theta_0$$

and

$$\tan C_1 = \tan \theta_0 / (\text{ctn } \beta / \text{COS } \theta_0) \quad (\text{D-36})$$

as illustrated by Figure D-3.

Also verification of equation (D-27) can be obtained by the squaring of equations (D-34) and (D-35) adding and taking the square root of the sum; i.e.,

$$\frac{\text{ctn}^2 \beta}{\text{COS } \theta_0} = C_2 \text{COS}^2 C_1 \quad (\text{D-37})$$

$$\tan^2 \theta_0 = C_2 \text{SIN}^2 C_1 \quad (\text{D-38})$$

$$\therefore \sqrt{C_2} = \sqrt{\tan^2 \theta_0 + \frac{\text{ctn}^2 \beta}{\text{COS}^2 \theta_0}} = \frac{(\text{ctn}^2 \beta + \text{SIN}^2 \theta_0)^{1/2}}{\text{COS } \theta_0} \quad (\text{D-39})$$

and

$$\left. \begin{aligned} \text{SIN } C_1 &= \text{SIN } \theta_0 / (\text{ctn}^2 \beta + \text{SIN}^2 \theta_0)^{1/2} \\ \text{COS } C_1 &= \text{ctn } \beta / (\text{ctn}^2 \beta + \text{SIN}^2 \theta_0)^{1/2} \end{aligned} \right\} \quad (\text{D-40})$$

To proceed with the analytical solution of the Lagrangian equation, the time dependency of equation (D-6) must be eliminated. Rewriting the equation to reflect a conservative system (as previously required) results in

$$\frac{d^2 r}{dt^2} - r \dot{\theta}^2 - (r \text{COS}^2 \theta) \dot{\lambda}^2 + \frac{\mu}{r^2} = 0$$

Introducing the dimensionless expression (ratio of the earth's equatorial radius to the equatorial component of the missile's spatial position)

$$W \equiv R / r \text{COS } \theta \quad (\text{D-41})$$

the first and second time derivatives of r , (with the expression for the angular momentum) becomes:

$$\frac{d}{dt} r = \frac{H}{r^2 \text{COS}^2 \theta} \frac{d}{d\lambda} \left(\frac{R}{W \text{COS } \theta} \right) \quad (\text{D-42})$$

and

$$\frac{d^2 r}{dt^2} = \frac{H}{r^2 \text{COS}^2 \theta} \frac{d}{d\lambda} \left(\frac{dr}{dt} \right)$$

resulting in

$$\frac{d^2 r}{dt^2} = \frac{H}{r^2 \cos^2 \theta} \frac{d}{d\lambda} \left\{ \frac{H}{(R/W)^2} \frac{d}{d\lambda} \left(\frac{R}{W \cos \theta} \right) \right\}$$

$$\frac{d^2 r}{dt^2} = \frac{H^2 W^2}{R^3} \left\{ W \frac{d^2}{d\lambda^2} \sec \theta - \sec \theta \frac{d^2 W}{d\lambda^2} \right\} \quad (D-43)$$

In addition, the second term of equation (D-9) may be rewritten as:

$$r \dot{\theta}^2 = r \left[\left(\frac{d\theta}{d\lambda} \right) \left(\frac{d\lambda}{dt} \right) \right]^2$$

By substituting the value for $d\lambda/dt$, derived in equation (D-14), the above equation reduces to

$$r \dot{\theta}^2 = r \left(\frac{d\theta}{d\lambda} \right)^2 \left(\frac{H^2}{(R/W)^3 \cos \theta} \right) \quad (D-44)$$

resulting in

$$r \dot{\theta}^2 = \frac{H^2 W^3}{R^3} \sec \theta \left(\frac{d\theta}{d\lambda} \right)^2 \quad (D-45)$$

The third term in equation (D-9), reduces to

$$(r \cos^2 \theta) \dot{\lambda}^2 = \frac{H^2 W^3}{R^3} \cos \theta \quad (D-46)$$

Substituting the above results into equation (D-9) yields

$$\sec \theta \frac{d^2 W}{d\lambda^2} - W \left\{ \frac{d^2}{d\lambda^2} \sec \theta - \sec \theta \left(\frac{d\theta}{d\lambda} \right)^2 - \cos \theta \right\} = g \cos^2 \theta \quad (D-47)$$

where the quantity $H^2 W^2 / R^3$ was factored out and by definition

$$g \equiv \mu R / H^2 \quad (D-48)$$

Dividing the above equation (D-47), by the $\sec \theta$ and evaluating the derivatives of the $\sec \theta$, yields the following linear differential equation of 2nd order, i.e.,

$$\frac{d^2 W}{d\lambda^2} + W = \frac{g}{\sec^3 \theta} \quad (D-49)$$

where

$$\sec \theta \equiv [1 + C_2 \sin^2 (\lambda + C_1)]^{1/2} \quad (D-50)$$

The general solution to the above non-homogeneous linear equation is made up of the sum of the complementary function and the particular integral. The solution involves two independent arbitrary constants and is given by

$$W = W_c + W_p \quad (D-50)$$

where $W = W_c$ is the general solution of the homogeneous equation (right-hand-side of equation (D-49) replaced by zero) and $W = W_p$ is the particular integral. Following the procedure outlined in any differential equations textbook, the general solution is given by

$$W = \frac{g}{(1+C_2)} [1 + C_2 \sin^2 (\lambda + C_1)]^{1/2} + K_1 \sin(\lambda + C_1) + K_2 \cos(\lambda + C_1) \quad (D-51)$$

where K_1, K_2 are constants of integrations to be defined and C_1 and C_2 are the integration constants, previously defined by equations (D-33) and (D-27).

To evaluate the undefined integration constants K_1, K_2 , differentiate equation (D-51), with respect to the independent variable λ which is the longitudinal coordinate of the missile. Multiplying W by the $\sin(\lambda + C_1)$ and its derivative $dW/d\lambda$ by the $\cos(\lambda + C_1)$, adding the two resulting equations and solving for K_1 (by rearranging the terms), yields

$$K_1 = W \sin(\lambda + C_1) + \frac{dW}{d\lambda} \cos(\lambda + C_1) - \frac{g}{(1+C_2)} \left\{ [1 + C_2 \sin^2 (\lambda + C_1)]^{1/2} + \sin(\lambda + C_1) + \frac{C_2 \sin(\lambda + C_1) \cos^2(\lambda + C_1)}{[1 + C_2 \sin^2 (\lambda + C_1)]^{1/2}} \right\} \quad (D-52)$$

The K_2 constant of integration value can be obtained by multiplying equation (D-51) by the $\cos(\lambda + C_1)$ and $dW/d\lambda$ by $\sin(\lambda + C_1)$. Subtracting the two resulting equations and solving for K_2 , yields

$$K_2 = W \cos(\lambda + C_1) - \frac{dW}{d\lambda} \sin(\lambda + C_1) - \frac{g}{(1+C_2)} \left\{ \sec \theta \cos(\lambda + C_1) - \frac{C_2 \sin^2(\lambda + C_1) \cos(\lambda + C_1)}{\sec \theta} \right\} \quad (D-53)$$

Imposing the previously defined set of initial boundary values, i.e.,

$$r \rightarrow r_0, \theta \rightarrow \theta_0, \lambda \rightarrow \lambda_0 \rightarrow 0$$

the above constants of integration reduce to:

$$\text{and} \quad \left. \begin{aligned} K_1 &= W_0 \sin C_1 + \frac{dW}{d\lambda} \Big|_0 \cos C_1 - g \cos \theta_0 \sin C_1 \\ K_2 &= W_0 \cos C_1 - \frac{dW}{d\lambda} \Big|_0 \sin C_1 - \frac{g}{(1+C_2)} \cos \theta_0 \cos C_1 \end{aligned} \right\} \quad (D-54)$$

Additional mathematical exercise, enables K_2 to be written as,

$$K_1 = K_2 \tan C_1 + \frac{dW}{d\lambda} \bigg|_0 \sec C_1 - \frac{g}{(1+C_2)} \sin C_1 \cos \theta_0 \quad (D-55)$$

where

$$W_0 = \frac{R}{r_0} \sec \theta_0 = \frac{R}{r_0} [1 + C_2 \sin^2 \alpha^2]^{1/2} \quad (D-56)$$

and

$$\left. \begin{aligned} \frac{dW}{d\lambda} \bigg|_0 &= \frac{R \sec \theta_0}{\cos \beta} [\tan \theta_0 \cos \beta - \cot \gamma] \\ \text{or} \quad \frac{dW}{d\lambda} \bigg|_0 &= \frac{W_0 r_0}{\cos \beta} [\sqrt{C_2} \sin C_1 \cos \beta - \cot \gamma] \end{aligned} \right\} \quad (D-57)$$

The analytical solutions to the set of 2nd order ordinary differential equations given by

$$\frac{d^2 r}{dt^2} - r \dot{\theta}^2 - (r \cos^2 \theta) \dot{\lambda}^2 + \frac{\mu}{r^2} = 0 \quad (D-9)$$

$$\frac{d}{dt} (r^2 \dot{\theta}) + \frac{(r^2 \sin 2\theta)}{2} \dot{\lambda}^2 = 0 \quad (D-10)$$

and

$$(r^2 \cos^2 \theta) \dot{\lambda} = \text{constant} \quad (D-8)$$

can now be summarized. Since the system is conservative (an imposed constraint), equation (D-8) can be conveniently integrated to obtain the total extrinsic angular momentum equation.

$$\left. \begin{aligned} H &= (r^2 \cos^2 \theta) \dot{\lambda} = \text{constant} \\ H &= r_0 V_0 \cos \theta_0 \sin \gamma \sin \beta \end{aligned} \right\} \quad (D-11)$$

that is functionally dependent upon the parameters of the initial state vector.

With the above relationship, the time derivatives in equations (D-9), (D-10) can be eliminated, and the functional dependency of θ on λ , yields the following analytical solution:

$$\theta = \theta(\lambda) = \arctan [\sqrt{C_2} \sin (\lambda + C_1)] \quad (D-29)$$

or

$$\theta(\lambda) = \text{ARC SEC} [1 + C_2 \sin^2 (\lambda + C_1)]^{1/2} \quad (D-30)$$

where

$$C_1 \equiv \arctan (\sin \theta_0 \tan \beta) \quad (D-36)$$

$$\sqrt{C_2} = \sec \theta_0 (\cot^2 \beta + \sin^2 \theta_0)^{1/2} \quad (D-27)$$

$$(1 + C_2) = \csc^2 \beta \sec^2 \theta_0 \quad (D-58)$$

These solutions were extensively used to eliminate the time derivatives in equation (D-10), thus yielding an analytical solution that relates the functional dependency of r on λ given by:

$$\frac{R}{r} = W \cos \theta = \frac{W}{[1 + C_2 \sin^2 (\lambda + C_1)]^{1/2}} \quad (D-59)$$

where

$$W = \frac{g}{(1 + C_2)} [1 + C_2 \sin^2 (\lambda + C_1)]^{1/2} + K_1 \sin (\lambda + C_1) + K_2 \cos (\lambda + C_1) \quad (D-51)$$

and

$$K_1 = K_2 \tan C_1 + \left. \frac{dW}{d\lambda} \right|_0 \sec C_1 - \frac{g}{(1 + C_2)} \sin C_1 \cos \theta_0 \quad (D-55)$$

$$K_2 = W_0 \cos C_1 - \left. \frac{dW}{d\lambda} \right|_0 \sin C_1 - \frac{g}{(1 + C_2)} \cos \theta_0 \cos C_1 \quad (D-54)$$

$$W_0 = R/r_0 \cos \theta_0 \quad (D-56)$$

$$\left. \frac{dW}{d\lambda} \right|_0 = \frac{W_0 r_0}{\cos \beta} [\sqrt{C_2} \sin C_1 \cos \beta - \cot \gamma] \quad (D-57)$$

Note that the above solution is analogous to the two-dimensional 'hit' equation derived in Appendix E.

APPENDIX E EVALUATION OF APPROXIMATE VALUES OF THE TWO DIMENSIONAL BALLISTIC MISSILE PARAMETERS

In the planar representation of the free-flight trajectory, the equations, derived from the Lagrangian function, are defined by the in-plane polar coordinates (r, θ) , i.e., $\lambda = 0$. Thus, for a predetermined surface range, constraints are imposed on the burnout parameters (v_0, r_0, γ) to assure this objective. In the following derivations, these parameters will be shown to be functionally dependent on this range. The in-plane representation of equations (D-9) and (D-10) is given by:

$$\left. \begin{aligned} \frac{d^2 r}{dt^2} - r \dot{\theta}^2 + \frac{\mu}{r^2} &= 0 \\ \frac{d}{dt} (r^2 \dot{\theta}) &= 0 \end{aligned} \right\} \quad (E-1)$$

The second equation expresses the conservation of angular momentum in the central force field and may be expressed as:

$$H = r^2 \dot{\theta} = r v \sin \gamma = r_0 v_0 \sin \gamma \quad (E-2)$$

where the burnout velocity vector is specified by its speed (v_0) and flight path angle with respect to the local vertical (γ) . Thus, at burnout i.e., $t = 0$, the velocity components in the spherical polar coordinate system (r, θ, λ) , at $r = r_0, \theta = \theta_0$ and $\lambda = 0$ are given by:

$$\left. \begin{aligned} \left. \frac{dr}{dt} \right|_0 &\equiv \dot{r}_0 = v_0 \cos \gamma \\ \left. \frac{d\theta}{dt} \right|_0 &\equiv \dot{\theta}_0 = \frac{v_0}{r_0} \sin \gamma \\ \left. \frac{d\lambda}{dt} \right|_0 &\equiv \dot{\lambda}_0 = 0 \end{aligned} \right\} \quad (E-3)$$

where the angles are illustrated in Figure E-1.

Since the solution to the Lagrangian equation requires finding r and θ as functions of time, this dependency may be eliminated by rewriting the equation of motion into a differential form $r(\theta)$, thus eliminating the parameter t . From the expression for angular momentum (equation (E-2)), the differential change dt is related to a corresponding change $d\theta$:

$$\frac{d}{dt} \equiv \frac{d\theta}{dt} \frac{d}{d\theta} = \frac{H}{r^2} \frac{d}{d\theta} \quad (E-4)$$

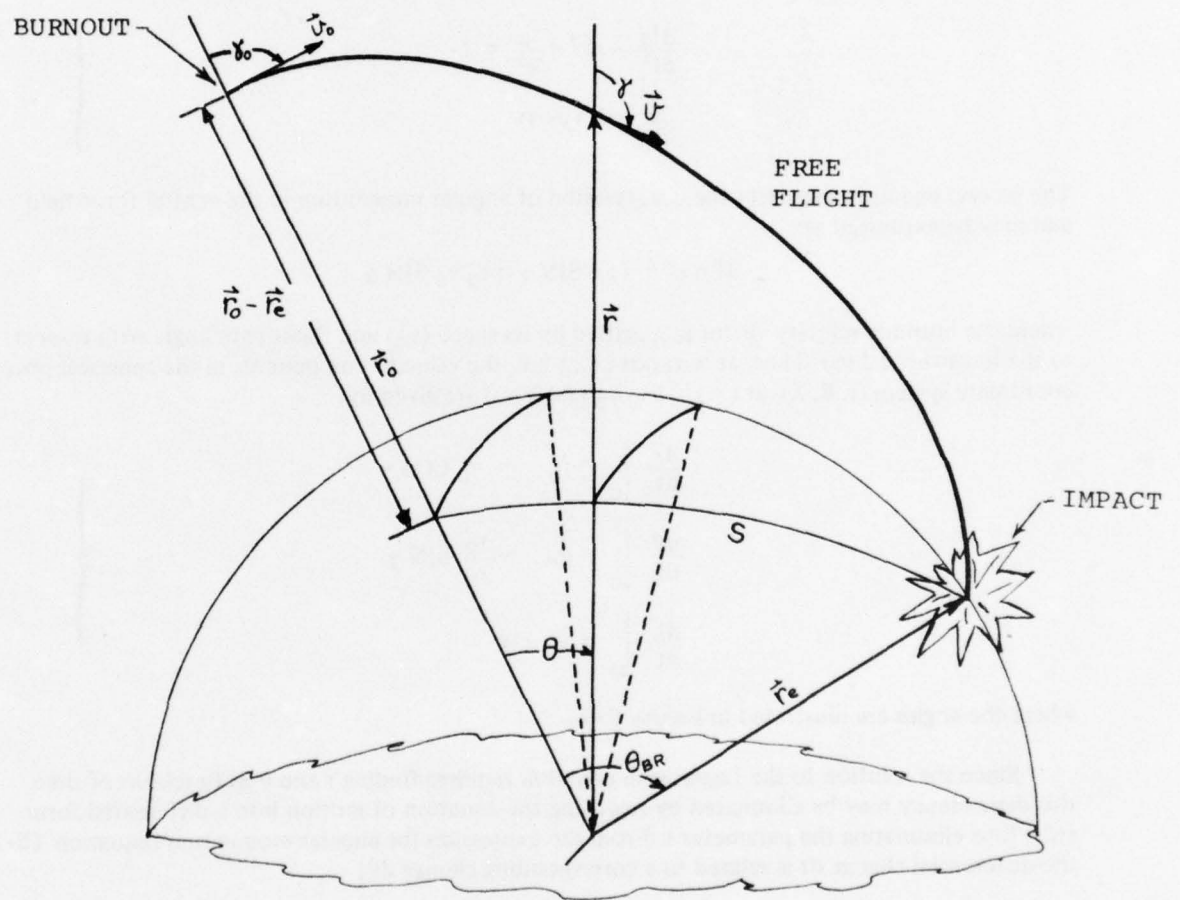


Figure E-1 – Illustration of the Free Flight Ballistic Missile Geometry

and the second derivative with respect to t and θ is

$$\frac{d^2}{dt^2} = \frac{H}{r^2} \frac{d}{d\theta} \left(\frac{H}{r^2} \frac{d}{d\theta} \right) \quad (E-5)$$

The Lagrangian equation becomes

$$\frac{H}{r^2} \frac{d}{d\theta} \left(\frac{H}{r^2} \frac{dr}{d\theta} \right) - \frac{H^2}{r^3} = -\frac{\mu}{r^2} \quad (E-6)$$

Since

$$\frac{1}{r^2} \frac{dr}{d\theta} \equiv -\frac{d}{d\theta} (1/r) \quad (E-7)$$

and by introducing a new variable $u(\theta) = 1/r(\theta)$, the differential equation for the orbit becomes

$$H^2 u^2 \frac{d^2 u}{d\theta^2} + H^2 u^3 = -\mu u^2 \quad (E-8)$$

or

$$\frac{d^2 u}{d\theta^2} + u = -\frac{\mu}{H^2} \quad (E-9)$$

with a solution given by

$$\left. \begin{aligned} u &= K_1 \cos(K_2 - \theta) + \mu/H^2 \\ du/d\theta &= K_1 \sin(K_2 - \theta) \end{aligned} \right\} \quad (E-10)$$

where K_1, K_2 are constants of integration solvable with the initial conditions

$$\left. \begin{aligned} u_O &\equiv u(0) \equiv 1/r_O \\ \dot{u}_O &= -\dot{r}_O/r_O^2 \\ \left. \frac{du}{d\theta} \right|_O &= \frac{du_O}{d\theta_O} = -\frac{\dot{r}_O}{H} \end{aligned} \right\} \quad (E-11)$$

The above expressions are solved for the constants of integrations, where $K_1 \cos K_2 = u_O - \mu/H^2$

and

$$\left. \begin{aligned} K_1 \sin K_2 &= -\dot{r}_O/H \\ \therefore \left(u - \frac{\mu}{H^2} \right) &= \left(\frac{1}{r_O} - \frac{\mu}{H^2} \right) \cos \theta - \frac{\dot{r}_O}{H} \sin \theta \end{aligned} \right\} \quad (E-12)$$

which reduces to the expression

$$u(\theta) r_O = \frac{1 - \cos \theta}{C \sin^2 \gamma} + \frac{\sin(\gamma - \theta)}{\sin \gamma} \quad (E-13)$$

The parameter C is a dimensionless ratio of twice the initial kinetic energy to the potential energy at burnout:

$$C \equiv v_O^2 / (\mu/r_O) \quad (E)$$

The burnout speed is given by:

$$v_O^2 = \frac{\mu C}{r_O} = \frac{\mu}{r_O} \left[\frac{(1 - \cos \theta)}{r_O u \sin^2 \gamma + \sin(\theta - \gamma) \sin \gamma} \right] \quad (E)$$

To insure that a ballistic trajectory will actually impact at a predetermined range, a particular combination of the burnout parameters (\vec{v}_O , \vec{r}_O , γ) is necessary to achieve a specific range angle θ_{BR} . When the ballistic missile trajectory intersects the earth's surface the above expression (equation E-13) becomes known as the "hit" equation, i.e.,

$$\frac{|\vec{r}_O|}{|\vec{r}_E|} = \frac{1 - \cos \theta_{BR}}{C \sin^2 \gamma} + \frac{\sin(\gamma - \theta_{BR})}{\sin \gamma} \quad (E)$$

The burnout speed required to impact at a range θ_{BR} , is given by:

$$|\vec{v}_O|^2 = \frac{\mu}{|\vec{r}_O|} \left[\frac{1 - \cos \theta_{BR}}{(|\vec{r}_O|/|\vec{r}_E|) \sin^2 \gamma + \sin(\theta_{BR} - \gamma) \sin \gamma} \right] \quad (E)$$

where

\vec{r}_E = spherical earth radius vector

and

θ_{BR} = in-the-plane range angle,
related to the surface range S by

$$\theta_{BR} = S/60.039 \text{ (DEG.)}$$

$$\therefore \theta_{BR} \text{ (DEG)} = |\vec{r}_E| \theta_{BR} \text{ (RAD)} / 60.039 \quad (E)$$

Specifying a set of burnout velocities (incremented by 2000. ft/s in magnitude and by 2.0 degrees in direction) at a specific burnout altitude ($|\vec{r}_O - \vec{r}_E|$) the free flight surface range, θ_{BR} , was calculated and plotted as a function of the burnout reentry angle, γ . Illustrated by Figure E-2, each iso-velocity curve (15,000. ft/s to 25,000 ft/s) achieves a maximum surface range at a specific value of γ and denotes a minimum energy condition.

To generate these minimum energy trajectories requires the knowledge of the magnitude and direction of the missile burnout velocity vector that will maximize its surface range. Given the desired surface range of the missile - θ_{BR} , the functional dependence of the reentry angle - γ , is obtained by setting with respect to γ , the partial derivative of equation E-16, i.e.,

$$(\partial \theta_{BR} / \partial \gamma) = 0 \quad (E)$$

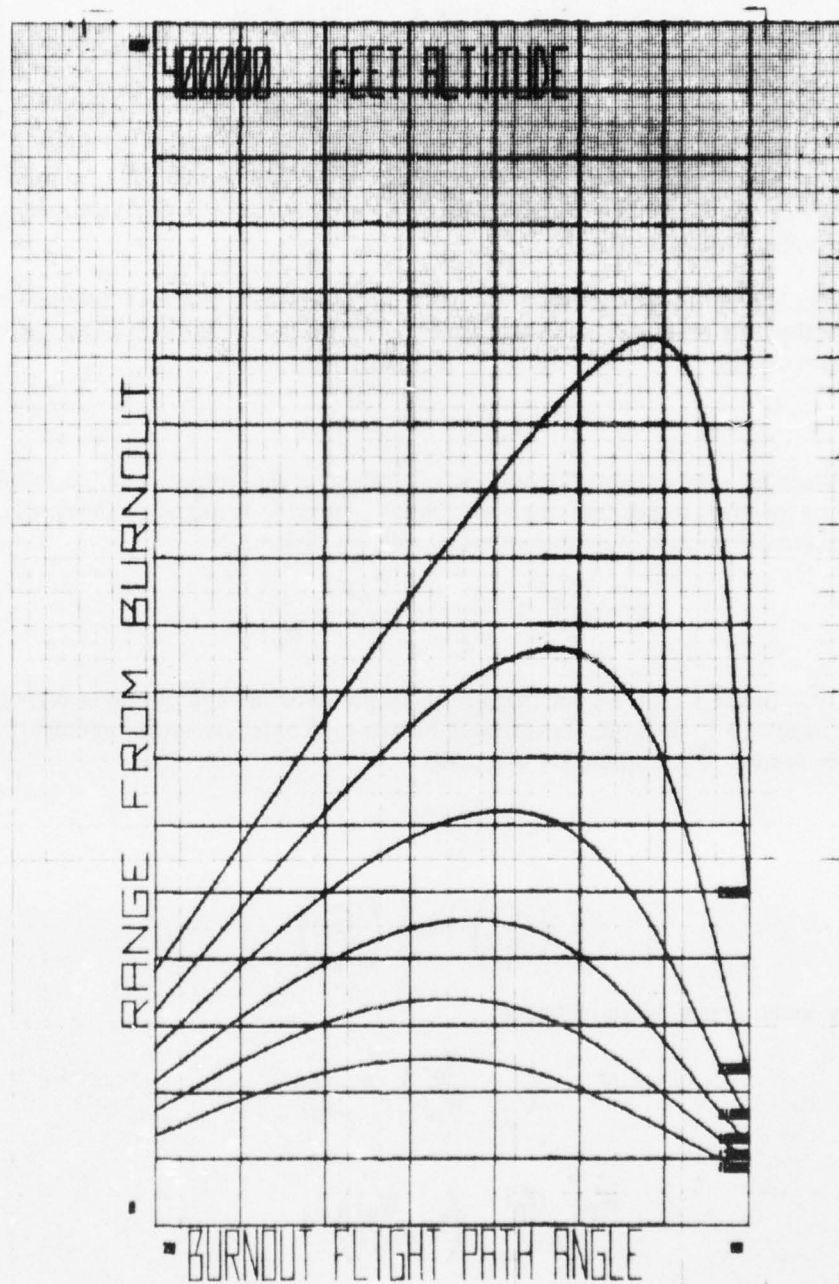


Figure E-2 - Range Angle (Degrees) versus Burnout Reentry Angle (Degrees) for a Family of Constant Burnout Velocity Magnitude

resulting in

$$\tan 2\gamma = \frac{\sin \theta_{BR}}{(\cos \theta_{BR} - |\vec{r}_O|/|\vec{r}_E|)} \quad (E-20)$$

or

$$2\gamma = \pi - \arctan \left\{ \frac{\sin \theta_{BR}}{(|\vec{r}_O|/|\vec{r}_E|) - \cos \theta_{BR}} \right\}$$

With these values of the basic parameters, the calculation of the magnitude of the burnout velocity can be obtained from equation E-20. Thus, for a given value of burnout altitude, these calculated values are illustrated in Figure E-3.

To clarify and bound the previously introduced dimensionless parameter C (defined by equation (E-14)) the total energy of the conservative system is given by the sum of the kinetic and potential energies, i.e.,

$$E = T + V = \text{constant} \quad (E-21)$$

where: T and V are the total extrinsic kinetic and potential energies, respectively. Since the TOTAL energy is invariant to position, the above equation may be evaluated at the apogee and perigee positions in the interest of mathematical expediency. Therefore

$$E = \frac{|\vec{v}_a|^2}{2} - \frac{\mu}{|\vec{r}_a|} = \frac{|\vec{v}_p|^2}{2} - \frac{\mu}{|\vec{r}_p|} \quad (E-22)$$

where $|\vec{v}_a|$, $|\vec{v}_p|$ and $|\vec{r}_a|$, $|\vec{r}_p|$ are the magnitudes of the velocities and positions at apogee and perigee, respectively. From the general expression for the total extrinsic angular momentum of the conservative system, $\vec{r} \times \vec{v}$ at apogee and perigee

$$|\vec{r}_a| |\vec{v}_a| = |\vec{r}_p| |\vec{v}_p| = \text{constant} \quad (E-23)$$

resulting in

$$\left(\frac{|\vec{v}_a|}{|\vec{v}_p|} \right) = \left(\frac{|\vec{r}_p|}{|\vec{r}_a|} \right) \quad (E-24)$$

and the energy equation may be rewritten as:

$$|\vec{v}_p|^2 \left\{ 1 + \frac{|\vec{v}_a|}{|\vec{v}_p|} \right\} = \frac{2\mu}{|\vec{r}_p|} \quad (E-25)$$

or

$$\frac{|\vec{v}_p|^2 |\vec{r}_p|}{2\mu} \left(1 + \frac{|\vec{r}_p|}{|\vec{r}_a|} \right) = 1 \quad (E-26)$$

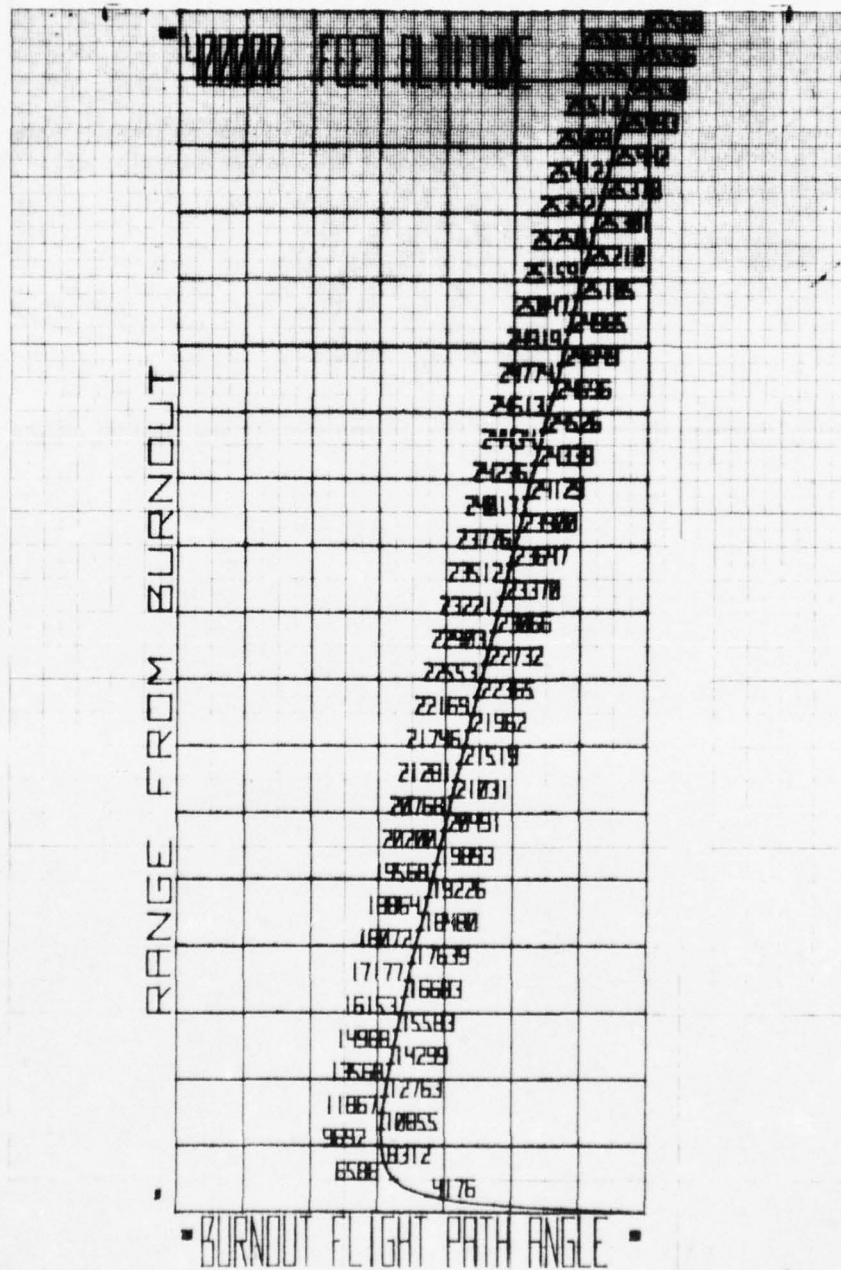


Figure E-3 - Minimum Energy Velocity Requirement (FT/S)

$$\begin{aligned} \therefore E &= \frac{|\vec{v}_p|^2}{2} - \frac{\mu}{|\vec{r}_p|} = -\frac{\mu}{|\vec{r}_p|} \left\{ 1 - \frac{|\vec{v}_p|^2 |\vec{r}_p|}{2\mu} \right\} \\ E &= \frac{-\mu}{|\vec{r}_p|} \left\{ 1 - \frac{1}{1 + |\vec{r}_p|/|\vec{r}_a|} \right\} = \frac{-\mu}{(|\vec{r}_a| + |\vec{r}_p|)} \end{aligned} \quad (E-27)$$

Thus, the total energy for any position on the closed elliptical orbit depends only upon the magnitude of the apogee-perigee position vectors, since the total energy is negative and since the total energy at burnout may be written as:

$$E = \frac{|\vec{v}_0|^2}{2} - \frac{\mu}{|\vec{r}_0|} \quad (E-28)$$

$$\frac{|\vec{v}_0|^2}{2} < \frac{\mu}{|\vec{r}_0|} \Rightarrow C < 2 \quad (E-29)$$

where $|\vec{v}_0|$ and $|\vec{r}_0|$ represent the magnitudes of the missile's velocity and position vectors respectively.

APPENDIX F

GRAPHICAL SOLUTION FOR A QUICK ASSESSMENT OF THE DETECTION PROBLEM

To aid the analyst in determining the visibility of an object (whether it be a satellite and/or missile) in the space-time domain, a rapid method of plotting the earth track (latitude and longitude) for a specific sensor(s) location(s) was derived. Using a Mercator Projection Map of the earth (illustrated in Figure F-1, the spatial object's ground trace was plotted on the HP 9862A Plotter. Also, the volumetric coverage for a specific sensor location and its associated visibility parameters was plotted. The contour (illustrated by Figure F-2) is generated from the projected spatial points on the circumference of the base for a right-circular cone. This cone, with apex at the sensor's location, is generated by specifying a set of visibility (constraint) parameters, i.e., elevation angle and slant range. (Ref. 5).

To plot the visibility contours on the mercator projection map requires a set of transformation equations that will define the geographical arc length between the set of projected spatial points and the specific sensor's location. Referring to Figure F-3 from the law of cosines equation for a spherical triangle, the cosine of the arc length is expressed by

$$\begin{aligned} \cos \alpha &= \sin \Phi_s \sin \Phi_p + \cos (\Delta\lambda) \cos \Phi_s \\ &\quad \cos \Phi_p. \end{aligned} \quad \left. \vphantom{\begin{aligned} \cos \alpha &= \sin \Phi_s \sin \Phi_p + \cos (\Delta\lambda) \cos \Phi_s \\ &\quad \cos \Phi_p. \end{aligned}} \right\} \quad (F-1)$$

where $\Delta\lambda \equiv \lambda_p - \lambda_s$ = longitudinal separation of the projected point and sensor, Φ_p, Φ_s = latitude of the projected point and sensor, respectively.

Since the arc length, α is equivalent to the subtended earth angle (illustrated in Figure F-4), its functional dependency on the sensor's detection range and elevation angle is given by:

$$\alpha = \arctan \left\{ \frac{R_s \cos E}{R_E + R_s \sin E} \right\} \quad (F-2)$$

where the sum and differences, i.e., $\alpha \pm \Phi_s$ defines the latitude of the most northerly and most southerly projected spatial points. Thus, the spatial object is said to be visible from a ground tracking sensor, if when viewed from the sensor, it lies at least E degrees above the true horizon of the sensor and within the specified detection range. A graphical display of the above equation, in Figure F-5 represents a sensor's viewing angle, α (degrees) as a function of slant range, R_s (NM) at detection for a specific set of elevation angles, E (degrees).

Since the Mercator Projection Map can only display a two-dimensional volumetric coverage, an intersecting ground trace (object's earth track) can indicate a possible detection provided the minimum altitude requirement is met. Referring to Figure F-4, the sensor's viewing angle may be expressed by;

$$\alpha = \arccos \left\{ \frac{R_E \cos E}{R_E + H} \right\} - E \quad (F-4)$$

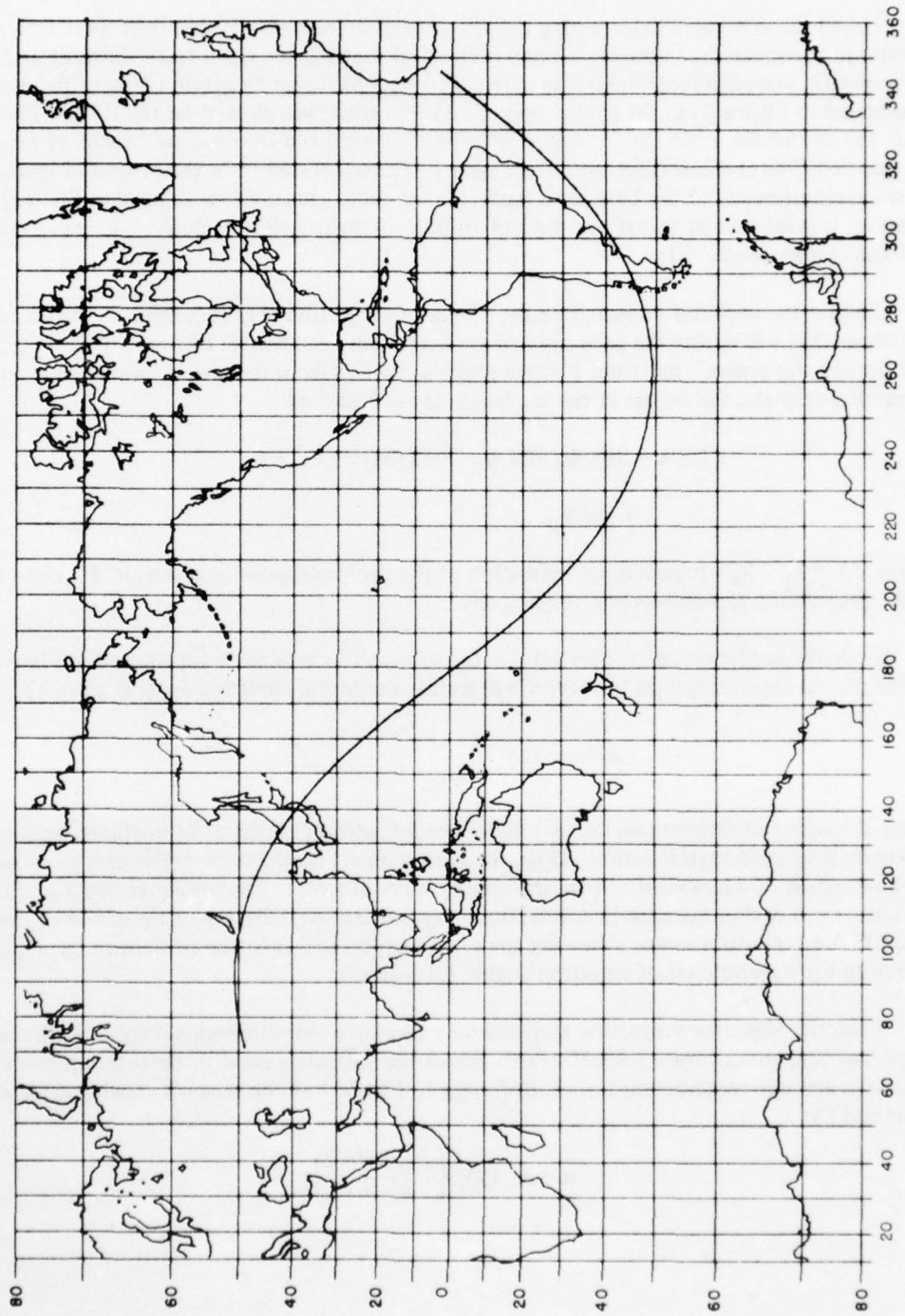


Figure F-1 Earth Track of a Typical Satellite Trajectory

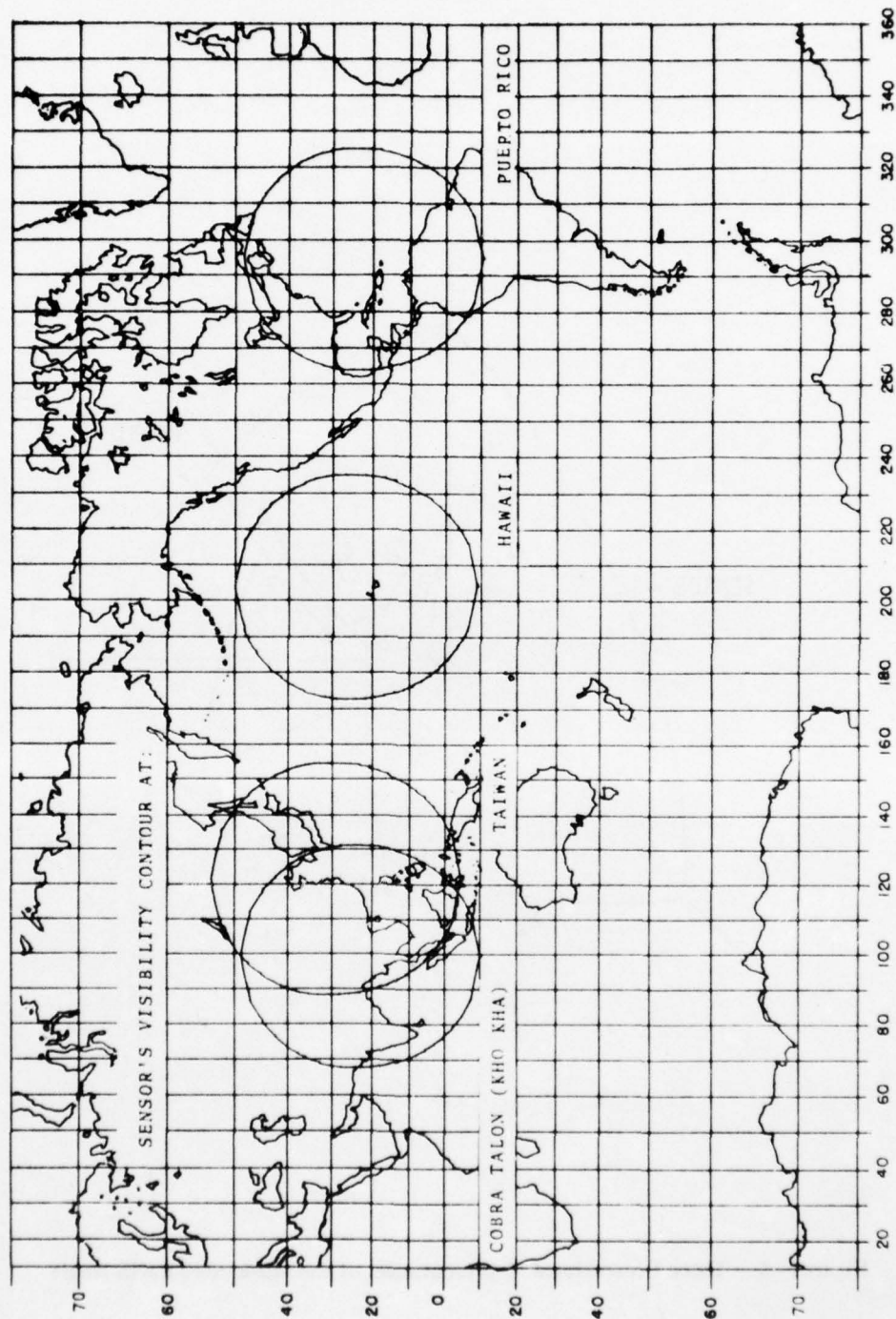


Figure F-2 - Visibility Contours for Specific Sensors (RS = 2000, NM, EL = 2.0°)

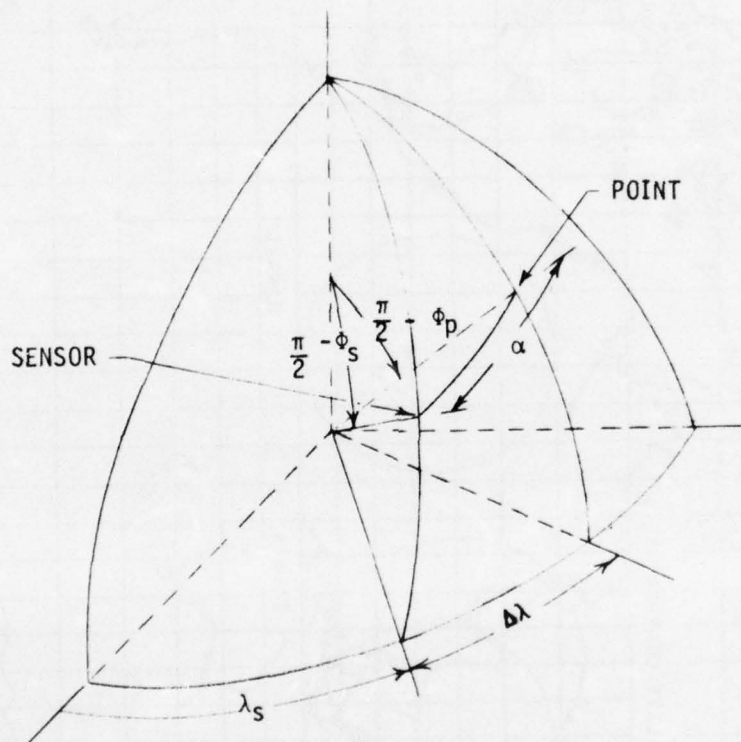


Figure F-3 – Three Dimensional Representation of the Subtended Earth Angle

SPHERE-CAPPED CONE

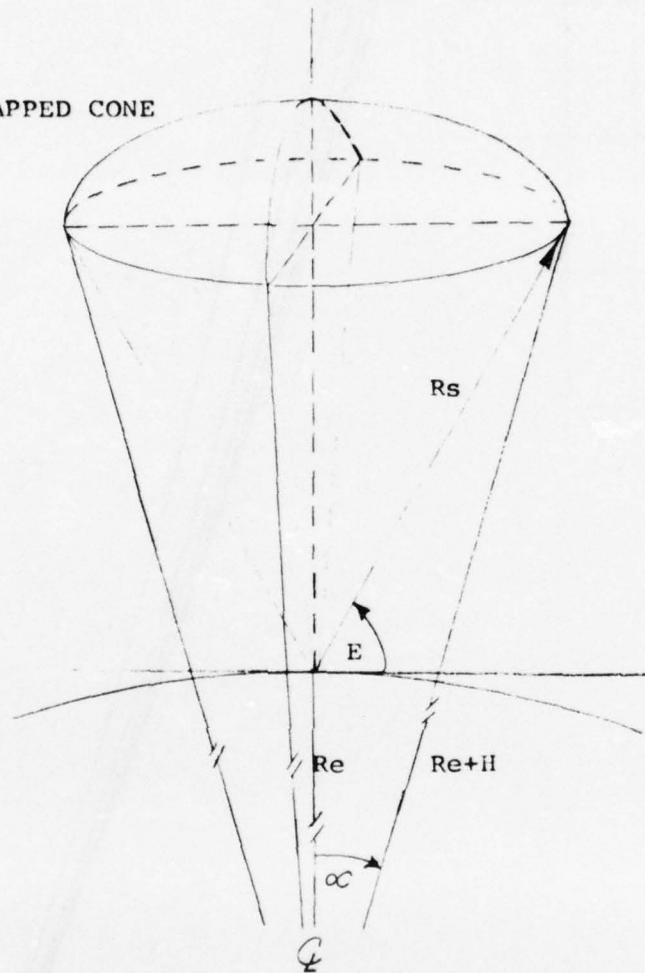


Figure F-4 - Sensor Volumetric Coverage Geometry

and is plotted (See Figure F-6) as a function of altitude, H (NM) for elevation angles of 0., 2.0 and 5.0 degrees. Thus, the detection of an object is conditionally dependent upon a specified set (unprimed) of constraint parameters. For example, if an object is confined to lie within a sphere-capped cone, its parameter set (primed) is described by;

$$R_s' \leq R_s$$

$$E' \geq E$$

$$H' \geq H$$

(F-4)

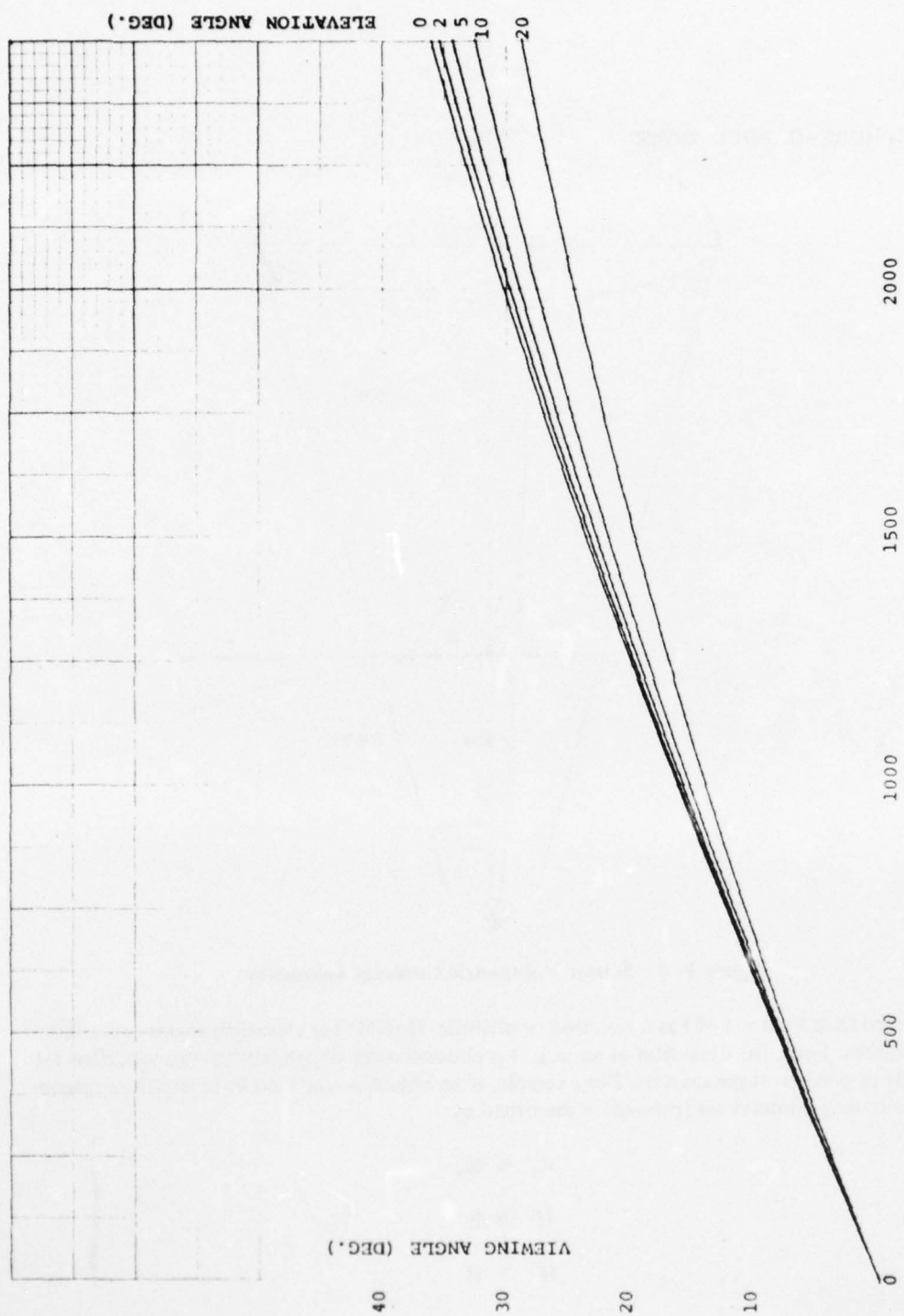


Figure F-5 - Viewing Angle vs. Slant Range (NM)

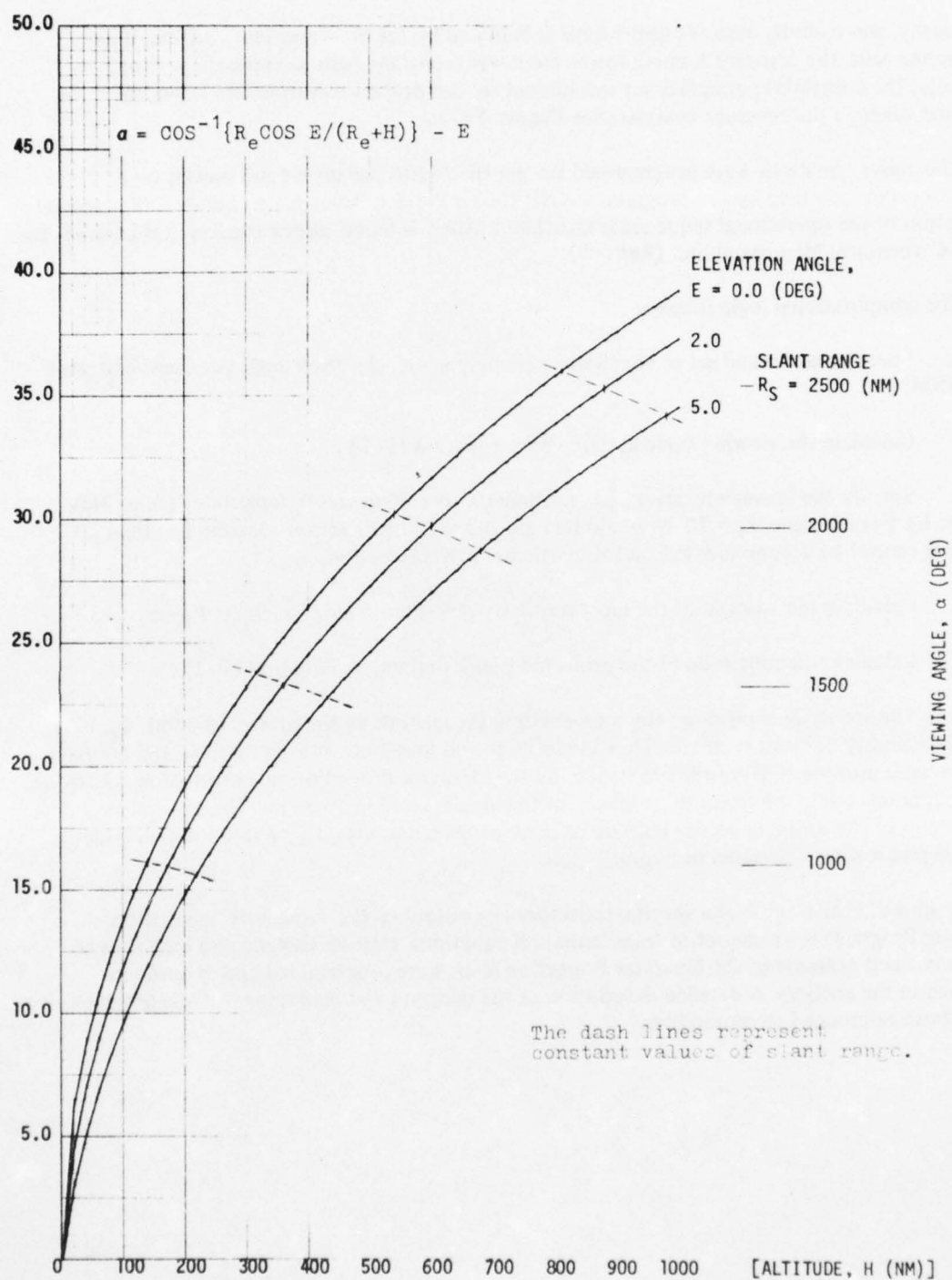


Figure F-6 Viewing Angle vs. Altitude

Graphically, the visibility region's upper limit is bounded by the $R_s = \text{constant}$, curve and its intersection with the constant E curve forms the lower (constant altitude) boundary value. Generally, the constraint parameter set was limited to: 2.0 degrees elevation and 2000 NM detection range in the coverage analysis (See Figure F-7).

The above equations were programmed for the HP 9820A calculator and plotter on a mercator projection map by the programmed HP 9862A Plotter. Referring to Figure F-8 a general description of the operational sequence is illustrated with a detailed description published in a RADC Technical Memorandum. (Ref. 5)

The computational logic follows:

1. Specify the desired set of constraint parameters i.e., elevation angle (degrees) and slant range (NM)
2. Calculate the viewing angle α , defined by equation (F-2).
3. Specify the sensor's location, i.e., latitude (0. to ± 90 degrees), longitude (20. to 360. degrees, E). For example, $\lambda_s = 70^\circ\text{W}$ would be inputted as 290° E. Sensor location less than 20 degrees E cannot be accommodated on this particular map projection.
4. Calculate the latitude of the most southerly projected point, i.e., $\Phi_p = \Phi_s - \alpha$
5. Calculate the longitude of the projected point, defined by equation (F-1).
6. The sequence is repeated (by incrementing the latitude of the projected point, $\Phi_p + \Delta$) until the visibility contour is closed. Thus the latitude and longitude of a set of projected points are translated into the X-Y coordinate system by the Mercator Projection transformation equations. These equations relate the linear dependency of the abscissa on longitude and the non-linear dependency of the ordinate on the latitude of these projected points. This relationship is evident from the grid scaling illustrated in Figure F-2.

To plot the earth trace of a specific trajectory (an output of the Trajectory Simulation Computer Program) the same set of transformation equations, relating latitude and longitude to the abscissa and ordinate of the Mercator Projection Map, were programmed and extensively employed in the analysis. A detailed description of the program and equations will be contained in the above referenced memorandum.

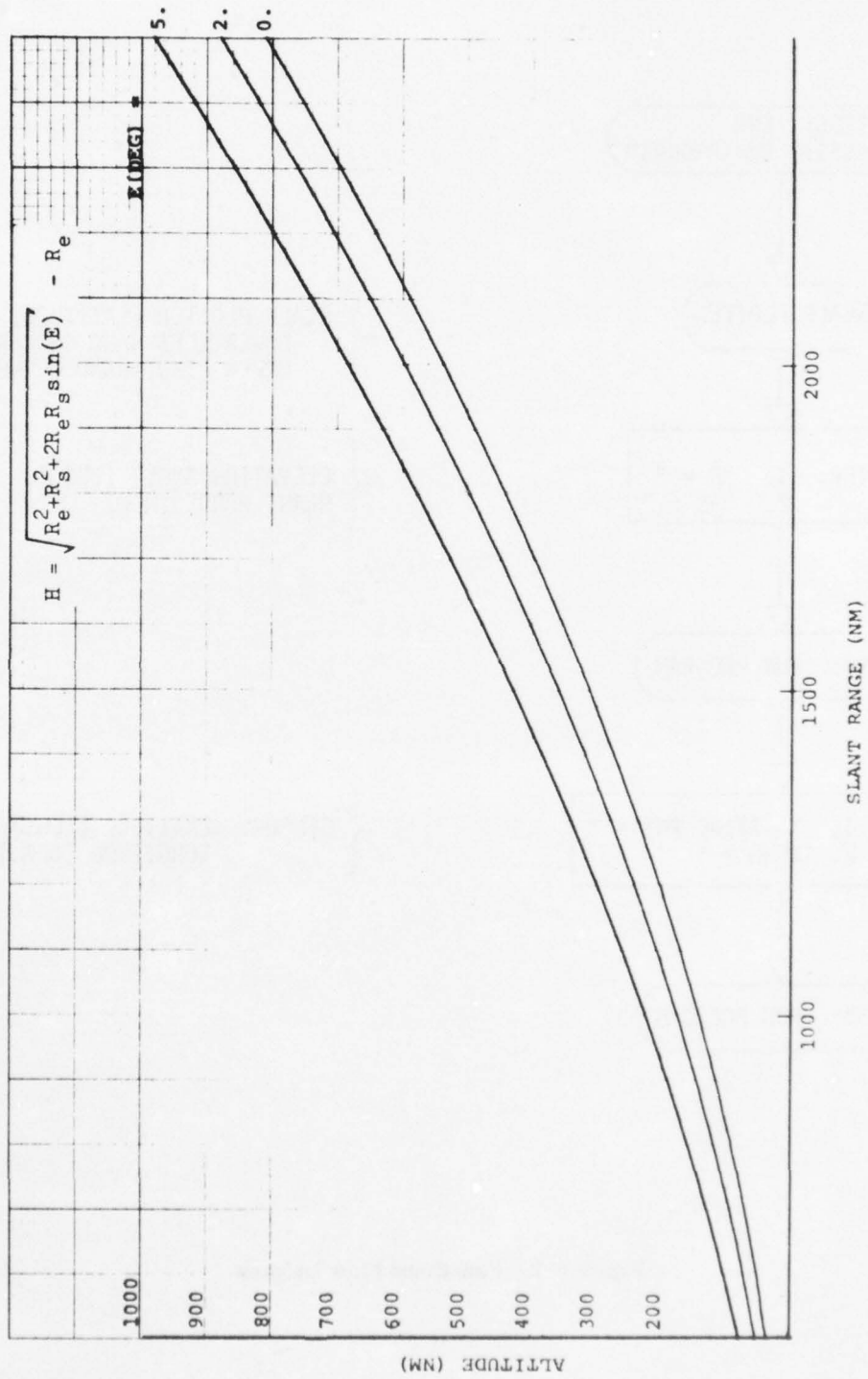


Figure F-7 — Slant Range versus Altitude for a Given Value of Elevation Range

AD-A033 712

ROME AIR DEVELOPMENT CENTER GRIFFISS AFB N Y
SPACE SURVEILLANCE SOFTWARE SUPPORT. VOLUME 1, PART 2. RADC TRA--ETC(U)
OCT 76 6 A ELLIS

F/8 15/3

UNCLASSIFIED

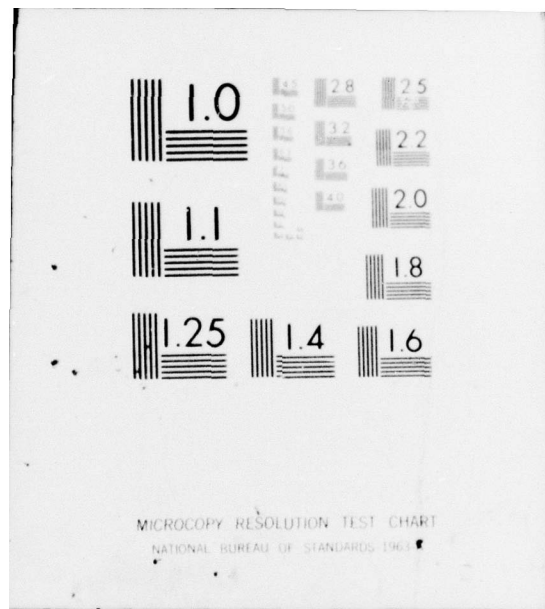
RADC-TR-76-261-VOL-1-PT-2 NL

2 of 2
AD
A033712



END

DATE
FILMED
2-77



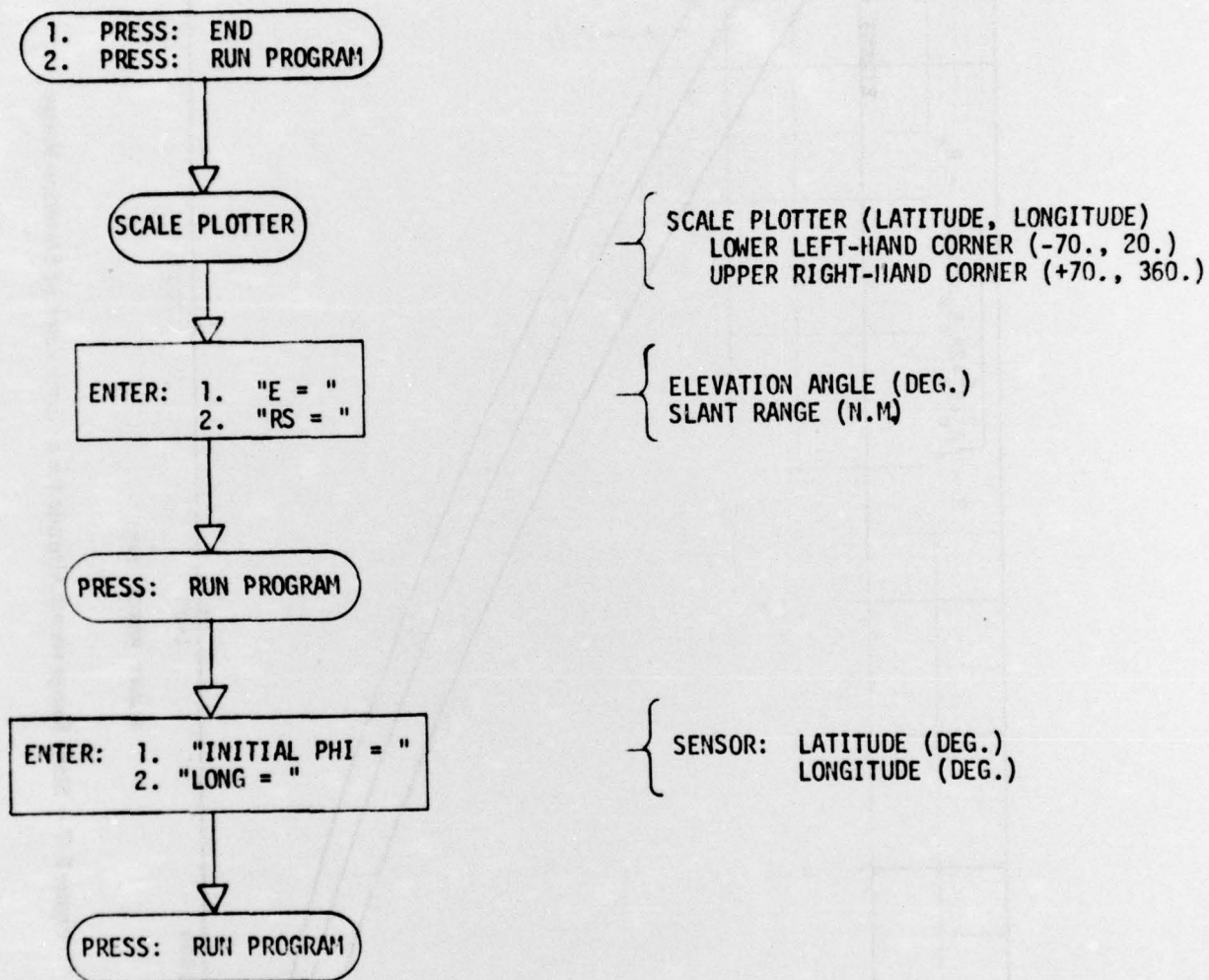


Figure F-8 - Functional Flow Diagram

MISSION *of* **Rome Air Development Center**

RADC plans and conducts research, exploratory and advanced development programs in command, control, and communications (C³) activities, and in the C³ areas of information sciences and intelligence. The principal technical mission areas are communications, electromagnetic guidance and control, surveillance of ground and aerospace objects, intelligence data collection and handling, information system technology, ionospheric propagation, solid state sciences, microwave physics and electronic reliability, maintainability and compatibility.



